# Condensation and T-dependent mobility of different vdW adsorbates within and across quantum confinements

## Inauguraldissertation

Zur

Erlangung der Würde eines Doktors der Philosophie

vorgelegt der

Philosophisch-Naturwissenschaftlichen Fakultät

der Universität Basel

von

Aisha Ahsan

aus Lahore (Pakistan)

Basel, 2018

**Genehmigt von der Philosophisch-Naturwissenschaftlichen Fakultät** auf Antrag von:

Prof. Dr. Thomas Jung
Prof. Dr. Ernst Meyer

Basel, 12.12.2017

Prof. Dr. Martin Spiess
Dekan

To my Mother and my family...

# Abstract

In this thesis a number of important and fundamental surface phenomena have been investigated in an unprecedented way: These involve the condensation of atomic (Xe, Ar) and molecular (cycloalkanes $C_5H_{10}$ to $C_8H_{16}$) gases within surface supported network architectures; the observation of surface phase transitions for the condensates in confinements and the diffusion of adsorbates across a complex nanostructured surface. Uniquely, all these phenomena are investigated under the Scanning Tunneling Microscope and with different adsorbates which predominantly interact by non-directional van der Waals interactions.

The substrate for all these investigations is provided by a complex surface architecture formed by a regular porous metal-coordinated network of perylene-derived molecules self-assembled on Cu(111). Each pore contains a characteristic confined state derived from substrate electrons, thus constituting a quantum confinement. Condensation of Xe is observed in the larger pores and on the smaller nodes of the network, as well as next to the network on the free metal Cu(111) surface. Xe, the first 'van der Waals' gas forms condensates comprising a different number of Xe atoms in different pores. The structural transitions of these condensates containing 1-9 Xe atoms in their hosting confinements have been investigated first (Chapter [[1]]). These transitions e.g. between the 'solid' condensed and the 'fluid' phase of a minimal amount of matter are attributed to different 'phase transition temperatures' and have been also induced *locally* by electric field excitation. In the second part of the thesis the unique and complex hierarchy of the Xe atoms' diffusion pathways within and across the surface nano-architecture is revealed with respect to their temperature dependent activation. The inter-pore diffusion at higher temperatures leads to a 'coarsening' of the condensates in that the lower populated ones disappear to the benefit of the larger condensates, in particular the 12 fold occupied 'full' pore (Chapter [[2]]). A unique chemical object has been identified in the form of a linear trimer which we attribute to the $Xe_3$ or the $Xe_3^+$ condensate (Chapter [[3]]). The last chapter discusses the condensation of the significantly larger cyclo-alkanes as they form aggregates with sizes incrementing from one to a max value which depends both on the size and also on the different possibilities for the stacking of the cycloalkanes in the nanopore confinements (Chapter [[4]]).

This work establishes a radically new approach to induce phase transition in minimal amount of matter in confinements embedded in on-surface porous networks. Moreover, it is shown that the quantum confinements can be used as nano-traps, offering real-space access to the phase transition and condensation proceeding under the influence of van der walls forces in an atom-by-atom and molecule-by-molecule way.

# List of publications / manuscripts

This thesis is based on four first-author manuscript and is provided in the 'cumulative' format. The manuscripts are listed below and are referred in the text by the double square brackets.

| | |
|---|---|
| [[1]] | **'Phase transitions' in confinements: Controlling solid to fluid transitions of Xenon atoms in an on-surface network**<br>Aisha Ahsan, S. Fatemeh Mousavi, Thomas Nijs, Sylwia Nowakowska, Olha Popova, Aneliia Wäckerlin, Jonas Björk, Lutz H. Gade, Thomas A. Jung., manuscript provisionally accepted in ***small*** journal. |
| [[2]] | **Kinetically controlled activation of diffusion pathways of Xe condensates in a surface metal organic network**<br>Aisha Ahsan, S. Fatemeh Mousavi, Thomas Nijs, Sylwia Nowakowska, Olha Popova, Aneliia Wäckerlin, Jonas Björk, Lutz H. Gade, Thomas A. Jung., manuscript submitted to ***small*** journal. |
| [[3]] | **$Xe_3^+$ Trimers: Stabilization of a linear Xe trimer in the DPDI quantum confinements**<br>Aisha Ahsan, S. Fatemeh Mousavi, Thomas Nijs, Sylwia Nowakowska, Olha Popova, Aneliia Wäckerlin, Jonas Björk, Lutz H. Gade, Thomas A. Jung., manuscript in preparation. |
| [[4]] | **Size dependent molecule-by-molecule condensation of cyclo-alkanes in nano-traps**<br>Aisha Ahsan, S. Fatemeh Mousavi, Thomas Nijs, Sylwia Nowakowska, Olha Popova, Aneliia Wäckerlin, Jonas Björk, Lutz H. Gade, Thomas A. Jung., manuscript in preparation. |

In addition, during my PhD studies I contributed following publications and manuscripts:

| | |
|---|---|
| [1] | **Molecular chessboard assemblies sorted by site-specific interactions of out-of plane d-orbital with a semimetal template**<br>Aneliia Wäckerlin, Shadi Fatayer, Thomas Nijs, Sylwia Nowakowska, S. Fatemeh Mousavi, Olha Popova, Aisha Ahsan, Thomas A. Jung, and ChristianWäckerlin. *Nano letters*, 17, 1956-1962 (2017)<br>[DOI: 10.1021/acs.nanolett.6b05344] |
| [2] | **Configuring Electronic States in an Atomically Precise Array of Quantum Boxes**<br>Sylwia Nowakowska, Aneliia Wäckerlin, Ignacio Piquero-Zulaica, Jan Nowakowski, Shigeki Kawai, Christian Wäckerlin, Manfred Matena, Thomas Nijs, Shadi Fatayer, Olha Popova, Aisha Ahsan, S. Fatemeh Mousavi, Toni Ivas, Ernst Meyer, Meike Stöhr, J. Enrique Ortega, Jonas Björk, Lutz H. Gade, Jorge Lobo-Checa and Thomas A. Jung.<br>***Small***, 12, 3757–3763 (2016). [DOI: 10.1002/smll.201600915] |
| [3] | **Adsorbate-induced modification of the confining barriers in a quantum array**<br>Sylwia Nowakowska, Federico Mazzola, Mariza N. Alberti, Fei Song, Tobias Voigt, Jan Nowakowski, Aneliia Wäckerlin, Christian Wäckerlin, Jérôme Wiss, W. Bernd Schweizer, Max Broszio, Craig Polley, Mats Leandersson, Shadi Fatayer, Toni Ivas, Milos Baljozovic, S. Fatameh Mousavi, Aisha Ahsan, Thomas Nijs, Olha Popova, Jun Zhang, Matthias Muntwiler, Carlo Thilgen, Meike Stöhr, Igor A. Pašti, Natalia V. Skorodumova, François Diederic, Justin Wells, Thomas A. Jung.<br>***ACS Nano***, 12, 768-778 ( 2017 ) [DOI: 10.1021/acsnano.7b07989] |
| [4] | **The different faces of 4'-pyrimidinyl functionalized 4,2':6',4''-terpyridines: environmental effects in solution and on Au(111) and Cu(111) surface platforms**<br>Thomas Nijs, Y. Maximilian Klein, S. Fatemeh Mousavi, Aisha Ahsan, Sylwia Nowakowska, Edwin C. Constable, Catherine E. Housecroftb and Thomas Jung.<br>***Journal of the American Chemical Society*** ( 2018 ) [DOI: 10.1021/jacs.7b12624] |

| | |
|---|---|
| [5] | **Thermally-activated Self-assembly and In Situ of a Reduced Decaazapentacene**<br>David Miklík, Seyedeh F. Mousavi, Anna Middleton, Yoshitaka Matsushita, Jan Labuta, Aisha Ahsan, Paul A. Karr, Pavel Švec, Filip Bures, Gary J. Richards, Toshiyuki Mori, Katsuhiko Ariga, Yutaka Wakayama, Francis D'Souza, Thomas A. Jung and Jonathan P. Hill.<br>In review ***Angewandte Chemie*** |

# Contents

# Abbreviations and molecules

**General acronyms**

| | |
|---|---|
| 2D | two dimensional |
| 3D | three dimensional |
| MON | metal organic network |
| DFT | density functional theory |
| DOS | density of states |
| LDOS | local density of states |
| UHV | ultra-high vacuum |

**Methods**

| | |
|---|---|
| STM | scanning tunneling microscopy |
| | scanning tunneling microscope |

**Molecules**

| | | |
|---|---|---|
| 3deh-DPDI | triply dehydrogenated 4,9-diaminoperylene quinone-3,10-diimine | 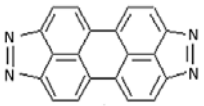 |

| | | |
|---|---|---|
| $C_5H_{10}$ | Cyclopentane | 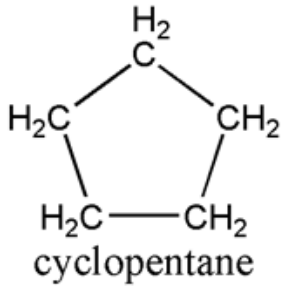 cyclopentane |
| $C_6H_{12}$ | Cyclohexane | 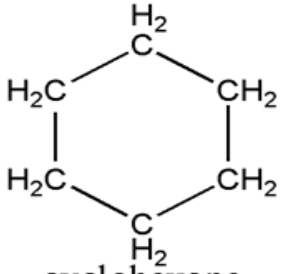 cyclohexane |
| $C_7H_{14}$ | Cycloheptane | 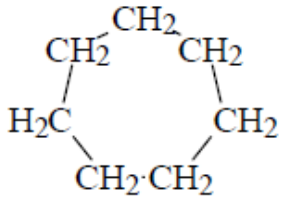 Cycloheptane |
| $C_8H_{16}$ | Cyclooctane |  Cyclooctane |

# Introduction

For more than a century, physicists and chemists were developing the concepts of chemistry in their drive to explain the world until Boltzmann and his peers developed the powerful instrument of statistical mechanics. Would any of these scientists have anticipated that it may be possible to see how e.g. few atoms form condensates, get transformed into fluid mode by either thermal excitation or by stimulating electric fields and re-condense in different forms.

In his famous 1959 lecture 'There is plenty of room at the bottom' R.P Feyman stated: 'What I want to talk about is the problem of manipulating and controlling things on the small scale'[1] He provided an amazingly complete account of different possibilities towards miniaturization. He talked about controlling individual atoms, as later pioneered by D. M. Eigler and coworkers at IBM Almaden. Further he discussed the art of 'writing small' and more generally the concept of information stored on a small scale. In his estimates he assumes a technological 'bit' to be stored in 5 x 5 x 5 atoms i.e. 125 atoms and he compares this value to the information density of DNA which is 50 atoms per bit. What Would Feynman think to see that only 3-12 Xe atoms can be used for one bit and that a whole landscape of equally spaced bits can be produced by self-assembly?

Why is this possible now and here? This thesis is standing on different pillars in the form of scientific knowledge:

- *Coordination chemistry and supramolecular chemistry* – a unique symbiosis with the metal substrate – provide the grounds for making the template.
- *Gas theory* which revealed an early entry point into the study of interatomic and intermolecular interactions, e.g. via the mathematical description of 'real' gases and the consequent derivation of the van der Waals potential.
- *Adsorption and desorption*, a pair of properties which are fundamental in surface/interface science on one side for the investigation and use of desorption and evaporation procedures on the other side for the controlled deposition and growth of thin films.
- *Phase transitions*, in particular solid to fluid transitions of small condensates of matter can be investigated e.g. in cluster beams and may depend on the number of atoms in a certain cluster – or in a confinement as it is the case in our studies.
- *Atomic diffusion* as it has been long-investigated and as it occurs at surfaces and interfaces.
- Crystal engineering and crystal structure analysis provide a versatile mean to investigate

interatomic and intermolecular forces – even more so if, as it is the case in this thesis – if very small condensates can be investigated in an atom by atom or a molecule by molecule way. Here different noble gases and the larger cycloalkanes have been chosen as the first objects of investigation along these lines.

James Clerk Maxwell stated in his famous lecture that *"there can be no doubt that the name of van der Waals will soon be among the foremost in molecular science"*. Historically van der Waals interactions are described first to explain non ideal behavior of gases that ought to be ideal (i.e. noble gases)

Before the start of this thesis, it was recognized that the fluids under condition of spatial confinements (3D nanopores or films) often exhibit physical properties different from those found in their bulk states.[2–12] This is brought about by (a) the introduction of additional interactions with the pore walls and (b) the confinement effects (from finite-size effects or effects of reduced dimensionality). This geometric confinement can give rise to restricted diffusion, which is widely used as a tool for structural characterization.[13,14] So spatial confinements lead to size-dependent alterations of the phase equilibria characteristics, such as the equilibrium transition temperature or pressure.[15–17] Due to the van der Waals interaction of guest molecules they can adhere to each other or adhere at the outer wall of the confinement as it is recognized to modifiy the phase equilibria in such confinements.[13]

We aim to study the power of vdW forces of adsorbants in 2D on-surface nano-sized confinements. Self-assembly plays a crucial role in the construction of the quantum confinement architectures, as the periodic (metal-)organic porous networks are confining the surface state electrons in their pores, hence acting as quantum confinement arrays without the need of controlling top-down processes.[18] Notably, on-surface 2D periodic networks, apart from their ability to confine the surface state electrons, can also trap different adsorbates.[19] In earlier work the interactions between the quantum state localized in the confinements and the adsorbates therein have been investigated.[20,21] Towards improving the control of such 2D architectures and in particular for controlling their functionality e.g. for catalyzing reactions, it is essential to understand the adsorption state and the mobility of the different adsorbed species. The behavior of noble gases in such confinements can serve as a model system to understand condensation and diffusion processes in these confinements.[22,24] The thermal energy (kT) activates atomic and molecular libration, rotation and diffusion in the confinements.[25] In addition to the van der Waals interaction of the noble gas guest atoms with the confining walls i.e. with the bottom substrate and the network, we expect that the centrally located quantum state will affect their temperature dependent behavior.

In case of the regular Cu-coordinated 3deh-DPDI network grown on Cu(111),[26] here we study the temperature dependent aggregation, libration, rotation of xenon atoms in these porous confinements, in addition to the phase transitions between '2D- fluid' and '2D solid' phases behaving on the number of guest atoms in confinements. In addition, the STM tip is used to exert local forces and electric fields to selected Xe occupied confinements. Thereby diffusion or liberation, processes can be excited in order to investigate the time the system needs to re-equilibrate with the environment. The fundamental interest, here, is to understand the new physics that occurs due to finite size effects, surfaces interactions and due to the reduced dimensionality of the host assembly with guest atoms and molecules. This thesis presents a first example of a real space investigation of atomic level phase transition induced *globally* by temperature changes and *locally* by electric field excursions in nano confinements (Chapter [[1]]), of the temperature dependent activation of diffusion/coarsening pathways across the network (Chapter [[2]]), of the remarkable observation of $Xe_3$ or $Xe_3^+$ and of the condensation / packing of cyclo-alkanes as guests in confinements (Chapter [[4]]). In this thesis and project STM proves, again, to be a powerful tool for the comprehensive exploration of atomic level phase transitions in 2D confinements. This way it has become possible to investigate the dynamics of phase transitions of different numbers of confined xenon atoms with varying temperature. Moreover, this system provides a fascinating possibility to investigate phase transitions, the coarsening and condensation under the interplay of van der Waals forces and in an atom-by-atom way. To investigate this system with more complex adsorbats, we also studied condensation behavior depending on the varying size of molecules in a molecule-by-molecule way. This is of fundamental relevance, given the fundamental role of the adsorption and condensation processes. Also owing to gain further insight into the predicted size effects on the nanometer scale, such atom-by-atom/molecule-by-molecule condensation/phase transition studies are conceptually desired.

The ultimate goal is to assemble a toolkit database about different atoms and molecules and their temperature dependent behavior in nanosized confinements allowing for the better understanding of complex condensation/structural transformation. Ultimately, an idea originating from gas theory and the underlying *van der Waals* forces is employed for forecasting condensation processes and structural transitions. The approach is mainly based on *physical* investigation methods revealing single atomic/molecular level modifications of the condensates and their interactions inside 2D nanometer sized confinements. Thereby this work provides a valid and characteristic example for the concept of Nanoscience.

# Methods

This section gives an overview of main experimental technique used in the research included in this thesis. For structural characterization of on-surface adsorbates in nano sized confinement arrays scanning tunneling microscopy (STM) is used.

**Scanning tunneling microscopy (STM)**

STM is a local imaging technique, in which a bias voltage is applied between a sharp tip and a sample. When the distance between these amounts to a few angstroms, the tunneling effect occurs. The subsequent tunneling current rest on exponentially on the sample-tip distance permitting for an unprecedented vertical resolution in the range of pm. The tip is mounted on a piezoelectric scanner, which images the sample via line-by-line in-plane movements with sub-angstrom precision. In the constant current mode, a feedback loop is keeping a constant value of the tunneling current by further vertical movements of a piezoelectric scanner, which then reflect the contour of local density of states (LDOS). In the constant height mode, the feedback loop is deactivated and the scanner moves the tip only vertically. The resulting tunneling current is used for accomplishing the LDOS contour.

# Chapter [[1]] and Supplementary Information

| | |
|---|---|
| [[1]] | **'Phase transitions' in confinements: Controlling solid to fluid transitions of xenon atoms in an on-surface network** |
| | Aisha Ahsan, S. Fatemeh Mousavi, T. Nijs, S.Nowakowska, Olha Popova, A. Wäckerlin, T. Nijs, J. Björk, L. H. Gade, T. A. Jung, *manuscript provisionally accepted in journal* ***small***. |
| | Contribution of A. Ahsan: carried out experimental investigations (STM), analysed and interpreted the data, wrote the manuscript. |

# Phase transitions in confinements: Controlling solid to fluid transitions of xenon atoms in an on-surface network

*Aisha Ahsan[a], S. Fatemeh Mousavi[a], Thomas Nijs[a], Sylwia Nowakowska[a], Olha Popova[a], Aneliia Wäckerlin[a], Jonas Björk[b], Lutz H. Gade[c], Thomas A. Jung[a,d]*

We report on 'phase' transitions of Xe condensates in on-surface confinements induced by temperature changes and local probe excitation. The pores of a metal-organic network occupied with 1 up to 9 Xe atoms have been investigated in their propensity to undergo 'condensed solid' to 'confined fluid' transitions. Different transition temperatures are identified, which depend on the number of Xe atoms in the condensate and relate to the stability of the Xe clustering in the condensed 'phase'. This work reveals the feature-rich behaviour of transitions of confined planar condensates which provide a showcase towards future 'phase-transition' storage media patterned by self-assembly. This work is also of fundamental interest as it paves the way to real space investigations of reversible solid to fluid transitions of magic cluster condensates in an array of extremely well-defined quantum confinements.

Phase transitions[1] play a pivotal role in many applications, such as in almost every implementation of data storage[2,3]. Ideally, at the ultimate limit, structural transitions[4–6] can be reversibly induced for a small, discrete number of atoms or molecules which can be addressed and operated without being diluted in a solid matrix. The addressing and manufacturing of such 'patterned media'[7,8] for data storage at the ultimate limit is facilitated by arrangements in less than three dimensions which do not require top-down nano-fabrication in their production. Importantly, bottom-up molecular self-assembly has been proven successful for the manufacturing of well-ordered templates which can host atoms and molecules in a controllable manner[9]. Inevitably for a discrete number of atoms/molecules, components in one 'information bit' may occupy different discernible positions, which are characterized by, for example, different bonding geometries for 'internal', 'surface', 'surface-edge' or 'surface-kink' positions. Therefore, the energy landscape becomes heterogeneous and site-specific. The homogeneity, as implied by the term 'phase' is thus lost and structural transitions will occur in a more complex way. Atoms/molecules at some sites require lower activation energy barriers to become mobile as observed for the phenomenon of 'surface melting'[10,11].

In the following, the terms 'phase' and 'phase transition' are meant to denominate the transition between condensed/static (solid) and mobile (2D fluid also including lattice-gas) forms of the atoms in the confinements[9], despite the non-uniformity of such discrete systems comprising atoms held in a potential but at discernible sites. Being 'small' with reference to the range of the dominant interaction force, such heterogeneous systems[12] provide a challenge to a thermodynamic treatment. On the other hand, they are relevant for the behaviour of bio-molecular machines and protein action, and in many other fields including nuclear and

[a]Department of Physics, University of Basel, 4056 Basel, Switzerland. [b]Department of Physics, Chemistry and Biology, IFM, Linköping University, Linköping 581 83, Sweden. [c]Anorganisch-Chemisches Institut, Universität Heidelberg, Im Neuenheimer Feld 270, 69120 Heidelberg, Germany. [d]Laboratory for Micro- and Nanotechnology, Paul Scherrer Institut, 5232 Villigen PSI, Switzerland. Correspondence and requests for materials should be addressed to A.A (aisha.ahsan@unibas.ch), or to L.H.G (lutz.gade@uni-hd.de) or to T.A.J. (thomas.jung@psi.ch)

astrophysics. A simple system like the one at hand may provide a suitable model case e.g. for the possibly retarded equilibration between different compartments; here Xe atoms hosted in a 2D metal-organic framework. This motivates real space investigations of size dependent structural ('phase') transitions of a small discrete number of atoms held in surface confinements [13,14].

We report an experimental study of the structural (~'phase') transitions of Xe condensates within the confinements of a highly ordered surface lattice which are induced by temperature as well as by local electronic excitations. These experiments have been performed for discretely incremented Xe filling levels ($1 \leq n \leq 9$) of the confinements.

**Results and Discussion**

In this study, a previously reported hexagonal surface network has been employed, composed of Cu-coordinated, triply dehydrogenated 4,9-diaminoperylene quinone-3,10-diimine (3deh-DPDI) molecules on Cu(111)[15]. The network is highly stable (up to 300 ºC) and its pores represent a 2D periodic array of confinements, each containing a discrete electronic quantum state created by the interaction of the periodic network with the underlying Shockley surface state[16]. Xenon gas, chosen for the minimal directional character of its Van der Waals attractive interactions, has been deposited into these 'quantum confinement' arrays[17,18]. The gas is dosed onto samples prepared in Ultra High Vacuum conditions to minimize the presence of other adsorbates, that condense in the pores of the network and on the vacant Cu(111) substrate. This has given rise a broad range of pore occupancies by condensed Xe "clusters" which are monitored by time lapse imaging sequences in STM at progressively increased temperatures. Typically, in one experiment, the temperature is raised from the thermal equilibrium in the He cryostat (~4.2K) by resistive heating to a maximum temperature of 16K by using a temperature controller [LakeShore-331] at 0.2 K/min, while STM micrographs and experiments are performed at each required temperature after switching off the temperature ramping. To further assess the dynamics within the confinements, the STM tip is used as a fixed probe at certain positions of the pores to measure the tunnelling current fluctuations which are caused by the presence or absence of Xe. The latter is dependent on the diffusive motion of the Xe in the pore. Finally, the STM tip has been used as an actuator, exerting a field/current at specific positions above the confinements.

With the adsorption of Xe in the pores of the periodic network on exposure, a statistical filling of the pores is achieved which has been described previously[17]. At 4 K, the Xe atoms appear static for different pore occupancies on the time-scale of the STM experiments, as exemplified in Fig. 1d for the cases of seven-fold occupancy (**occ-7**), and single occupancy (**occ-1**). Upon heating to 16 K, dynamic exchange of pore positions sets in: the **occ-7** case shows a ring like shape while **occ-1** appears as a six-star shape at 16 K as depicted in Fig 1e. Notably, the spatial distribution of the dynamic xenon atoms in **occ-1** and **occ-7** indicates that Xe is not moving freely across the pore, but stays near the outside rim. As it will be discussed in more detail below, we attribute this observation to attractive interactions with the bordering network components as well as repulsive interactions with the confined surface state (cSS) centrally located in each confinement[17,18]. To investigate the site dependence of the Xe diffusion in confinements, STM micrographs have been acquired at variable temperature for initial pore occupancies from single to nine-fold (**occ-1—occ-9)** and with increasing temperature from 4 to 16 K (SI 1).

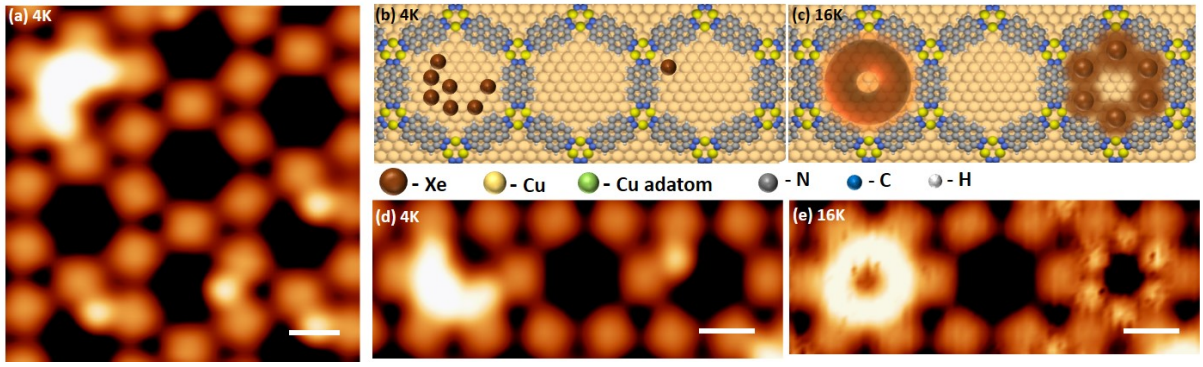


**Figure 1: Temperature induced 'phase' transition in confinements.** STM image **(a)** shows different condensates in networks especially **occ-7** and **occ-1**. **(d, e)** In the bottom row scanning tunnelling micrographs of three neighbouring pores containing (from left to right) 7, 0 and 1 xenon atoms (**occ-7**, **occ-0**, **occ-1**), respectively, are shown at low ~4K (d) and elevated ~ 16K (e) temperatures. The Xe generally shows the highest contrast in STM irrespective of its adsorption site, the 3deh-DPDI backbone is characterized by medium contrast while the empty pores and the sites of the coordinating nodes appear black at the imaging parameters used (10 pA, 1V). The atomic positions of Xe adsorbed in the network have been marked brown in the structural model **(b, c)**. All here shown Xe condensates are immobile at 4K (left) while at 16K, the **occ-7** condensate inside the confinement appears as a ring and the **occ-1** condensate as 6 star-shaped which is the sign of a significant diffusion or hopping along the perimeter of the confinement. All scale bars are 1nm.

The 16 K upper limit has been fixed to avoid changes in pore occupancy that sets in at higher temperatures. The STM data is displayed in a matrix arrangement in Fig. 2 with Xe occupancy at the horizontal axis and vertical axis indicates provided temperature. The transition from 'solid' (static) to 'fluid' (dynamic) phase is indicated by the blue and green frames, respectively. With progressively increased temperature, mobility slowly sets on, as indicated by the "noisy" STM Xe patterns. Detectable noise indicates that the timescale of the data acquisition (~ 8 msec / pixel) is in the same order of magnitude of the Xe atoms fluctuating between different positions in the confinement. At temperatures above this transitional regime the tip records the time averaged distribution of the confined atoms. As mentioned above, the onset of Xe motion occurs along the periphery of the confinement in all cases. In the case of **occ-1** the particular 'star-like' shape of the Xe in motion suggests that in this case Xe is diffusively hopping in a 'lattice-gas'[19] manner and the Xe residency time in the 6 corner positions of the confinement is dominant even up to 16 K. The asymmetry of this system indicates that the nodes are more attractive for Xe condensation than alternative positions within the individual pore (e.g. close to the 3deh-DPDI units). It is instructive to compare this specific case with the other occupancies in a display of the diagonal cross section profiles for the dynamic systems as extracted from the STM data which are displayed in Fig. 3.

Importantly, Fig. 2 indicates that the transition between the 2D-solid and 2D-fluid phases critically depends on the number of guest atoms inside the pore. In case of **occ-1—occ-6** mobility starts at 8 K, in case of **occ-7** at 10 K, while **occ-8** at 14 K. The **occ-9** as a whole becomes mobile at 12K but it is important to note that the 9$^{th}$ Xe atom which is in a less favoured adsorption site[17] becomes dynamic already at 8K (SI 2). This reflects the inequivalent bonding of this atom compared to the others. Surface melting, non-uniform phase transitions

in small clusters of atoms as well as the observations of 'magic' and more diffusive 'non-magic' surface islands provide other cases of the special thermodynamic evolution of few inequivalently interacting subsystems[20–26]. The reorientation of the larger condensates (**occ-7—occ-8**) occurs before a complete melting, at distinct temperatures i.e. 8K, 12K respectively.

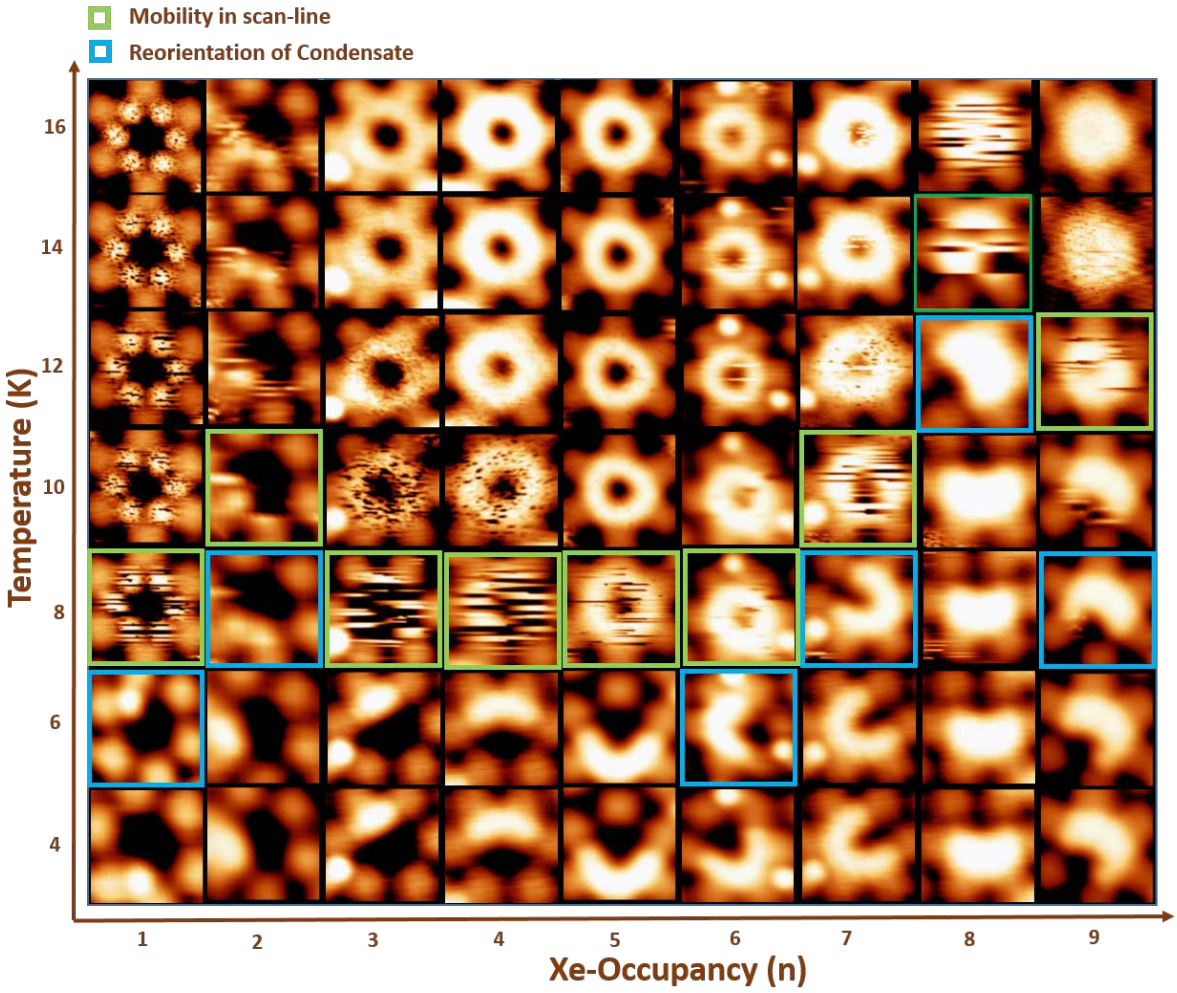


**Figure 2: Temperature dependent phase transition of Xe condensates in confinements with occupancies incremented in single Xe atom steps.** The horizontal axis denotes the Xe-occupancy of the pore; the vertical axis denotes the temperature which has been incremented by 2 K from row to row. All data have been recorded with the same imaging parameters to facilitate for the interpretation of the mobility patterns. The onset of mobility with increasing temperature is indicated by blue (green) outline, as specified in the legend. In the case of Xe re-arrangements per frame of 128 seconds (Xe re-arrangements per line ~ 500 msec). At 8 K the **occ-1—occ-6** become dynamic on the timescale of the experiment, **occ-7** at 10 K, **occ-9** at 12K while the temperature for the onset of diffusion dynamics is highest for **occ-8** at 14 K. See main text for further discussion (STM scanning parameters: V =1000 mV, $I_t$ =10 pA, 3 nm x 3 nm, scan speed 6 nm/sec)

The high melting temperature for **occ-8** indicates the higher stability of this cluster comprising two tetrameric subunits of sites which are in registry with the favoured adsorption site on the extended Cu(111) terrace. The stability of **occ-8** correlates well with its frequent occurrence

after deposition of Xe onto the hosting network[17]. Notably similar phase transitions have been observed in case of Kr condensates within Cu coordinated 3deh-DPDI pores, although transition temperatures are lower than in the Xe case (SI 3). This difference is consistent with the smaller radius and lower polarizability of the Kr electron shell according to vdW theory[27,28]. The Xe density distribution detected in STM is of toroidal or donut shape (Fig. 3). While the outer perimeter, bordering on the confining network wall, does not significantly change with increasing Xe population, the line profile (Fig. 3a) is progressively shifted to higher z-elevations and the center of the pore is gradually more occupied. This filling dependent asymmetry between the inner and outer perimeter of the Xe distribution in the pore reflects to the steeper repulsive potential at the outside of the Xe torus due to Pauli / Lennart Jones repulsion with the DPDI wall. The shallower, also repulsive interaction on the inside corresponds to the Xe repelling the cSS. With increased occupancy from 1 to 7, the cSS is also shifted towards the Fermi level while being increasingly localised along the z-axis[18,29] (see also the discussion of T-dependent line profile Fig. SI 6 and further below).

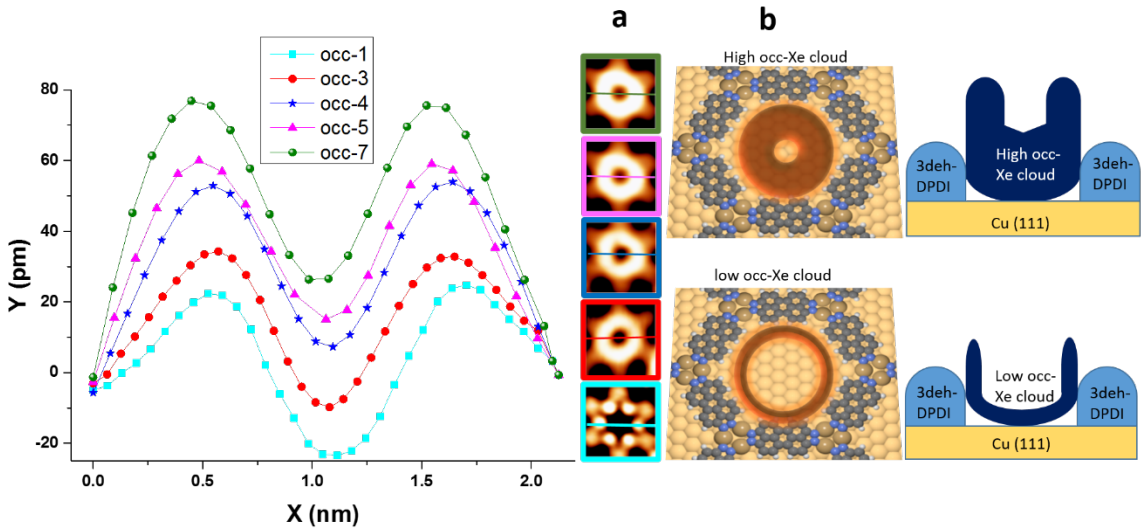


**Figure 3: Diagonal cross section profile analysis of the time-averaged mobility pattern of differently Xe populated confinements. (a)** Cross sections of **occ-1,3,4,5,7** have been extracted from the corresponding STM data taken at 16 K. At higher occupancy the center is becoming narrower and the rim of the ring is also progressively elevating. **Occ-7** exhibits a significantly narrower central hole width compared to **occ-1**. We attribute the significant difference to our observation that **occ-1** is in a lattice gas hopping mode between the 6 corner positions of the pore, while in all other cases (beyond occ-2, see SI 5-b) the diffusive motion also reaches other positions at the rim of the pore. With gradually increased population more and more incidents reach the pore center (see Fig. SI 5,6), thereby the time average of the Xe populated pore is characterized by a shallower inner center. **(b)** Representation of the structural position of ring of dynamic xenon atoms inside the surface pore.

In order to assess the temperature induced Xe hopping[30] in the time domain, the tip excursions at fixed positions of the STM tip have been analysed at different positions in the pore and at different temperatures, allowing the determination of the Arrhenius activation energy for the site exchange (Fig 4). The observed hopping rate of Xe in the confinements depends on the occupancy as well as the temperature. The activation energy for **occ-1** equals to 5.8 ± 0.05 meV and for **occ-3** is 6.9 ± 0.21 meV. For **occ-2** the determined activation energy is the lowest,

3.62 ± 0.61 meV, reflecting a low binding energy in agreement with its low frequency of occurrence in the statistical regime.[17] Notably, the Arrhenius plot presented for **occ-1** and **occ-3** describes a diffusive mode which involves individual Xe hopping processes distributed around the periphery while for **occ-2** the Xe atoms appear to remain condensed and do not fully spread along the whole periphery, possibly as a Xe-Xe dimer under the influence of a condensation energy. Furthermore, the STM fingerprint of the hopping signal and the width distribution of the tip excursions indicate that in case of threefold occupancy atoms diffuse in a more 'condensed' form, whereas at the high temperature limit the **occ-1** and **occ-3** cases are indistinguishable (see Fig 4 a,b & SI 4) indicating separate motion of individual atoms. For **occ > 3** and also above 10 K, the extraction of hopping rates is precluded due to the limited time resolution (~msec) of STM as the residence time gets too low for the detection electronics.

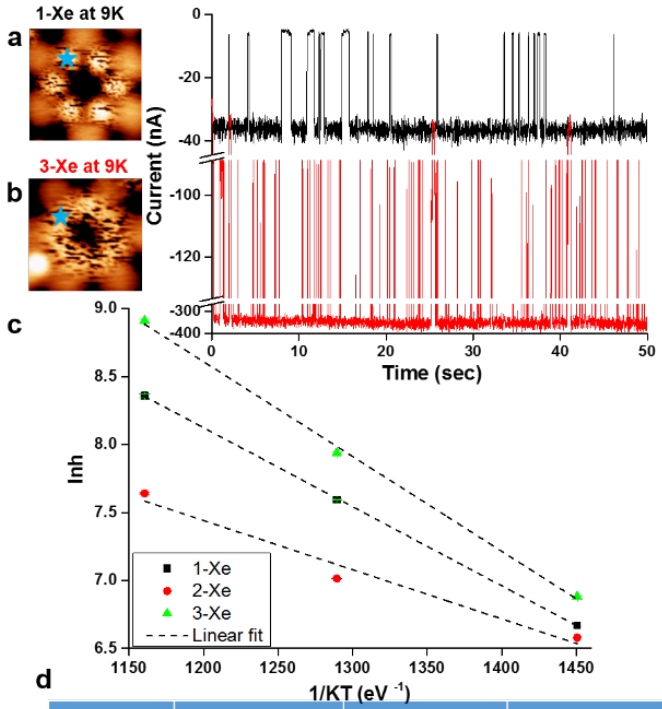


d

| Occupancy | 1-Xe | 2-Xe | 3-Xe |
|---|---|---|---|
| $E_a$ | 5.82 ± 0.05 meV | 3.62 ± 0.61 meV | 6.98 ± 0.21 meV |
| $h_o$ | 15.1 ± 0.06 | 11.7 ± 0.7 | 16.9 ± 0.3 |

**Figure 4: Temperature dependent hopping of Xe atoms inside the confinements. a, b)** Current versus time I(t) plot recorded at 8 K in the pore containing 1 and 3 Xe atoms respectively. The measurement has been performed at the tip position indicated by the blue star in the STM micrograph (inset). The spikes in the tunnelling current provide evidence for the presence of a Xe atom below. **c)** The **occ-1—occ-3** cases were investigated in the temperature range of 4 – 10 K. From these measurements hopping rates were extracted. For each Xe occupancy the data was fitted with the Arrhenius dependence in order to determine the activation energy as tabulated in **(d)**.

The thermally induced phase transitions inside the confinements motivated investigations towards the excitation of transitions by local stimuli. At 4K, 'High' (~ -3 V) sample bias voltage excursions with the STM tip above the center of a selected box were inter alia transforming statically adsorbed Xe atoms into a 'fluid' state. In reverse, sample bias voltage excursions of +5 V applied to a confined fluid phase induced phase transformations leading to condensation

of the mobile Xe inside the confinements (see Fig. 5). In both directions a reliability of ~75% for the state switching was found. The observation of the metastable fluid state at 5K is remarkable: The persistent delocalized mobility of Xe at close to 5K suggests that the Xe is mechanically and thermodynamically weakly interacting with the heat sink of the sample/cryostate. The dynamicity of Xe in the fluid persists in spite of the sample being held at close to 5K and suggests that the Xe is thermodynamically weakly coupled to the heat sink of the sample/cryostate. Notably the metastable state is occurring by the voltage stimulus as well spontaneously after Xe dosing and is consistently observed in the analysis of tip-excursion statistics, and of static images as well as time-lapse sequences taken by STM.

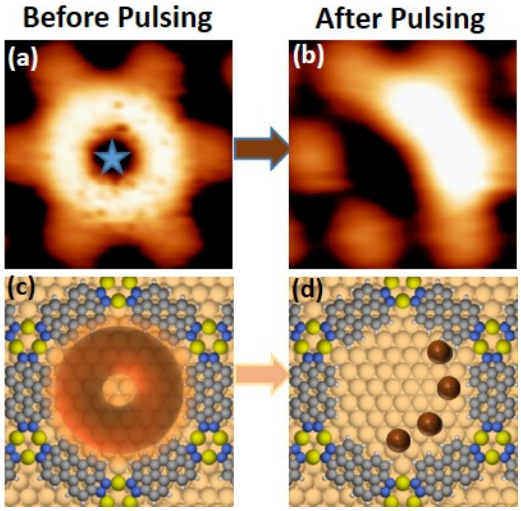


**Figure 5: STM bias voltage induced phase transition in confinements. a)** STM micrographs of confinement containing 4 Xe atoms measured in constant height mode before and after **(b)** a voltage ramp has been provided with a holding time of 300 – 2000 msec. Upon applying a voltage ramp with a peak voltage of +5 V to the sample, **(a)** the initially mobile **occ-4** is forced to condense **(b)**. The blue asterisk indicates the position of STM tip upon applying the voltage ramp. In the second row, corresponding atomic models have been provided **(c, d)**. (STM images size 3 nm x 3 nm, tunnelling parameters: I = 10pA, V = 1V, scan speed = 6 nm / sec, time scan = 128 sec; STM pulse parameters tunnelling current = 10pA, bias voltage = 1000 mV, Voltage ramp +5 V, pulse width = 2 sec).

The system at hand is remarkable in several aspects: It provides a case of "small system thermodynamics"[12], in that it comprises a finite number of components and is of a size comparable to the range of forces between its constituents. The inequivalence of the Xe adsorption sites in a specific pore occupied with a certain number of Xe atoms is the result of the geometrical preferences of the planar Xe (Van der Waals) clustering (such as the diamond-shaped Xexenon tetramers) as well as the repulsive interaction between Xe and the lobe shaped cSS in each pore. The former depends on the dispersive interactions of Xe with its nearest neighbours, and the interaction with the confining barrier of the coordination network. On the other hand, the interaction with the cSS is reduced as the latter is successively pushed towards the Fermi level with increasing Xe population in the pore(**occ(n)**)[18]. The adsorption of Xe with the underlying Cu substrate is thus governed by dispersion forces type while the repulsive Pauli-type interactions between the Xe and the cSS state depend on the specific profile of the

electronic state(s) in the confinement.
This combination of attractive and repulsive interactions is also reflected in the trend of Xe to occupy 'non-registry' positions different from the 'on-top' sites which are favoured for extended Xe layers on Cu(111). At low occ(n), with greater repulsion between the Xe and the cSS, occupation of a certain number of non-registry sites is prevalent which may also explain the spontaneously occurring 'fluid' states. On the other hand, for **occ(7)** and above a rather systematic filling pattern is observed with only one non-registry case i.e. the ninth Xe in occ(9) which escapes isolation next to the two registry-compliant tetramers. The cSS with its centrally located maximum gives rise to the donut-shaped spatial Xe distribution in the confining pore discussed above. This together with the 'soft' response of the inner perimeter of the "donut" with increased T and **occ(n)** (Fig. 3, SI 6) completes this picture.
With regard to the physics involved in the 'small system thermodynamics' at hand it is important to discuss the most likely macroscopic case: this derives from the picture of 'lattice gas' diffusion of adsorbates on surfaces where adsorption energies are generally higher by at least an order of magnitude than the barrier for diffusion[19,29,31,32]. The diffusion in these systems is characterized by 'lattice gas' motion i.e. by their temperature-induced ($\sim k_B T$) hopping between different quasi stable adsorption positions given by the lattice of surface Cu atoms in our case. We have shown two effects: (1) the behaviour of the system at slow variation of temperature (which reflects expected macroscopic behaviour) as well as (2) the non-thermally equilibrated 'slow motion/slow relaxation' of the observed 'metastable' states occurring spontaneously by Xe deposition and accordingly after Xe clusters have been excited by a voltage ramp. We tentatively assign these 'excited' systems to Xe atoms suspended by repulsion with the cSS and thus interact weakly with the hosting pore and substrate. Such a scenario goes beyond the lattice gas picture which is characterized by a considerable residence time in comparison to the lateral hopping. Force measurements[28] of the Xe in different excited states and at different positions may provide deeper insight in future studies.
In conclusion, we have shown that the thermal activation of the phase transitions of discrete Xe condensates in the confinements between their (static) condensed state and a mobile fluid can be initiated by variation/increase of the temperature and depends on the Xe occupancy of the confinements. This behaviour is reminiscent of earlier adatom and vacancy island diffusion studies[31]. The observed dependence upon the occupancy is a characteristic for discrete condensation nuclei undergoing complex interactions. This is also evidenced by the observation that energetically privileged ('magic') arrangements can be found and extra Xe atoms start diffusing at lower activation energy than their clustered neighbours even within the same confinement (see Fig. 2_occ-9, S2_occ-7b). We have also demonstrated that excursions in the local electric field applied at the position of the confinements provide a (non-thermal!) local, external stimulus[33]. To what extent the complexity of the present 'small system' is governed by the complex quantum mechanical interaction with and within the pores is an interesting topic for future experimental and theoretical investigations. The possibility to actively switch between mobile and static states for confined ensembles of xenon atoms may provide a means for reversible two-dimensional patterning which underlies the development of data storage systems on the level of single atoms.

## References


1. Transitions in focus. *Nat. Phys.* **4,** 157–157 (2008).
2. Wuttig, M. & Yamada, N. Phase-change materials for rewriteable data storage. *Nat. Mater.* **6,** 824–832 (2007).
3. Giusca, C. E. *et al.* Confined Crystals of the Smallest Phase-Change Material. *Nano Lett.* **13,** 4020–4027 (2013).
4. Torchet, G., Farges, J., Feraudy, M. F. & Raoult, B. Structural transition in SF6 clusters. *Z. F*[illegible]*r Phys. At. Mol. Clust.* **12,** 93–96 (1989).
5. Farges, J., de Feraudy, M. F., Raoult, B. & Torchet, G. Structure and temperature of rare gas clusters in a supersonic expansion. *Surf. Sci.* **106,** 95–100 (1981).
6. Lee, J. W. & Stein, G. D. Electron diffraction experiments on argon clusters nucleated in helium using Laval nozzle beams. *Surf. Sci.* **156,** 112–120 (1985).
7. Dong, Q. *et al.* A Polyferroplatinyne Precursor for the Rapid Fabrication of $L1_0$ -FePt-type Bit Patterned Media by Nanoimprint Lithography. *Adv. Mater.* **24,** 1034–1040 (2012).
8. Yang, X., Wan, L., Xiao, S., Xu, Y. & Weller, D. K. Directed Block Copolymer Assembly *versus* Electron Beam Lithography for Bit-Patterned Media with Areal Density of 1 Terabit/inch $^2$ and Beyond. *ACS Nano* **3,** 1844–1858 (2009).
9. Müller, K., Enache, M. & Stöhr, M. Confinement properties of 2D porous molecular networks on metal surfaces. *J. Phys. Condens. Matter* **28,** 153003 (2016).
10. Frenken, J. W. M. & Veen, J. F. van der. Observation of Surface Melting. *Phys. Rev. Lett.* **54,** 134–137 (1985).
11. Feenstra, R. M., Slavin, A. J., Held, G. A. & Lutz, M. A. Surface diffusion and phase transition on the Ge(111) surface studied by scanning tunneling microscopy. *Phys. Rev. Lett.* **66,** 3257–3260 (1991).
12. Gross, D. H. E. *Microcanonical thermodynamics: phase transitions in 'small' systems*. (World Scientific, 2001).
13. Klein, J. & Kumacheva, E. Confinement-Induced Phase Transitions in Simple Liquids. *Science* **269,** 816–819 (1995).
14. Alba-Simionesco, C. *et al.* Effects of confinement on freezing and melting. *J. Phys. Condens. Matter* **18,** R15–R68 (2006).
15. Matena, M. *et al.* On-surface synthesis of a two-dimensional porous coordination network: Unraveling adsorbate interactions. *Phys. Rev. B* **90,** (2014).

16. Lobo-Checa, J. *et al.* Band Formation from Coupled Quantum Dots Formed by a Nanoporous Network on a Copper Surface. *Science* **325,** 300–303 (2009).
17. Nowakowska, S. *et al.* Interplay of weak interactions in the atom-by-atom condensation of xenon within quantum boxes. *Nat. Commun.* **6,** 6071 (2015).
18. Nowakowska, S. *et al.* Configuring Electronic States in an Atomically Precise Array of Quantum Boxes. *Small* (2016). doi:10.1002/smll.201600915
19. Berner, S. *et al.* Adsorption and two-dimensional phases of a large polar molecule: Sub-phthalocyanine on Ag(111). *Phys. Rev. B* **68,** (2003).
20. Schmidt, M. & Haberland, H. Phase transitions in clusters. *Comptes Rendus Phys.* **3,** 327–340 (2002).
21. Kellogg, G. L. Atomic view of cluster diffusion on metal surfaces. *Prog. Surf. Sci.* **53,** 217–223 (1996).
22. Levitas, V. I. & Samani, K. Size and mechanics effects in surface-induced melting of nanoparticles. *Nat. Commun.* **2,** (2011).
23. *HANDBOOK OF NANOPHYSICS: clusters and fullerenes.* (CRC PRESS, 2017).
24. Echt, O., Sattler, K. & Recknagel, E. Magic Numbers for Sphere Packings: Experimental Verification in Free Xenon Clusters. *Phys. Rev. Lett.* **47,** 1121–1124 (1981).
25. Widmer, R., Passerone, D., Mattle, T., Sachdev, H. & Gröning, O. Probing the selectivity of a nanostructured surface by xenon adsorption. *Nanoscale* **2,** 502 (2010).
26. Dil, H. *et al.* Surface Trapping of Atoms and Molecules with Dipole Rings. *Science* **319,** 1824–1826 (2008).
27. Hamaker, H. C. The London—van der Waals attraction between spherical particles. *Physica* **4,** 1058–1072 (1937).
28. Kawai, S. *et al.* Van der Waals interactions and the limits of isolated atom models at interfaces. *Nat. Commun.* **7,** 11559 (2016).
29. Forster, F., Hüfner, S. & Reinert, F. Rare Gases on Noble-Metal Surfaces: An Angle-Resolved Photoemission Study with High Energy Resolution †. *J. Phys. Chem. B* **108,** 14692–14698 (2004).
30. Yitamben, E. N. *et al.* Tracking Amino Acids in Chiral Quantum Corrals. *J. Phys. Chem. C* **117,** 11757–11763 (2013).
31. *Surface science: an introduction.* (Springer, 2003).
32. Silvestrelli, P. L., Ambrosetti, A., Grubisiĉ, S. & Ancilotto, F. Adsorption of rare-gas atoms on Cu(111) and Pb(111) surfaces by van der Waals corrected density functional theory. *Phys. Rev. B* **85,** (2012).
33. Wortmann, B. *et al.* Reversible 2D Phase Transition Driven By an Electric Field: Visualization and Control

on the Atomic Scale. *Nano Lett.* **16,** 528–533 (2016).

**Acknowledment**
The work was supported by the Physics Department of the University of Basel, Swiss Nanoscience Institute, the Swiss National Science Foundation (Grant: 200020_162512, 206021_144991, 206021_121461), the Swiss Commission for Technology and Innovation (CTI, 16465.1 PFNM-NM) and the Swiss Commission for Swiss Government Excellence Scholarship Program for Foreign Scholars (2013.0492). M. Martina and M. Senn provided valuable technical assistance. We sincerely thank to Shigeki Kawai and Robert Skonieczny for support during the measurements.

**Author contributions**
A.A., S.F.M., T.N., S.N., O.P., and A.W., led the STM measurements and examined the data under the supervision of T.A.J., and L.H.G. A.A., T.A.J. and L.H.G. wrote the manuscript.
**Additional Information:** Supplementary information of this article accompanies in a separate file.
**Competing financial interest:** The authors found no competing interests.

# SUPPORTING INFORMATION

## "Phase transitions" in quantum confinements: inducing mobility of Xenon atoms in a porous surface network

**Contents**



### 1. Methods

**Sample preparation and STM measurement:**
The samples are prepared and examined in an ultrahigh vacuum (UHV) system with a base pressure of 6 x $10^{-10}$ mbar. The Cu(111) crystal (MaTecK GmbH) is prepared by rounds of $Ar^+$ sputtering with E = 1 keV performed at room temperature followed by annealing at 480 $^oC$. The DPDI molecules are deposited with the use of nine-cell commercial evaporator (Kentax, GmbH, Germany) on the Cu(111) by sublimation at ~240 $^oC$ and the rate is controlled before deposition by a quartz crystal microbalance (QCMB). After deposition, the sample is annealed to 300 $^oC$ in order to convert DPDI into 3deh-DPDI, which crafts the Cu-coordinated network[15]. Xe of purity 99.99% is dosed to the sample placed in the STM (Omicron Nanotechnology GmbH) operated at 4.2 K, with the cryoshields open and the leak valve opening on the vacuum side being in a straight line with the sample. SI-1_a presents STM data acquired after exposure of the Cu-coordinated 3deh-DPDI network to 120 L of Xe. The

exposure has been performed at a pressure of 1.3 x $10^{-7}$ mbar for 1,200 s causing the increase in the sample temperature to 9 K. Xe is found to be adsorbed in the pores as well as in the nodes of the network[17]. After Xe exposure the cryo-shields are closed, the sample temperature re-equilibrates to the temperature in the He cryostat (~4.2K). Using a temperature controller [LakeShore-331] set to a heating rate of 0.2 K/min, STM experiments are performed at step by step increased sample temperatures. At each required temperature by switching off the temperature ramping.

STM measurements have been performed in the constant current mode with Pt–Ir tips (90% Pt, 10% Ir), prepared by mechanical cutting followed by sputtering and controlled indentation in the bare Cu(111) surface. The STM images shown in Figure 1—5, SI 1—6 have been acquired with such prepared metallic tip. To avoid modification of the condensates by interaction with the tip, a sample bias of 1V has been selected whereas the tunnelling current has been set to 10 pA. To further assess the dynamics within the confinements, the STM tip has been used as a fixed probe at certain positions (center and periphery) of the pores to measure the tunnelling current fluctuations which are caused by the presence or absence of Xe, which is dependent on the diffusive motion of the Xe in the pore. These tip excursion plots have been used to prepare the Arrhenius plot with sample bias = 2 volts, set current = 60pA, sweep time = 102 s and an initial setting time of 5 msec.

In the STM voltage ramp induced Xe condensates dynamics, the STM tip has been used as an actuator, exerting a field/current at middle of the DPDI pore. Here tunnelling parameters during the ramping sequence correspond to the typical STM imaging conditions i.e. I = 10pA, V = 1000 mV, Voltage ramp +5 V, width of the ramp = 2 sec) and normal scanning parameters are I = 10pA, V = 1V, scan speed = 6 nm / sec, time scan = 128 sec.

## 2. Overview image of Xe populated confinements

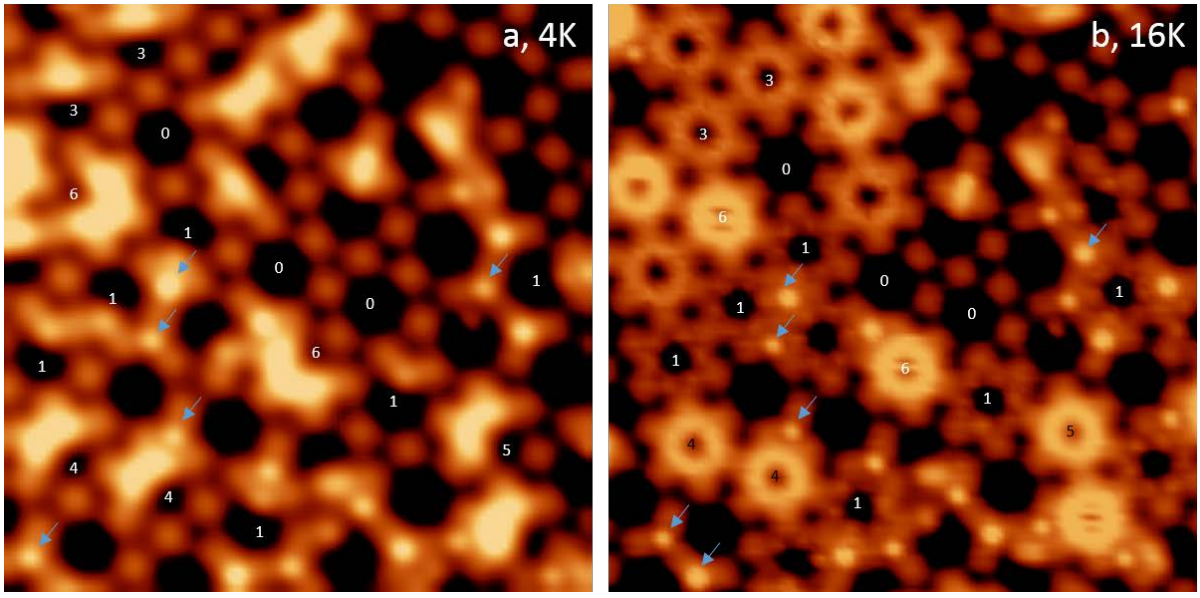


**Figure SI 1: Overview image of Xe populated confinements at 4K and 16K (a)** Overview image acquired at 4K and **(b)** at 16K. **(a)** All depicted Xe are in their frozen state; the numbers indicate the Xe occupancy in the individual pores. **(b)** All Xe adsorbed in one or the other confinement is in the hopping diffusion or fluid state; the numbers indicate the Xe occupancy in the individual pores as determined

from a previously acquired image taken at 4K. This assignment is validated by observations that below 18K there are no exchange processes between the pores and the decorated coordination nodes where ad-Xe remains static at 16K. (indicated by arrows). Scanning parameters: STM image 15 nm x 15 nm, tunnelling current 10 pA, bias voltage 1000 mV.

### 3. Phase transition of occ-7b, occ-9 in confinements

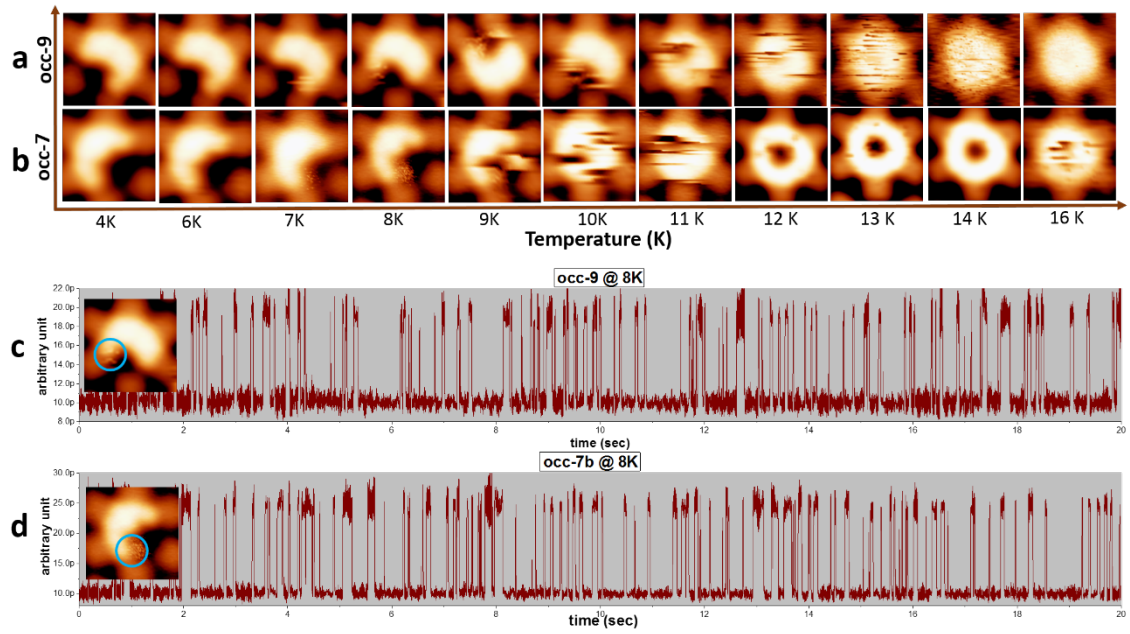


**Figure SI 2: Temperature dependent phase transition of occ-7b, occ-9 Xe in confinement. a)** array of STM images taken of a single pore occupied with 9 Xe atoms i.e. **occ-9** Xe at 1K increment between 4K and 16K. Note that the single Xe atom which initiates diffusion at 7K, 2K below the temperature facilitates the collective reorientation of the whole condensate already as low as at 9K. **b)** occ-7b case, note that the single Xe atom, located at a lower coordination site starts hopping at 7K. This is before the 6 Xe atoms start to move which are more stably adsorbed in a tetramer pattern ('magic island'In both cases, the Xe atom which initiates the hopping process is located at off-registry positions on the Cu(111) substrate[17]. **c)** and **d)** The STM tip excursions perpendicular to the substrate as they are caused by the Xe atoms hopping in and out of the non-registry positions for **occ-7b** and for **occ-9** recorded at 8K. The blue circle indicates the position of the STM tip during the experiments.

## 4. Phase transition of Kr in confinements

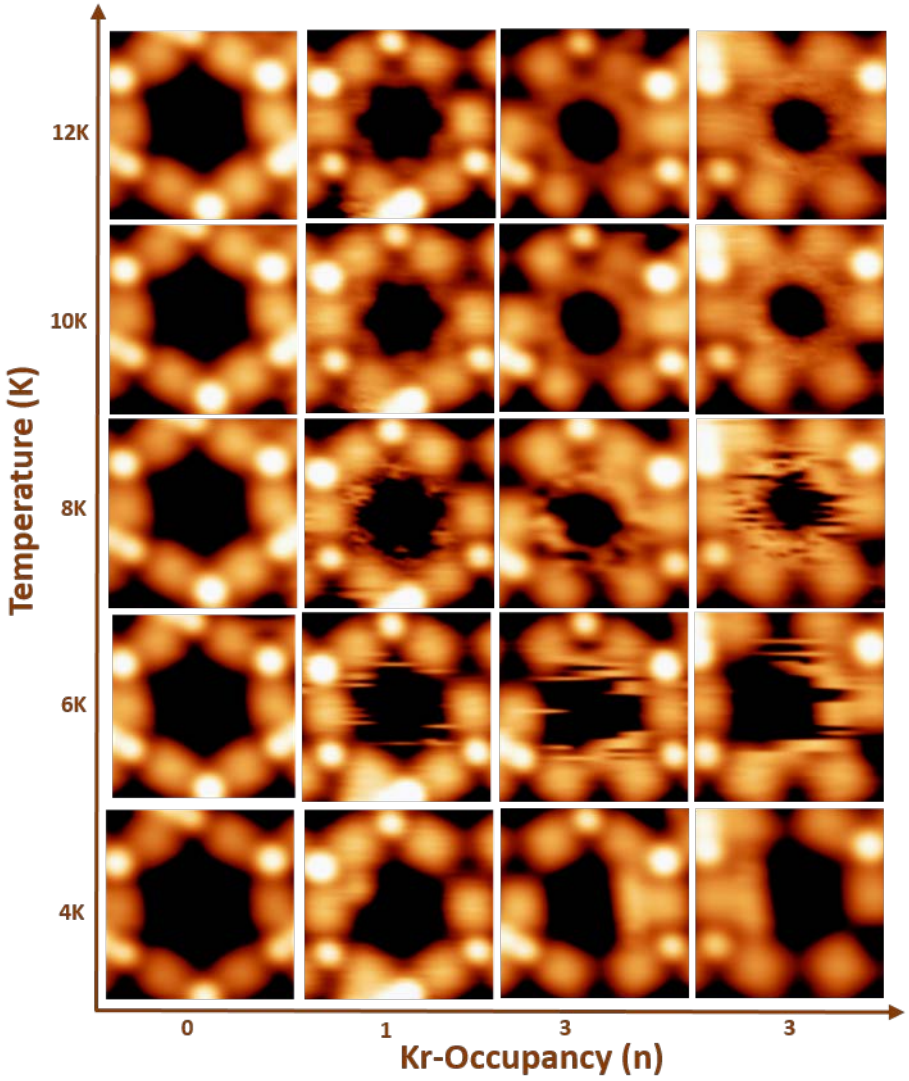


**Figure SI 3: Atom by atom temperature dependent phase transition of Kr in confinements.** The horizontal axis denotes the Kr-occupancy of the pore; the vertical axis denotes the temperature which has been incremented by 2 K from row to row. All data have been recorded with the same imaging parameters to facilitate for the interpretation of the mobility patterns. The onset of mobility with rise of temperature in the case of Kr re-arrangements per frame of 128 seconds (Kr re-arrangements per line ~499 seconds). The phase transition behaviour of Kr inside confinements is similar to the behaviour of Xe in the confinements. At 6 K the **occ-1, occ-3** become dynamic on the timescale of the experiment. (STM scanning parameters: V=1000 mV, I=10 pA, Scan speed 9.8 nm/sec, 2.6 x 2.3 $nm^2$)

## 5. Different modes of hopping

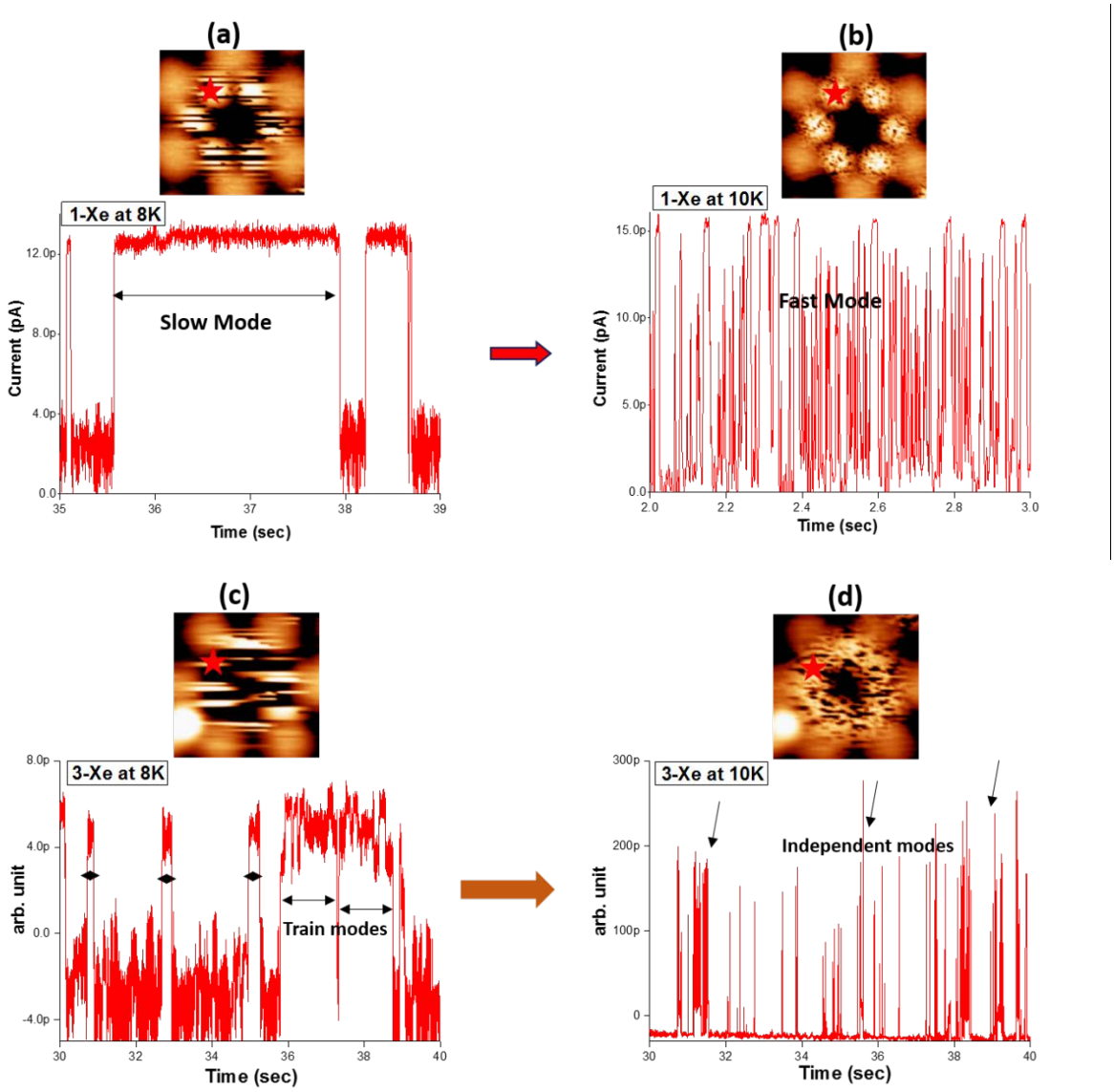


**Figure SI 4: Different time structure of 1-Xe and 3-Xe hopping in confinement:** (a) Shows slow (~2 sec) mode at 8K while (b) shows the much faster (~50 msec) hopping at 10K between the corner positions of one confinement box. (c) Shows slow train mode hopping of the surface at 8K of **occ-3** while (d) shows fast individual hoping of xenon atoms in **occ-3.**

## 6. Hopping in center and periphery of pore

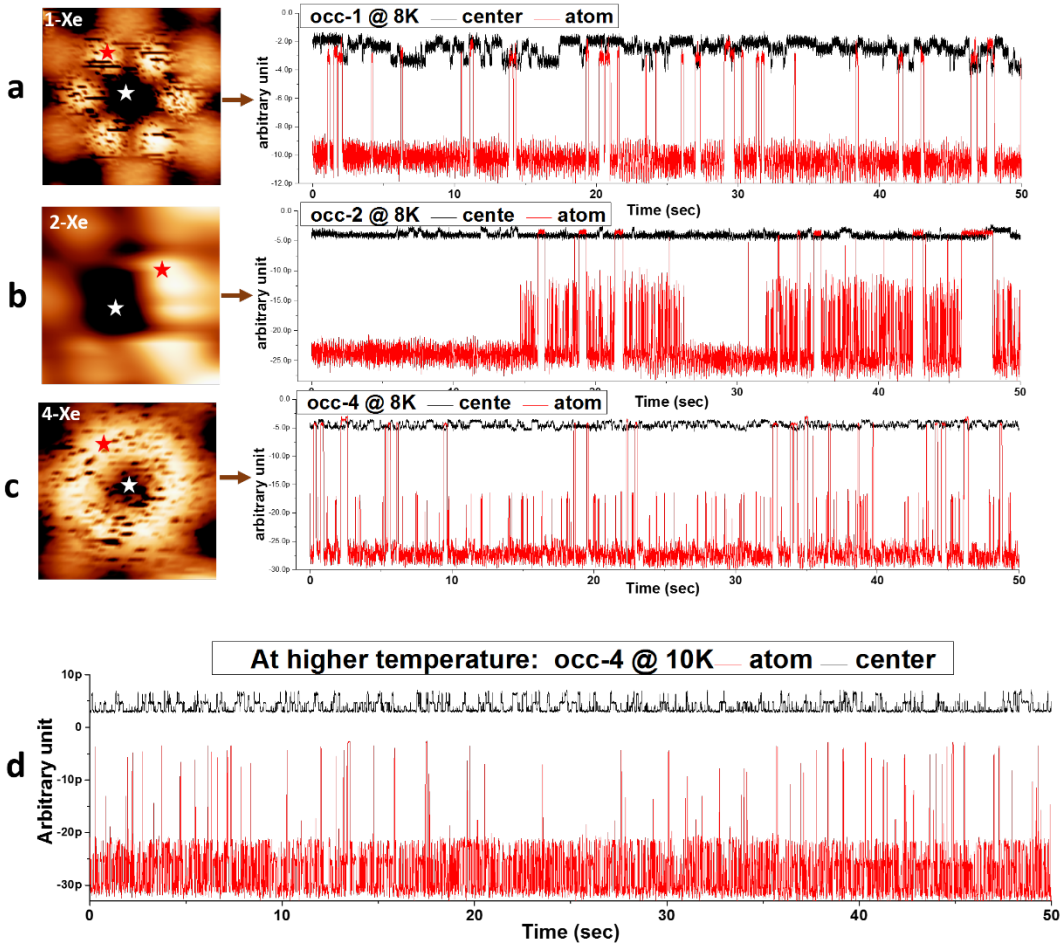


**Figure SI 5: Comparison of Xe diffusion between corner position and center position for 1-Xe, 2-Xe and 4-Xe in confinement.** The red asterisk indicates the tip position at the corner of the confinement where the I(t) trace in red has been sampled. The white asterisk indicates the center position where the trace in black has been sampled. Note that the top and bottom plots have been taken at different times and cannot be correlated. **(a)** 1-Xe hopping in confinement at 8K **(b)** 2-Xe hopping in confinement at 8K. It is a reproducible characteristic of all 2-Xe that they remain confined to a single corner up to about 10K. We attribute this with their condensation energy and with the presence of the quantum well state which is comparably less disturbed at low Xe occupancy of the pores. **(c)** 4-Xe hopping in confinement at 8K. **(d)** 4-Xe hopping in confinement box at 10K, with increasing temperature in comparison to (c) and higher occupancy, Xe is more frequently present in the centre, either as the thermal energy is then sufficient to overcome the repulsive interaction with the quantum well state or (also) as the latter fluctuates more at this temperature.

## 7. Diagonal profile analysis of occ-7 with increment of temperature

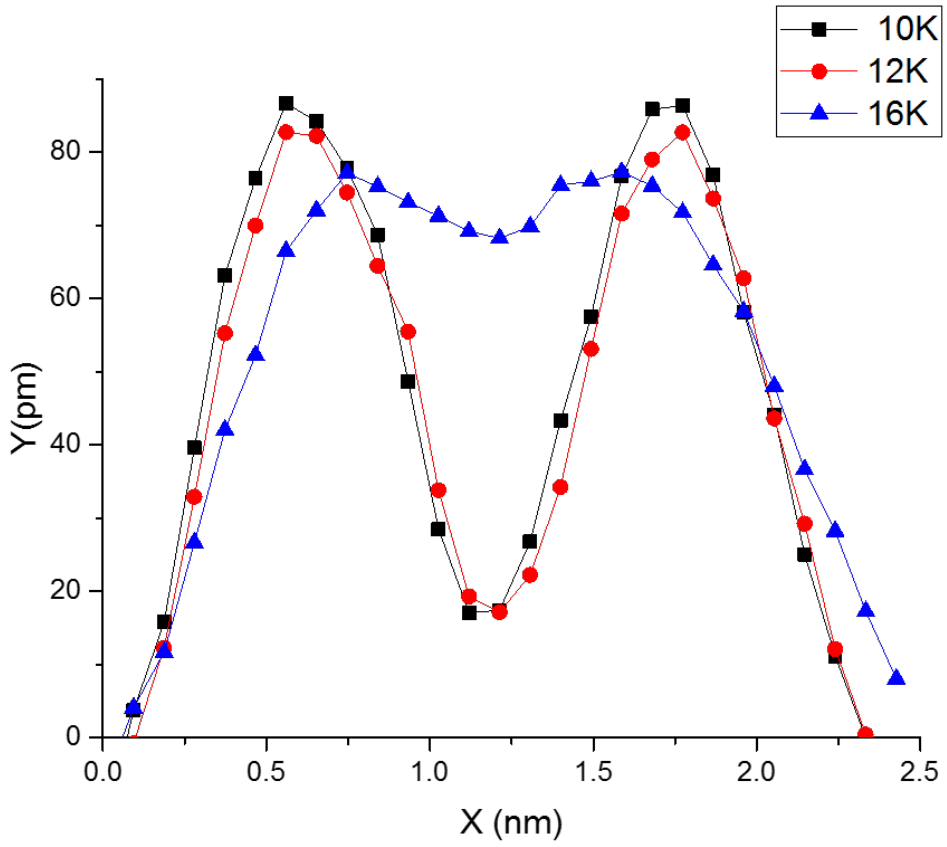


**Figure SI 6: Diagonal cross section profile analysis of the time-averaged mobility pattern of occ-7 Xe populated confinement with increment of temperature.** (black) Cross sections of **occ-7** has been extracted from the corresponding STM data taken at 10 K (red) at 12K and at 16K (blue). At the higher temperature, 16K, the center is becoming narrower and the rim of the ring is also progressively depressing, which indicates the diffusive motion reaches other positions at the rim of the pore. By the gradual increase of temperature more and more incidents reach the pore center. Thus, the time average of the Xe populated pore is characterized by a less shallow in inner center.

# Chapter [[2]] and Supplementary Information

| | |
|---|---|
| [[2]] | **Kinetically controlled activation of diffusion pathways of Xe condensates in a surface metal organic network** |
| | Aisha Ahsan, S. Fatemeh Mousavi, T. Nijs, S.Nowakowska, Olha Popova, A. Wäckerlin, T. Nijs, J. Björk, L. H. Gade, T. A. Jung, manuscript submitted to ***small*** journal. |
| | Contribution of A. Ahsan: carried out experimental investigations (STM), analysed and interpreted the data, wrote the manuscript. |

# Kinetically controlled activation of diffusion pathways of Xe condensates in a surface metal organic network

Aisha Ahsan[a], S. Fatemeh Mousavi[a], Thomas Nijs[a], Sylwia Nowakowska[a], Olha Popova[a], Aneliia Wäckerlin[a], Jonas Björk[c], Lutz H. Gade[d], Thomas A. Jung[a,e]

[a]Department of Physics, University of Basel, 4056 Basel, Switzerland.
[b]Nanoscale Materials Science, Empa, Swiss Federal Laboratories for Materials Science and Technology, 8600 Dübendorf, Switzerland.
[c]Department of Physics, Chemistry and Biology, IFM, Linköping University, Linköping 581 83, Sweden.
[d]Anorganisch-Chemisches Institut, Universität Heidelberg, Im Neuenheimer Feld 270, 69120 Heidelberg, Germany.
[e]Laboratory for Micro- and Nanotechnology, Paul Scherrer Institut, 5232 Villigen PSI, Switzerland.

## ABSTRACT:

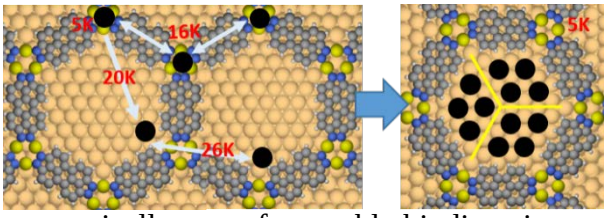


The temperature activated diffusion of Xe between different compartments of an on-surface metal organic coordination network has been monitored. Xe atoms adsorbed at lower energy sites become mobile with increased temperature and gradually populate energetically more favourable binding sites or remain in a delocalized 'fluid' form confined to diffusion along a topological subset of the on-surface network. These diffusion pathways can be studied individually under kinetic control via the chosen thermal energy kT of the sample and are determined by the network and sample architecture. The spatial distribution of Xe in its different modes of mobility and the time scales of the motion is revealed by Scanning Tunneling Microscopy (STM) at variable temperatures up to 40K and subsequent cooling to 4K. The system provides insight into the diffusion of a van der Waals gas on a complex structured surface and its nucleation and coarsening / growth into larger condensates at elevated temperature under thermodynamic conditions.

## INTRODUCTION:

Thermally activated Brownian motion and, in the presence of concentration gradients, diffusion[1] has been widely studied at the ensemble level, but remains difficult to trace at the level of atoms and molecules. This applies particularly to the motion of molecules across non-uniform sample architectures. With the recent advancement of microscopic techniques, it has become possible to observe and investigate diffusion processes on the atomic scale [2–13]. The thermodynamic and kinetic evolution of different atomic sites, such as steps[14,15], kinks, adatoms and (vacancy) islands affect, inter alia, the formation of surface reconstructions[16], the evolution of growth processes[17–19] and surface chemical conversions[20]. Most of the systems investigated have been composed of only a few atomic species – mostly metals – for which diffusion processes in the surface plane were found to lead to coarsening phenomena: Characteristic features (such as "sticky" atomic sites or smaller on-surface islands or vacancy islands), representing local minima of the energy landscape, tend to disappear and to evolve into energetically more favoured features[21–26]. Most of what is known about the surface dynamics of complex structured systems has been deduced from studies of simpler cases[27] rather than by direct probing.

The emergence of on-surface chemistry[28,29] has considerably broadened the basis for the generation of complex and atomically precise functional sample architectures without the need to control top-down processes. The investigation of rare gases on structured surfaces[28,29] can serve as a model to understand the diffusion processes of small molecules in the presence of traps (attractive sites) or antitraps (repulsive sites) [30,31]. For example, the diffusion of ad-atoms on surfaces is strongly modified by the presence of such traps and this is even more pronounced for porous on-surface networks[32,33]. The cavities of the pores may provide attractive sites for the adsorption of guest molecules by non-directional, weak (e.g. van der Waals) interactions. In other cases, the pores interact with the surface electrons in the underlying substrate and form quantum well states[34][-] which display repulsive interactions with Xe atoms. It has been found that such local interactions can be overcome upon increasing the number of Xe atoms available for in-pore adsorption [35] and at higher (> 40K) temperatures.

Here we provide an account of the temperature dependent equilibration of ad-Xe diffusing between different sites and compartments in, on and near a two-dimensional metal organic coordination network (MON) as well as the atomically clean Cu(111) substrate. The network gives rise to a multitude of different compartments (traps) which can host Xe atoms. It also mediates the exchange of Xe between neighbouring sites/compartments. We report how experimentally observed diffusion pathways change with increasing temperature, how they may be addressed under "kinetic control", i.e. by addressing their characteristiv threshold energies, and how the diffusing Xe atoms nucleate to clusters within the pores under "thermodynamic control" at elevated temperature which allows the access to all the exchenge pathways.

**RESULTS AND DISCUSSION**

A Cu-coordinated porous surface network with pore size of 1.4 nm was formed on an atomically clean Cu(111) surface by temperature induced reactive dehydrogenation of 4,9-diaminoperylene quinone-3,10-diimine (DPDI) at ~300 $^{o}$C to the triply dehydrogenated '3deh-DPDI' form and the coordination of the latter to thermally emitted Cu adatoms.[32] Xenon was chosen as the test adsorbate both due to its size and the minimal directionality of the van der Waals interaction characteristic of a noble gas.

**1. Equilibration of the distribution of Xe atoms across the structured surface: High initial pore occupancies act as attractors at the expense of low occupancies**

To study the thermodynamic re-equilibration occurring with increased temperature, a random population of Xe was generated by 180 L exposure of Xe to the on-surface network held at >6 Kelvin (K). Figure 1(**a**) displays the random absorption of Xe on the nodes and in differently occupied pores. After annealing up to 40 K for 30 minutes and after cooling down to 5K most of the pores were filled to their maximum occupancy (12) of guest atoms [Figure 1(**b**)] while others were completely empty. It is worth to note that a substantial share of the Xe atoms filling the pores was initially captured on the network-free substrate surface, and then relocated into the pores by the temperature increase. The data thus indicate that the 12-fold occupied pore is the *energetically* most favoured state which is attained under conditions which would *entropically* favour a more uniform distribution between the different adsorption sites on the uncovered metal substrate, the network structure and the pores within it. This evolution is represented in Figure 1(c) which provides a histogram plot of the transition of the Xe

distribution in the pores by the annealing process. A number of barriers have to be overcome to reach this fully equilibrated state and thus thermodynamically controlled distribution of the adsorbate on the structured surface. To trace the individual atomic motions and their thermal regimes a variable temperature STM study was carried out (vide infra). This was also aimed at providing insight into the observed dehomogenization (coarsening) of the pore occupancy and the criteria for partially filled pores acting as attractors for further xenon atoms, while others, in contrast, appear to be depleted upon annealing. As will be discussed below, this behaviour may be traced in part to the specific electronic interaction of the metal-organic network and the underlying metal surface.

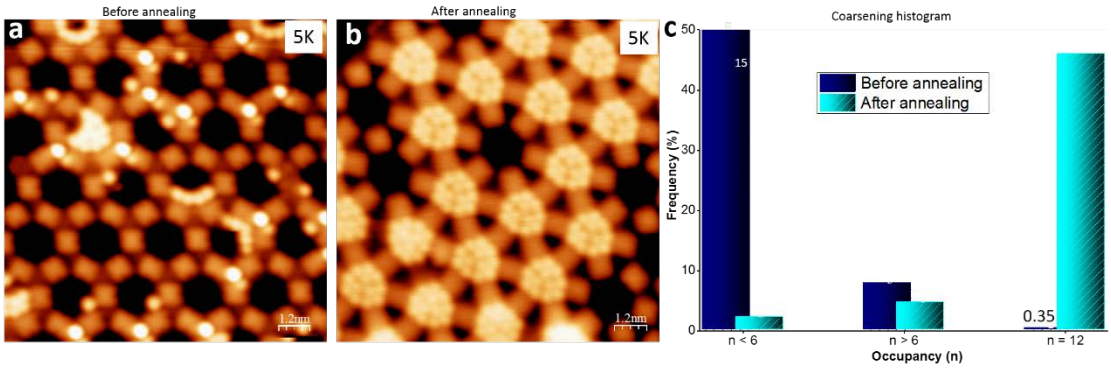


**Figure 1. Coarsening of Xe atoms inside nano-sized cavities of MONs.** *(a)* STM micrograph of a DPDI network on Cu(111) exposed to Xe gas (180 L) at 9K results in the adsorption of Xe atoms on nodes, in pores and in 2D periodic ad-Xe islands nucleating at the border of the porous network *(b)* after annealing the sample at 40K for 30 minutes and then cooling down to 5K a maximum number of pores are filled to their maximal i.e. 12-fold degree. STM acquisition parameters (V=1000 mV, I=10 pA, image size 12nm x 12nm), data taken at 5K. *(c)* In a histogram representation, the coarsening of the average island size upon annealing is clearly identifiable. Pores with occupancies lower than 6 were depleted while higher occupancy pores filled up to 12 fold occupancy in progress of the coarsening phenomenon.

## 2. The kinetically controlled motion of Xe atoms in and across the surface network: Identification of thermal motion regimes by variable temperature STM

In the temperature dependent diffusion studies, the individual experiment was started at the equilibrated initial temperature, and the sample was then resistively heated to a maximum temperature of 40 K by using a temperature controller at a rate of 1 K/min. STM micrographs and position dependent tip excursion statistics were acquired at different selected temperatures. After the initial decoration of the porous network with Xe we observed three stable adsorption sites; the nodes of the honeycomb network, the pores and near-network-on-terrace adsorption. The nodal site was found to be mostly singly occupied, while the occupancies within the pores after initial deposition followed a particular distribution of occupancies between 0 and 12[35].
The different mobility patterns observed in the present study are illustrated schematically in the top left section of Figure 2: As a guide to the eye, green arrows and an alphabetic red letter code for the observed thermal activation of each path have been added (a—g). The initial condensates are static (a_static); at temperatures above 8K diffusional exchange processes

inside some of the pores start (b_8K); at 16K diffusional exchange between the nodes of the coordination network is activated (c_16K); at 20K Xe moves from the node sites of the network into the pores (d_20K); at 26K the coarsening of the condensates from less filled (n<6) to highly filled (n>6) pores starts (e_26K); at 30K Xe is diffusing in a single line along the edges (boundaries) of the network (f_30K); at 35 K the Xe atoms initially adsorbed in near network islands on the bare Cu surface start moving all across the network and lead to complete filling of the partially filled (n>6) pores to fully filled 12-Xe (g_35K). At this point, equilibration between all locations for the xenon atoms on the outside and within the network sets in. This results in the redistribution of the Xe: some of the network pores are filled to the maximum of 12-fold occupiancy while the neighbouring lower occupancy pores are emptied as shown in Figure 1.

The thermal activation of the different equilibration pathways between the different minimal energy sites gives rise to the interesting global transition mentioned above: The 12-fold, fully filled pore which provides one of many possible configurations under the kinetic constraints of the Xe dosing becomes the dominant, saturated configuration. The threshold temperatures T* corresponding to the described modes of diffusion ***(a—g)*** gradually increase from 5 K to 35 K. ( Figure 1 ).

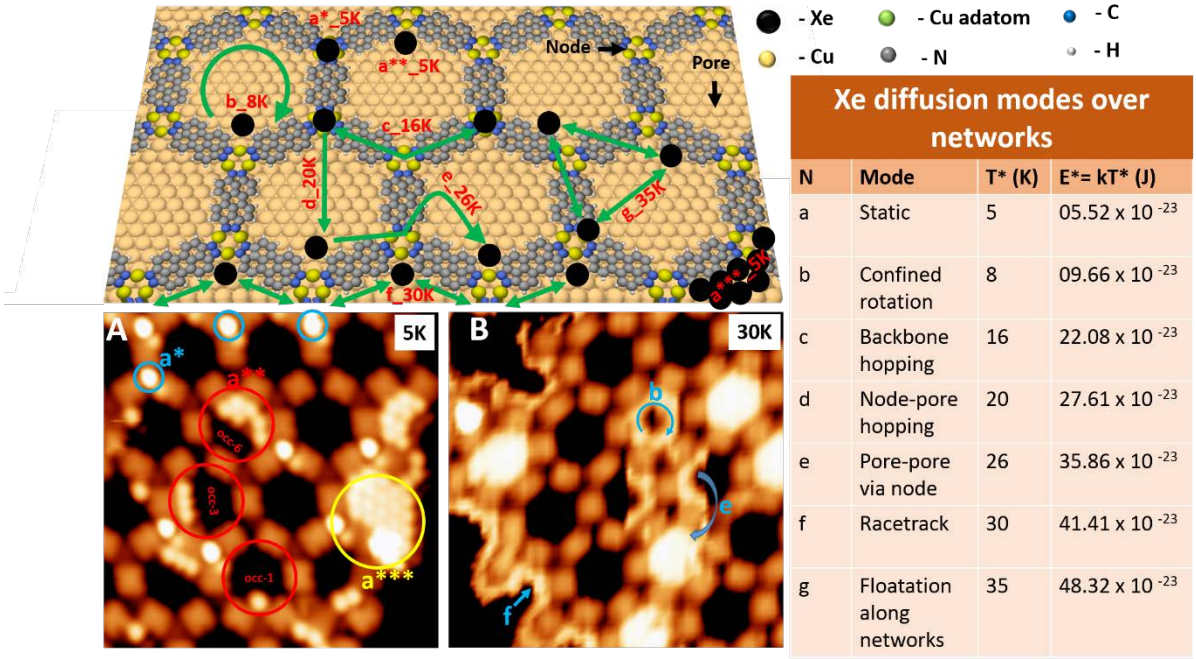


**Xe diffusion modes over networks**

| N | Mode | T* (K) | E*= kT* (J) |
|---|---|---|---|
| a | Static | 5 | 05.52 x $10^{-23}$ |
| b | Confined rotation | 8 | 09.66 x $10^{-23}$ |
| c | Backbone hopping | 16 | 22.08 x $10^{-23}$ |
| d | Node-pore hopping | 20 | 27.61 x $10^{-23}$ |
| e | Pore-pore via node | 26 | 35.86 x $10^{-23}$ |
| f | Racetrack | 30 | 41.41 x $10^{-23}$ |
| g | Floatation along networks | 35 | 48.32 x $10^{-23}$ |

**Figure 2. Diffusion pathways of Xe monomers across porous coordination networks.** *Top left:* Molecular model obtained by DFT optimisation[32] of dehydro-DPDI linked by three Cu adatoms in each node. Predominant adsorption sites (black spheres) and diffusion pathways (green arrows) are indicated; *Bottom left:* (A) STM data taken at 5K after initial adsorption of Xe on nodes (indicated by blue circles), inside pores (red circles) and around the boundary of the islands of the porous network (yellow circles), all showing a static mode of adsorption. Key adsorption sites have been marked in the STM data: a*) the node site on top of the Cu-trimer linking the network; a**) Xe occupied network pores showing six-fold occupancy (occ-6) composed of a tetramer and a dimer, a threefold occupancy (occ-3) as well as a singly occupied (occ-1) pore; a***) a Xe 2D aggregate on the metal surface at the outer border of the network. *Bottom right:* (B) shows the STM profile of the diffusive Xe migration at a temperature of 30 K with three states of motion, denoted *confined rotation (b)* for in-pore diffusion at and above 8K; *pore-*

*pore-via-node* exchange *(e)* i.e. for Xe diffusion across pores via the route of a temporarily occupied node and the *boundary mode (f)* the initially static atoms (a***) start moving around the boundary of the network. The table indicates the various Xe diffusion pathways as they are activated at certain threshold temperatures T* and with the corresponding thermal threshold energies E* = kT*.

First pathways for Xe atom mobility across the network may be identified in the two STM micrographs depicted in the bottom left corner of Figure 2. The STM image A.) taken at 5K illustrates the stable adsorption of Xe atoms on nodes (blue circles), in the pores of the network (red circles) and along the boundary of the network as islands on the bare Cu(111) surface (yellow circles). Image B.) was obtained at 30 K and represents different modes of diffusion/coarsening at higher temperature; the following three modes of diffusion are individually indicated: the *confined rotation* mode, the *pore-pore-via-node* coarsening mode and the *motion of Xe atoms* along the outer rim of the 2D network islands. Further insight was obtained upon stepwise increase of the temperature starting from below 14 K, at which the adsorbed Xe atoms appear static on the timescale on the experiment. Results of the system's reaction to such gradual heating are represented in Figure 3.

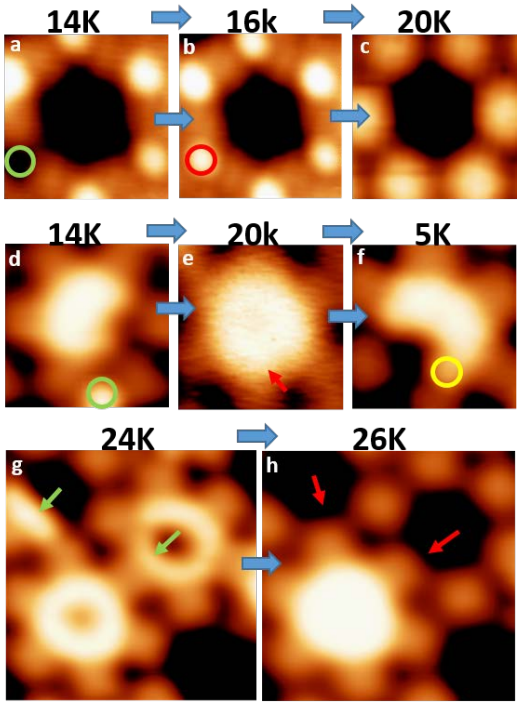


**Figure 3. Xe diffusion of and between condensates in the pores of 2D networks.** *First row (a) – (c):* Up to 14K, Xe atoms are localized on the nodes of the network; upon heating to 16K inter-node lattice gas diffusion starts; one Xe atom diffuses in and occupies the last vacant site among the six node sites around the imaged pore as indicated by the red circle in (b); upon heating to 20K all six node sites are vacant again. Notably in this case the initially empty center pore remains empty. *Second row (d) – (f):* At higher pore occupancies (8-fold in this case), mobile Xe atoms from the nodes (Xe at node position marked by green circle (d)) are filling up the pores by "jumping" from the nodes at 20K (e). This assignment is evidenced by re-measuring at 5K, indicated by the yellow circle marking the added ($9^{th}$) Xe atom in pore (f). *Bottom row (g) – (h) coarsening* of neighbouring condensates*:* Xe atoms are diffusing from the pores exhibiting lower Xe occupancy (marked by green arrows in (g)) to the neighbouring pore with higher occupancy (marked by red arrows in (h). STM image 3 nm x 3 nm (a—f), 5nm x 5nm (g, h) tunnelling current 10 pA, bias voltage 1000 mV.

Diffusional motion of Xe captured inside the pores starts at 8K, while the Xe atoms located on the nodes remain stably adsorbed up to 14 K as evidenced by their bright STM contrast (Figure 3 — a, g). At a temperature of about 16K the Xe atoms start diffusing between different nodes across the network (Figure 3b) as indicated by a red circle in the sequences 3a-c. The nodes are completely cleared from ad-Xe at 20K as it is visible in Figure 3c. Interestingly the destination of the Xe can be traced as shown in Figure 3d for a pore containing 8 Xe atoms and one Xe atom residing on the node (marked by a green circle). After increasing the temperature to 20K this Xe atom disappeared from the position indicated by a red arrow in Figure 3e. Subsequent cooling down to 4K and imaging of the same pore allows us to identify the increased Xe-population of the pore i.e. from 8-occ to 9-occ. (see Figure 3f where the additional Xe has been indicated by a yellow circle).

Note that for the zero occupancy cases depicted in Figures 3a-c, the initially empty pore remains empty, even if Xe is cleared from neighbouring node positions at temperatures above 20K. This result agrees well with our earlier observation that it is not possible to deposit Xe into pores with small initial fractional occupancy as determined by STM. This also agrees with the low probability of observing singly and doubly populated pores in the histogram distribution[35]. This apparent instability of the Xe atom adsorption in empty or low occupancy pores has been attributed to the strong Pauli repulsion between closed shell noble gas atoms and the occupied quantum well state which remains almost unperturbed at low occupancy. At higher occupancy, the Xe atoms repel the confined quantum well state and confine it to a narrower region in z direction. Consequently the state shifts towards the Fermi level in momentum space,[36] which leads to a flatter distribution of the paired spin density within the pores and, consequently, to the reduction of the repulsive force between the confined surface state and individual Xe adsorbate in the pore. Thus, at higher pore occupancy, the Xe atoms favour further adsorption inside the pore which is reminiscent of earlier observations on extended Cu(111) terraces (on-top adsorption in a M x M superstructure)[37,38]. Via this mechanism, the xenon atoms start to cluster in 2D patterns at occupancies higher than 6 at which point van der Waals attraction becomes dominant. Thus, at higher coverages pores with occupancies greater than 6 become *attractors* for further condensation events which explains the growth of almost filled pores at the expense of those with low occupancies under the conditions of thermal equilibration via inter-pore exchange.

This reversal of the Xe atom-pore interaction from repulsive to attractive is a remarkable feature of the complex balance of interactions involving the adsorbate, the adsorbent and the confined surface state – next to the rather hard wall of the confining 3deh-DPDI molecule(s). Note that the fully occupied sites provide the only observed case after annealing i.e. provide the highest Xe- binding energy sites available on the surface at this stage, not the on-terrace islands / layers. This implies that the (non-equilibrium) thermalisation of Xe during the deposition onto the pre-cooled structured substrate is ineffective in reaching this state. The cause might be assigned either to a kinetic retardation or to a certain threshold activation energy ($E_{barr}$) which is only overcome if Xe is directly captured by a pore during the thermalization. The latter is supported by the observation of the whole range of occupancies – at different probability -- in any dosing event[35].

At higher temperatures, between 24—26K, Xe atoms are diffusing from pore to pore via

neighboring node positions. The Xe occupancy histogram is evolving over time in this temperature range: Smaller Xe condensates disappear and fully filled pores become predominant as expected based on the observations and the rationale delineated above. This cross-pore coarsening process starts at 26K which results in a final state in which only empty and completely (12-fold) filled pores can be found to coexist in the network (vide infra). One example of this cross pore coarsening process is displayed in Figure 3g where green arrows indicate a 'ring' of moving Xe atoms in the pore next to two partially filled occupancies in the vicinity which disappear at 26K (indicated by red arrows in Figure 3h). The missing atoms to fill the pore to the left apparently traversed the pore boundary.

The possible diffusion pathways of Xe across the supramolecular porous network are further modified and extended at elevated temperatures: In Figure 4 STM data of a larger area of a network island and its border is shown at 5K, where Xe is at rest, and then at increased temperatures of 30 K, 35 K and 40 K. The dynamicity of the Xe can be deduced from the noisy or streaky features which appear in the data taken at the elevated temperatures. At 30K (Fig. 4b), Xe atoms start flowing in a chain around the network boundaries as indicated by blue arrows. Furthermore, condensates with occupancies > 6 appear as mobile discs indicated by green circles, while those with less than six Xe atoms give rise to mobile rings indicated by red circles. This provides indirect experimental evidence for the shifting and spreading of the surface state across the pore, as described above. At 35K (Fig. 4c), the mobile braid of xenon atoms at the network boundary is narrowed (marked by blue arrows in the STMs recorded at 30K and 35K), indicating depletion of these adsorption sites, and practically disappears at the higher temperature, indicating that Xe moves along other routes. (see Fig. 4d)

**3. Direct observation of adsorbed Xe atom in motion**

A new feature appears at 35K in the form of 'streaks' indicated by 'purple' arrows in Fig. 4c. This evidences that Xe atoms which have not yet been captured in pores are rapidly moving along the network backbone and collide with the scanning tip (at a frequency of interaction with the scanning tip of approximately one in every fourth line). At 40K (Fig. 4d) a considerable number of Xe atoms, which have not yet aggregated within pores above the condensation threshold, are moving across the network, as indicated by the increased number of streaks indicated by purple arrows. The number of streaks detected by collisions of the scanning STM tip, i.e. the observation of Xe diffusing along the network backbone is gradually increasing from 30 K to 40 K Fig. 4b-d). At this temperature, the frequency of interaction between the scanning tip and Xe atoms diffusing along the network is increased to approximately 5 per scanline. This collision statistics has been analysed and revealed an increase from $2.9 \times 10^4$ n at 30K to $5.0 \times 10^5$ n at 35K and then to $5.1 \times 10^6$ n at 40K [SI-2]. We note that Xe is now moving randomly across the (2-dimensional) network linking the pores as the pore occupancy further coarsens. The pores with close to complete occupancy appear as bright disks in the STM.

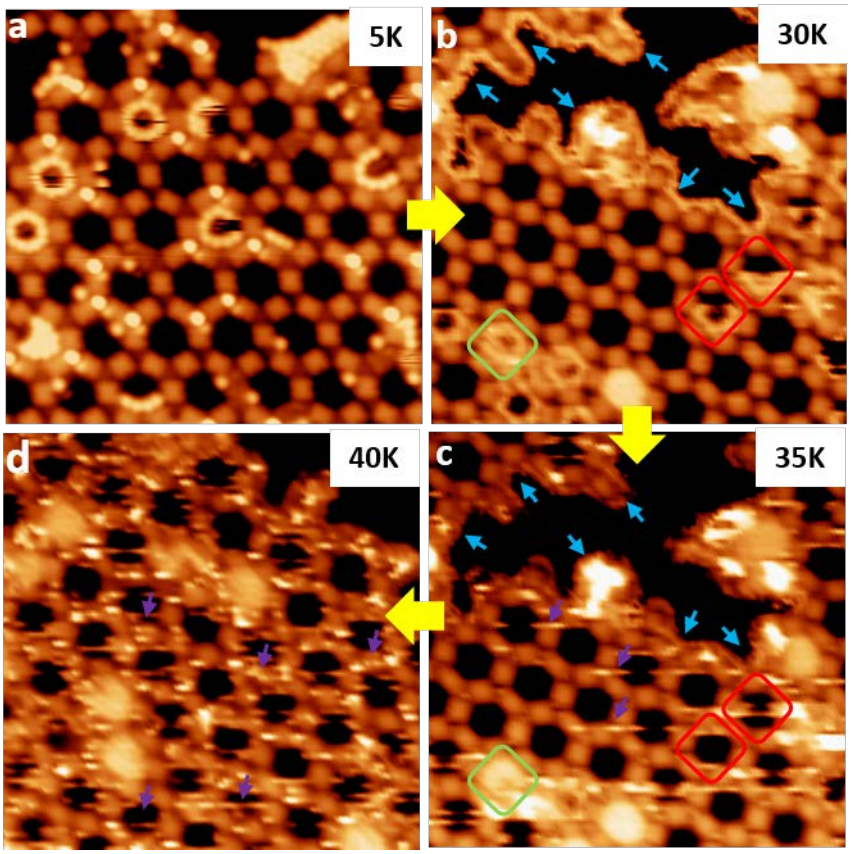


**Figure 4. Temperature dependent diffusion characteristics and coarsening of the Xe condensates in the DPDI network.** *(a)* At 4K most Xe atoms appear at fixed positions (frozen) on the nodes, inside the pores and as islands around the network boundary on the bare Cu(111) surface. *(b)* At 30K, characteristic signs of Xe mobility inside the pores appear (‘ring-like’ structures marked by green squares) as well as chains of mobile Xe atoms along the rims of the networks ('race track like’ lines along the network border, indicated by blue arrows). (c) At 35K the mobile Xe atoms at the borders virtually disappear (blue arrows and the partially filled pores in *(b)* appear to be depleted as marked by the ‘red squares’, while others have accumulated Xe significantly as indicated by ‘green squares’. This is also manifested in the observed bright disk-shaped features representing 12 fold occupied pores (established by STM analysis performed after cooling the sample to 5K, not shown). It is important to note that (b) and (c) were recorded at close to the same spot of the surface. *(d)* At 40K the frequency of interaction between the scanning tip and Xe atoms diffusing along the network is increased to the order of 5 per scanline. A larger fraction of DPDI pores appears close to fully Xe occupied (bright disks), a result of the ‘coarsening’ i.e. the increase of the larger condensates’ fraction at the expense of disappearing smaller condensates in other pores. Only the three higher T data sets depict the same area, because the thermal drift between 5K and 30K was too high. STM scanning parameters; (V=1000 mV, I=10 pA, image size 20nm x 20 nm).

## 4. Theoretical modelling of Xe pathways across the surface network

In order to better understand the preferred motion of the Xe atoms within the surface network we performed DFT modeling of several pathways. The self-diffusion process between two local minima was calculated by making a linear interpolation of the Xe motion between the two sites, and then optimizing the *z*-coordinate (perpendicular to the surface) for each state. The transition state separating the local minima was identified by a fine interpolation and optimization around the energy maximum of the curve. Due to the extremely flat energy

landscape of the system we could not use conventional methods for the determination of transition states, such as the nudged elastic band method.

The resulting pathways for Xe self-diffusion processes are summarized in Figure 5. The Xe atom starts in its most stable adsorption site inside the pore (**S0**), moves to the centre of the first node (**S1**), then across the molecular backbone to reach another (inequivalent) node (**S2**) and finally goes back into the pore of the network (**S3**). Considering these processes, the diffusion between two nodes has the lowest barrier (~60 meV). Furthermore, the barrier going from one of the nodes to the pore (~70 meV) is lower than the reverse process of going from the pore to a node (~80 meV). These barriers, in fact, follow the hierarchy of our experimental observations perfectly: The backbone hopping is activated at lower temperatures than the node-pore hopping, while the pore-pore hopping happens only at even higher temperatures. The reason for the pore-pore hopping to require higher temperatures than the node-pore hopping is simply because the adsorption within the pore is more stable than the adsorption on a node, and the pore-pore hopping involves the pore-node hopping. Although it is beyond our numerical capacity to provide an accurate quantitative description of the processes, the results provide a good qualitative picture of the experimentally observed diffusion behavior and confirm the temperature dependent hierarchy of the thermally activated diffusion pathways.

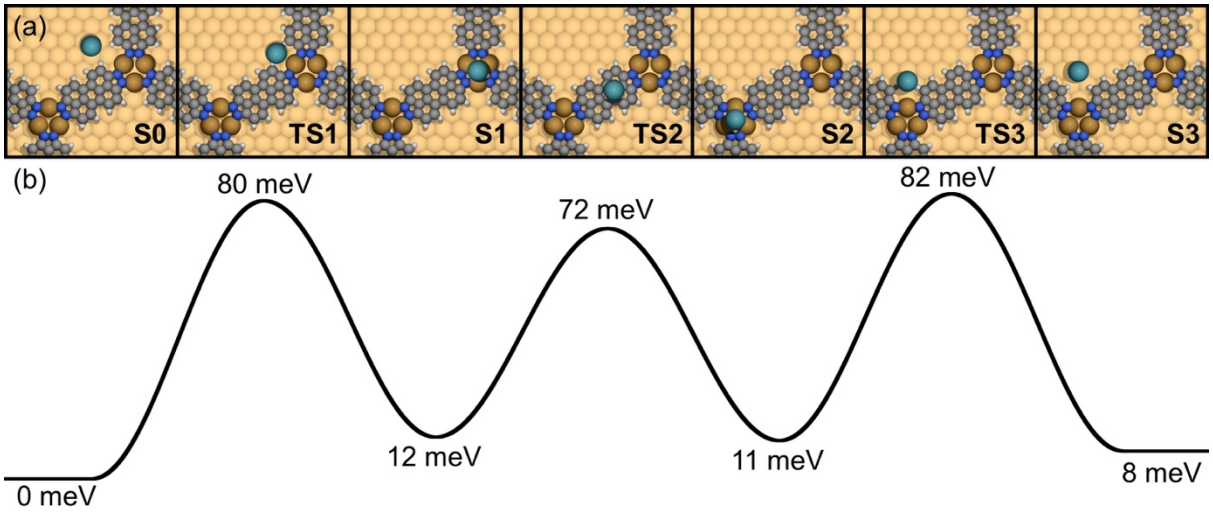


**Figure 5. Calculated pathway of the Xe moving across the surface network.** (a) Top and side views of local minima (**S0** – **S3**) and transition states (**TS1** – **TS3**) with (b) representation of the corresponding energy profile. The pathway for each separate step together with the full energy profile plotted with respect to the coordinate of the Xe movement is provided in the Supporting Information.

## CONCLUSION

In this study we have monitored and identified the complex temperature dependent diffusion pathways of the vdW adsorbate Xe across a metal organic on-surface network. The complexity of these pathways and their step-wise activation with increasing temperature has allowed for a certain kinetic control. This is in a way reminiscent of the kinetic retardation observed in the formation of surface reconstructions on e.g. Si(111), Au(111) but also for adsorbate induced reconstructions on Au(110) and Ag(110)[11,16,39].

Three different static adsorbate positions on the network-covered substrate, namely the node, the pore and the island sites provided the starting point for different diffusion trajectories along 0D to 2D confinements provided by the structurally patterned substrate: inside the pores (0D),

along the network boundary (1D) and along the porous network backbone (2D). The step-wise activation of these trajectories leads to a redistribution of Xe first 'in' and then 'between' different compartments (pores) and to a 'coarsening' of the Xe condensates: Lower occupancy (<6 Xe atoms) condensates disappear to the benefit of higher occupancy (≥6 Xe atoms) condensates (SI-1), ultimately leading to all pores being 12-fold Xe occupied. It is important to note that a significant role in this transition is assigned to the interaction of the different Xe condensates with the underlying surface states. Upon increased pore occupancy Pauli repulsion of the closed shell xenon atoms progressively shifts the quantum well state closer to the Fermi level, as recently reported[36]. This leads to an expansion and "flattening" of the confined surface states which in turn reduces their repulsive interaction with the gueat atoms. The latter experience increasing vdW attaction with growing occupancy. These two independent and counter-acting trends lead to the pores becoming attractors for additional Xe atoms at higher occupancies.

We also conclude that these 12-fold Xe occupied sites provide the highest binding energy sites available on the surface. This state is difficult to reach during the deposition process due to the presence of the surface state, but is demonstrated to be reached by the Xe diffusing across the surface. It is rather the frequency of Xe atoms impinging at the pore during the thermal equilibration at ~40K than the lower frequency of higher energy (~kT source i.e. 300K) Xe appearing during the dosing process (effective surface pressure of ~10-7 mbar).

## METHODS

### Sample preparation and STM measurement:

All samples were prepared and examined in an ultrahigh vacuum (UHV) system with a base pressure of 6 x $10^{-11}$ mbar. The Cu(111) crystal (MaTecK GmbH) was prepared by several rounds of $Ar^+$ sputtering at E = 1 KeV performed at room temperature followed by annealing at 480 $^oC$. The DPDI molecules were deposited with the use of a nine-cell commercial evaporator (Kentax, GmbH, Germany) on the Cu(111) by sublimation at ~240 $^oC$ and the rate was controlled by a quartz crystal microbalance. After deposition, the sample was annealed to 300 $^oC$ in order to convert DPDI into 3deh-DPDI, which generated the Cu-coordinated network [32]. Xe of purity 99.99% was dosed to the sample placed in the STM (Omicron Nanotechnology GmbH) operated at 4.2 K, with the cryoshields open and the leak valve being in straight shot with the sample. STM data were acquired after exposure of the Cu-coordinated 3deh-DPDI network to different exposure of Xe performed at a pressure equal to 1.3 x $10^{-7}$ mbar for corresponding time causing the increase in the sample temperature to 9 K.

Deposition times: 65L → 650s, 120L → 1,200s, 180L → 1,800s, 200L → 2,100s, 265L → 2,700s, 300L → 3,000s, 345L → 3,300s at 1.3 x $10^{-7}$ mbar.

Xe was found to be adsorbed initially in the pores as well as on the nodes of the network. Then with closed cryoshields, the temperature was progressively raised up from the thermal equilibrium in the He cryostat (~4.2K) by resistive heating to a maximum temperature of 40K by using a temperature controller [LakeShore-331] at 1K/min, experiments were performed at each chosen temperature by switching off the temperature ramping.

STM measurements were performed in the constant current mode with Pt–Ir tips (90% Pt, 10% Ir), prepared by mechanical cutting followed by sputtering and controlled indentation in the bare Cu(111). The STM images shown in Figure 1—4, SI 1—5 were acquired with metallic tips prepared in this way. To avoid modification in diffusion of the condensates via interaction with the tip, the sample bias was set at 1000 mV whilst the tunnelling current was set at 10 pA.

Periodic DFT calculations were done with the VASP code[40], using the projector-augmented wave method to describe ion-core interactions[41] and with planewaves expanded to a kinetic energy cutoff of 400 eV. The van der Waals density functional[42] described exchange-correlation effects, with the version by Hamada denoted as rev-vdWDF2[43] which provide an accurate description compared to experimental reference data of the DPDI network [Manfred 2014 PRB]. The Cu(111) surface was described by a six-layered slab with the bottom layer saturated by H atoms for a better description of the top layer's surface state. The surface network was geometrically optimized until the residual forces on all atoms (except the three bottom layers of the slab which were kept fixed) were smaller than 0.01 eV/Å. For the calculations with Xe in the network, only the Xe atom was allowed to relax while all other atoms were kept fixed.

**ACKNOWLEDGMENTS**

The work was supported by the Physics Department of the University of Basel, Swiss Nanoscience Institute, the Swiss National Science Foundation (Grant: 200020_162512, 206021_144991, 206021_121461), the Swiss Commission for Technology and Innovation (CTI, 16465.1 PFNM-NM) and the Swiss Commission for Swiss Government Excellence Scholarship Program for Foreign Scholars (2013.0492). We also acknowledge the support by the University of Heidelberg and the DFG (SFB 1249). M. Martina and M. Senn provided valuable technical assistance. We sincerely thank to Shigeki Kawai and Robert Skonieczny for support during the measurements.

**Author contributions**

A.A., S.F.M., T.N., S.N., O.P., and A.W., led the STM measurements and examined the data under the supervision of T.A.J., and L.H.G. A.A., T.A.J. and L.H.G. wrote the manuscript.

**Additional Information:** Supplementary information of this article accompanies in a separate file.

**Competing financial interest:** The authors found no competing interests.

## REFERENCCES


1. Lindner, B. & Nicola, E. M. Diffusion in different models of active Brownian motion. *Eur. Phys. J. Spec. Top.* **157,** 43–52 (2008).
2. Ehrlich, G. & Hudda, F. G. Interaction of Rare Gases with Metal Surfaces. I. A, Kr, and Xe on Tungsten. *J. Chem. Phys.* **30,** 493–512 (1959).
3. Silvestrelli, P. L., Ambrosetti, A., Grubisiĉ, S. & Ancilotto, F. Adsorption of rare-gas atoms on Cu(111) and Pb(111) surfaces by van der Waals corrected density functional theory. *Phys. Rev. B* **85,** (2012).
4. Thomas, P., Gray, J., Zhu, X. D. & Fong, C. Y. Surface diffusion of Xe on Nb(110). *Chem. Phys. Lett.* **381,** 376–380 (2003).
5. Morgenstern, K., Braun, K.-F. & Rieder, K.-H. Direct Imaging of Cu Dimer Formation, Motion, and Interaction with Cu Atoms on Ag(111). *Phys. Rev. Lett.* **93,** (2004).
6. Bendounan, A. Adsorption Properties of Xe on Ag/Cu(111) System: Real-Time Photoemission Investigation. *J. Phys. Chem. C* **120,** 24279–24286 (2016).
7. Xia, X. *et al.* On the role of surface diffusion in determining the shape or morphology of noble-metal nanocrystals. *Proc. Natl. Acad. Sci.* **110,** 6669–6673 (2013).
8. van Gastel, R., Somfai, E., van Albada, S. B., van Saarloos, W. & Frenken, J. W. M. Nothing Moves a Surface: Vacancy Mediated Surface Diffusion. *Phys. Rev. Lett.* **86,** 1562–1565 (2001).
9. Gomer, R. Diffusion of adsorbates on metal surfaces. *Rep. Prog. Phys.* **53,** 917–1002 (1990).
10. *Surface science: an introduction*. (Springer, 2003).
11. Perkins, L. S. & DePristo, A. E. Self-diffusion mechanisms for adatoms on fcc(100) surfaces. *Surf. Sci.* **294,** 67–77 (1993).
12. Ferrando, R. & Fortunelli, A. Diffusion of adatoms and small clusters on magnesium oxide surfaces. *J. Phys. Condens. Matter* **21,** 264001 (2009).
13. Rhead, G. E. Diffusion on surfaces. *Surf. Sci.* **47,** 207–221 (1975).
14. Schwoebel, R. L. Step Motion on Crystal Surfaces. II. *J. Appl. Phys.* **40,** 614–618 (1969).
15. Mugarza, A. *et al.* Modelling nanostructures with vicinal surfaces. *J. Phys. Condens. Matter* **18,** S27–S49 (2006).
16. Barth, J. V., Brune, H., Ertl, G. & Behm, R. J. Scanning tunneling microscopy observations on the reconstructed Au(111) surface: Atomic structure, long-range superstructure, rotational domains, and surface defects. *Phys. Rev. B* **42,** 9307–9318 (1990).
17. Chang, Y. J. & Phark, S. Direct Nanoscale Analysis of Temperature-Resolved Growth Behaviors of

Ultrathin Perovskites on $SrTiO_3$. *ACS Nano* **10,** 5383–5390 (2016).

18. Phark, S. & Chang, Y. J. Nucleation and growth of primary nanostructures in SrTiO3 homoepitaxy. *Nanoscale Res. Lett.* **10,** (2015).
19. Brune, H. Chapter 15 Creating Metal Nanostructures at Metal Surfaces Using Growth Kinetics. in *Handbook of Surface Science* **3,** 761–786 (Elsevier, 2008).
20. Kim, Y.-J. *et al.* Surface Chemical Conversion of Organosilane Self-Assembled Monolayers with Active Oxygen Species Generated by Vacuum Ultraviolet Irradiation of Atmospheric Oxygen Molecules. *Jpn. J. Appl. Phys.* **47,** 307–312 (2008).
21. Müller, B., Nedelmann, L., Fischer, B., Brune, H. & Kern, K. Initial stages of Cu epitaxy on Ni(100): Postnucleation and a well-defined transition in critical island size. *Phys. Rev. B* **54,** 17858–17865 (1996).
22. Unal, B. *et al.* Nucleation and growth of Ag islands on fivefold Al-Pd-Mn quasicrystal surfaces: Dependence of island density on temperature and flux. *Phys. Rev. B* **75,** (2007).
23. Heidorn, S.-C., Bertram, C. & Morgenstern, K. The fractal dimension of ice on the nanoscale. *Chem. Phys. Lett.* **665,** 1–5 (2016).
24. Müller, B., Nedelmann, L., Fischer, B., Brune, H. & Kern, K. Submonolayer Nucleation and Growth of Copper on Ni(100). in *Surface Diffusion* (ed. Tringides, M. C.) **360,** 151–159 (Springer US, 1997).
25. Linderoth, T. ., Horch, S., Lægsgaard, E., Stensgaard, I. & Besenbacher, F. Dynamics of Pt adatom and dimers on Pt(110)-(1×2) observed directly by STM. *Surf. Sci.* **402–404,** 308–312 (1998).
26. Hohage, M. *et al.* Atomic Processes in Low Temperature Pt-Dendrite Growth on Pt(111). *Phys. Rev. Lett.* **76,** 2366–2369 (1996).
27. Buchner, F. *et al.* Diffusion, Rotation, and Surface Chemical Bond of Individual 2 *H* -Tetraphenylporphyrin Molecules on Cu(111). *J. Phys. Chem. C* **115,** 24172–24177 (2011).
28. Widmer, R., Passerone, D., Mattle, T., Sachdev, H. & Gröning, O. Probing the selectivity of a nanostructured surface by xenon adsorption. *Nanoscale* **2,** 502 (2010).
29. Dil, H. *et al.* Surface Trapping of Atoms and Molecules with Dipole Rings. *Science* **319,** 1824–1826 (2008).
30. Pivetta, M., Pacchioni, G. E., Schlickum, U., Barth, J. V. & Brune, H. Formation of Fe Cluster Superlattice in a Metal-Organic Quantum-Box Network. *Phys. Rev. Lett.* **110,** (2013).
31. Müller, K., Enache, M. & Stöhr, M. Confinement properties of 2D porous molecular networks on metal surfaces. *J. Phys. Condens. Matter* **28,** 153003 (2016).

32. Matena, M. *et al.* On-surface synthesis of a two-dimensional porous coordination network: Unraveling adsorbate interactions. *Phys. Rev. B* **90,** (2014).
33. Shchyrba, A. *et al.* Controlling the Dimensionality of On-Surface Coordination Polymers via Endo- or Exoligation. *J. Am. Chem. Soc.* **136,** 9355–9363 (2014).
34. Lobo-Checa, J. *et al.* Band Formation from Coupled Quantum Dots Formed by a Nanoporous Network on a Copper Surface. *Science* **325,** 300–303 (2009).
35. Nowakowska, S. *et al.* Interplay of weak interactions in the atom-by-atom condensation of xenon within quantum boxes. *Nat. Commun.* **6,** 6071 (2015).
36. Nowakowska, S. *et al.* Configuring Electronic States in an Atomically Precise Array of Quantum Boxes. *Small* **12,** 3757–3763 (2016).
37. Seyller, T., Caragiu, M., Diehl, R. D., Kaukasoina, P. & Lindroos, M. Observation of top-site adsorption for Xe on Cu(111). *Chem. Phys. Lett.* **291,** 567–572 (1998).
38. Lazić, P., Crljen, ž., Brako, R. & Gumhalter, B. Role of van der Waals interactions in adsorption of Xe on Cu(111) and Pt(111). *Phys. Rev. B* **72,** (2005).
39. Diehl, R. D. *et al.* The adsorption sites of rare gases on metallic surfaces: a review. *J. Phys. Condens. Matter* **16,** S2839–S2862 (2004).
40. Kresse, G. & Furthmüller, J. Efficient iterative schemes for *ab initio* total-energy calculations using a plane-wave basis set. *Phys. Rev. B* **54,** 11169–11186 (1996).
41. Blöchl, P. E. Projector augmented-wave method. *Phys. Rev. B* **50,** 17953–17979 (1994).
42. Dion, M., Rydberg, H., Schröder, E., Langreth, D. C. & Lundqvist, B. I. Van der Waals Density Functional for General Geometries. *Phys. Rev. Lett.* **92,** (2004).
43. Hamada, I. van der Waals density functional made accurate. *Phys. Rev. B* **89,** (2014).

# Supporting Information (SI):
# Step-wise activation of diffusion pathways and coarsening of Xe condensates in metal organic networks

**Contents**



## 1. Energy level landscape for different pathways of diffusion and coarsening

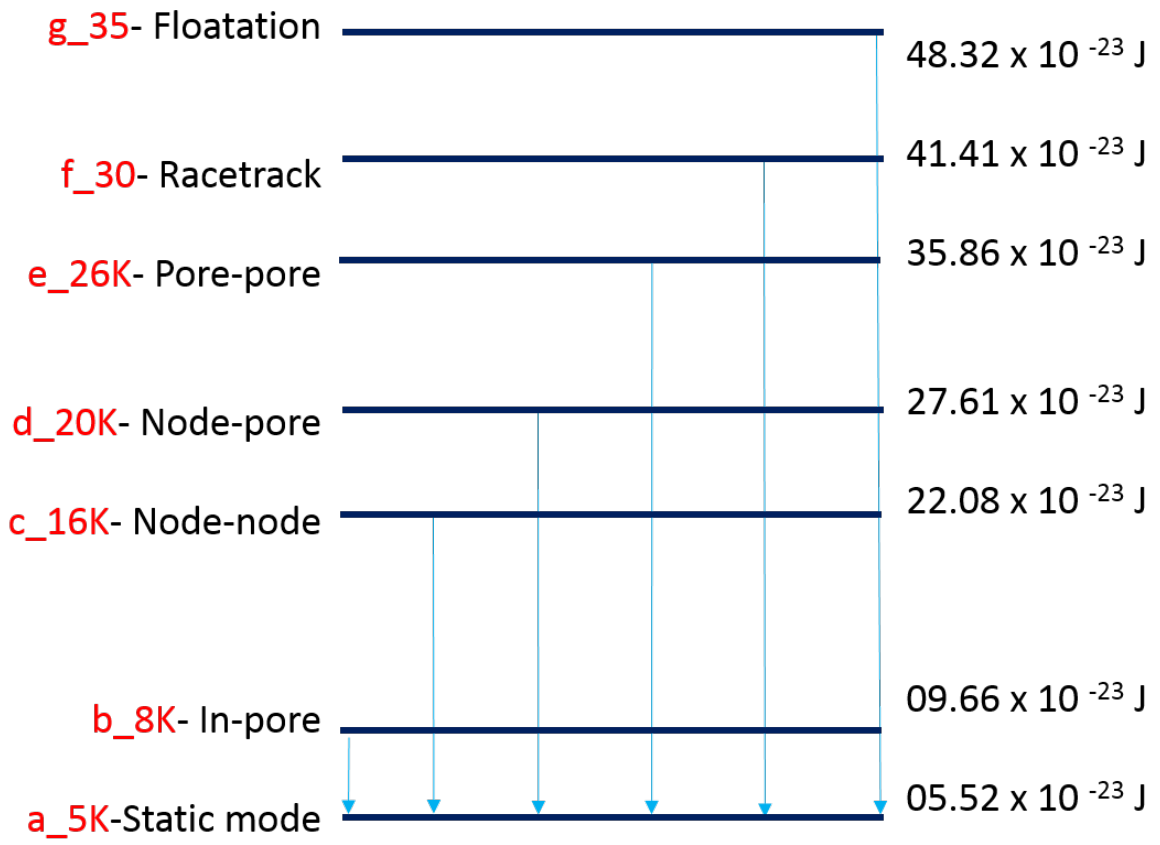


**SI-Graph1. Energy (kT) level landscape of coarsening pathways.** This graph shows the trend of increasing energy with different levels of diffusion.

2. **Coarsening of Xe condensates in networks DPDI**

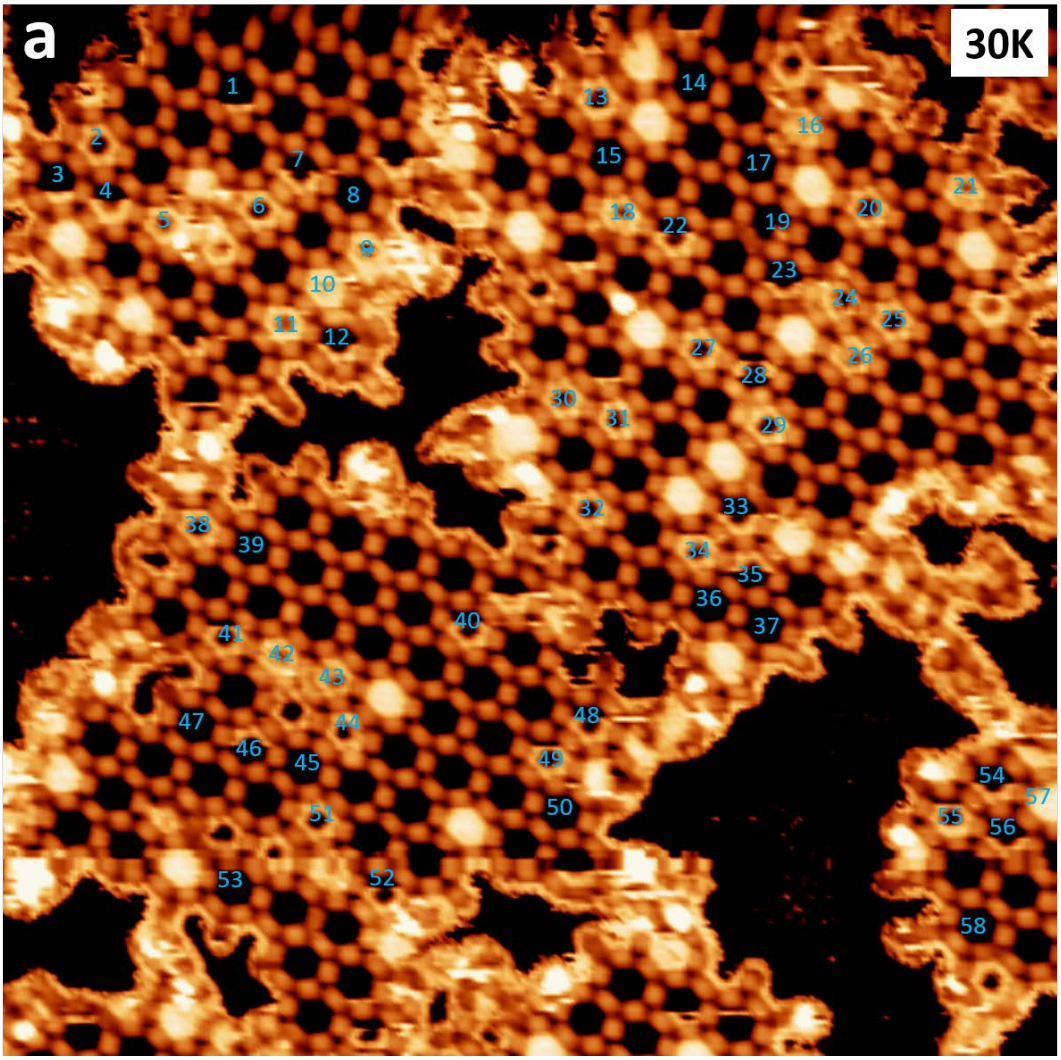

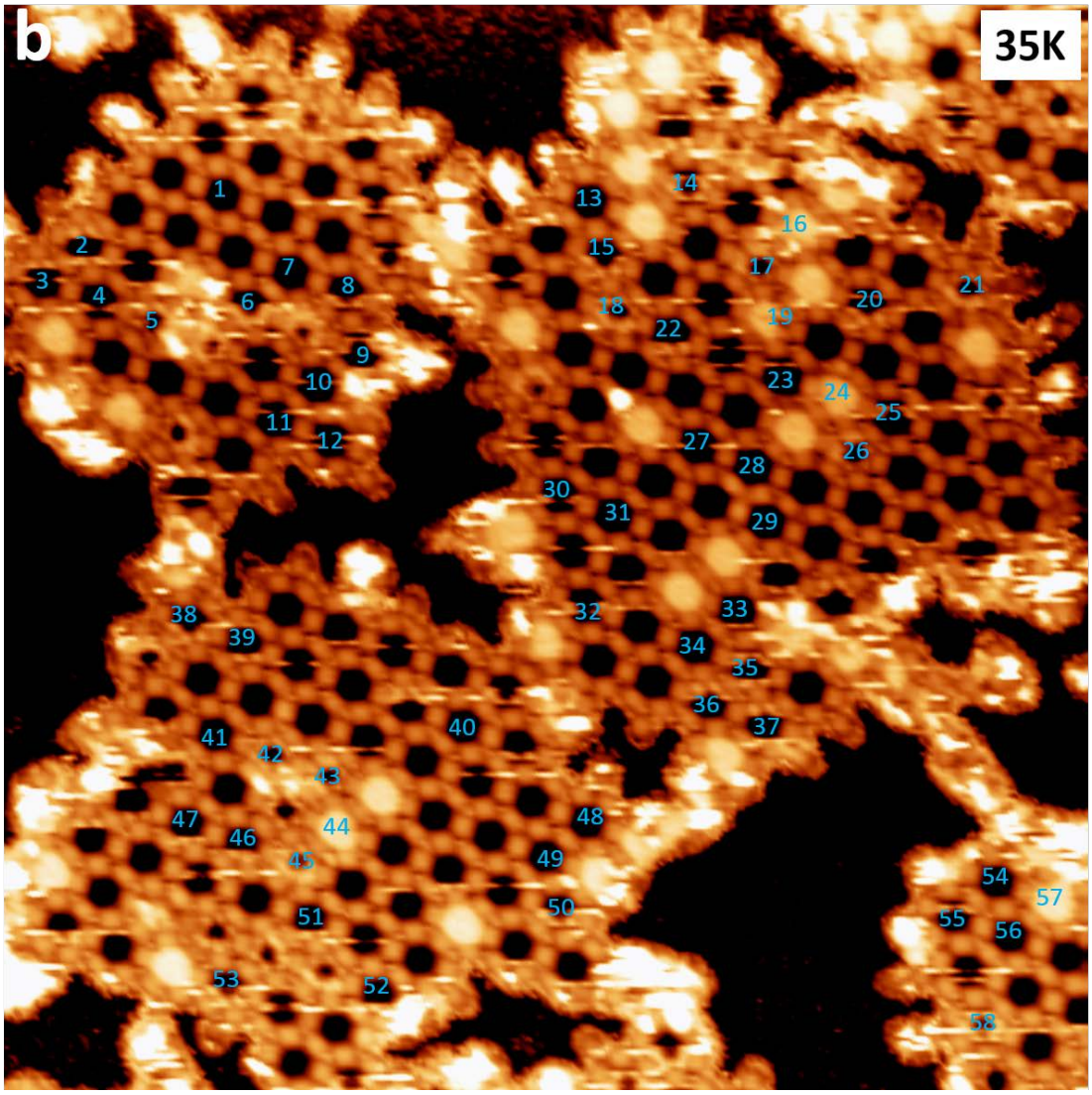


| Temperature | n=12 | n < 6 | n > 6 |
|---|---|---|---|
| 30K | 9% | 5% | 24% |
| 35K | 12% | 2% | 7% |

**SI-1. Coarsening of Xe condensates in DPDI networks.** (a) STM image taken at 30 K revealing the mobility of Xe within-pores and along the rim around the networks. The two dimensional diffusion of Xe over networks at 30K is associated with transient mobility. Different pores are numbered in blue (a) at 30K with the exactly corresponding pores labelled in the same way in (b) at 35K. The evolution of the occupancy of these pores has been listed in a table of which the summary is shown at the bottom of the figure. Clearly there is the trend of partially filled pores, both at lower than 6 occupancy (will be emptied) and at higher than 6 occupancy (will be filled) to disappear while the number of completely filled pores is increasing. STM scanning parameters (V=1 V, I=10 pA, image size 35nm x 35nm)

## 1. Evolution of Xe diffusion patterns

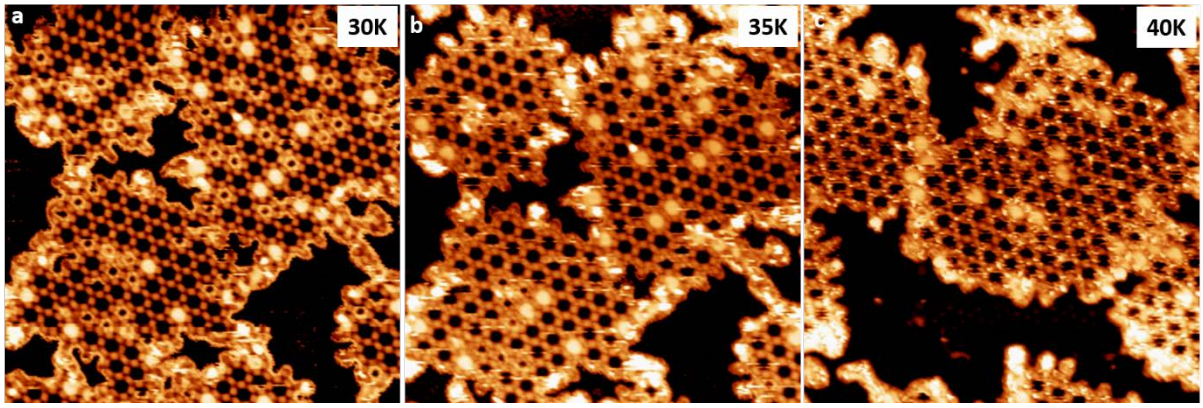


| Temperature (K) | 30K | 35K | 40K |
|---|---|---|---|
| No. of streaks (n) | 2.9 x $10^4$ n | 5.1 x $10^5$ n | 5.0 x $10^6$ n |

**SI-2. Sequence of consecutive images showing the evolution of Xe diffusion patterns: a)** at 30K, diffusion is predominantly occurring either inside the pores or along the network border. Pores with occupancies below 6 are recognized by ring like features with the STM virtual height dependent on the population of the number of diffusing Xe atoms. Pores with occupancy higher than 6 display disk shape patterns due to the presence of Xe which is closer to the center of the pore and the progressive shift of the quantum well state facilitating 2D diffusion inside the pore. A very low number of tip excursion 'streaks' is visible as the STM tip is scanning across the network backbone. **b)** at 35K, the diffusion along the outer rim is far less apparent, the coarsening of the filling patterns leads to less 'ring shape' and more 'disk shape' features. Indicating the coarsening pathway are the 'streaks' visible on the backbone of the DPDI network. We assign these 'streaks' to the presence of Xe diffusing along the network backbone, -and therefore forming a dynamic equilibrium between the pores of the different population which then results in the coarsening. From the scanning speed (36 nm) and the average length of the streak features in this data (~ 1.3 nm) we estimate a residence time of Xe to be in the order of some msec at the observation temperature. Note that this is only a rough estimate in presence of the electric field induced by the scanning tip among other potentially present interactions. **c)** at 40 K the mobile chains along the outer periphery of the network islands are completely gone and the number of 'streak' incidents increased even more significantly. The occurrence has been analysed by number of streaks (counted twice because of right and left STM tip scan) multiplied by area of scan, and the increased number of streaking frequency $10^4$ n→ $10^5$ n→ $10^6$ n as it evolves from 30K → 35K → 40K, respectively. This has been listed in the table below the figure. Note that there are no visible incidents of Xe adsorbing or diffusing across the Cu substrate at all these observation temperatures. STM scanning parameters (V=1 V, I=10 pA, image size 35nm x 35nm)

## 2. Different diffusion modes

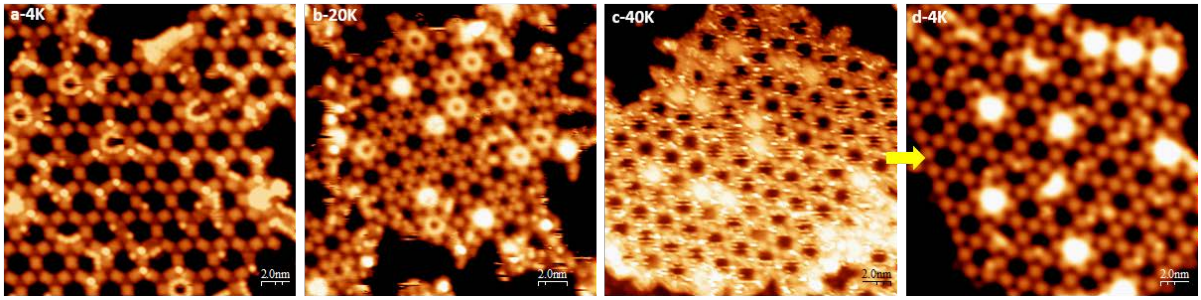


**SI-3. Diffusion from nodes, in-pore mobility, start-up of coarsening ended up with maximization of pore filling with Xe atoms.** (a) Xe atoms are static over nodes, in pores and around the networks at 4K with 0% dynamicity also 27% nodes occupancy with 48% pores occupancy. At 20K mostly atoms are mobile inside pores but not outside the networks with 0% dynamic channels. After annealing to 40K (c) and scanned back to 4K reveals most of pores are occupied with maximum 12 Xe atoms. STM scanning parameters (V=1 V, I=10 pA, image size 35nm x 35nm)

## 3. Coarsening of Xe condensates

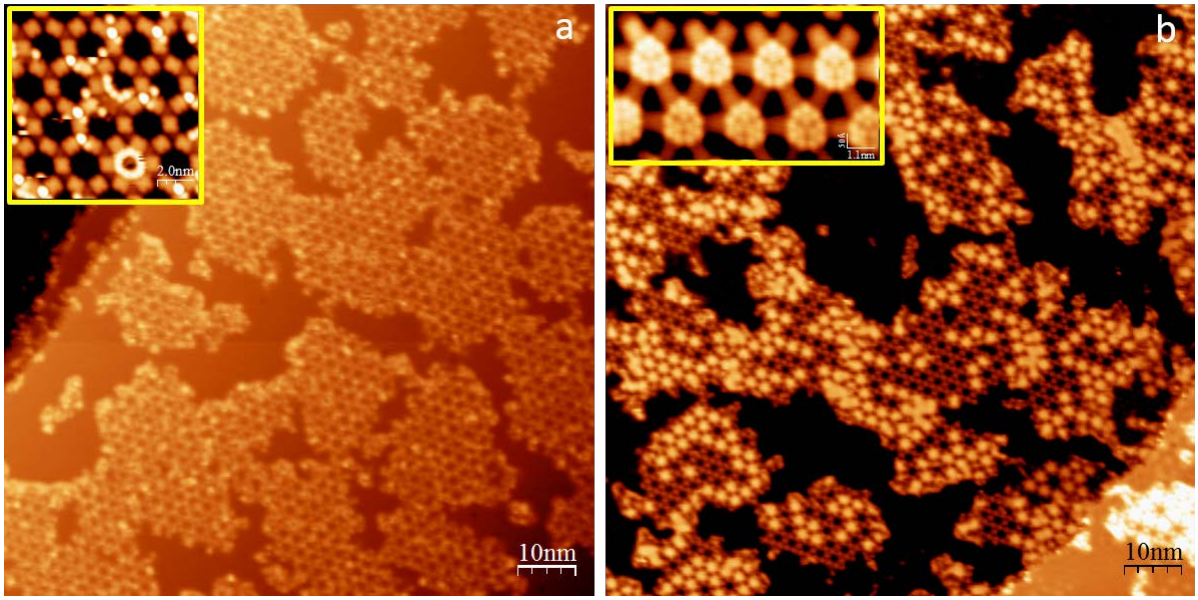


**SI-4. Coursening of Xe condensates in network cavities.** (a) STM image of network islands on Cu(111) after exposure with 240L-Xe. An irregular pattern of different adsorption sites is hosting the Xe: at the nodes on the network, in the pores with different occupancy, and also on the bare Cu(111) surface, but the latter only in small areas around the network boundaries. (b) after annealing to 40K for 30 minutes and STM inspection at 4K most of the Xe is found in fully (12-fold) occupied pores. Only some small or narrow pockets between neighbouring network islands are covered by larger Xe islands which are imaged by featureless bright areas. STM scanning parameters (V=1 V, I=10 pA, image size 100 nm X 100 nm).

## 4. Coverage dependent diffusion

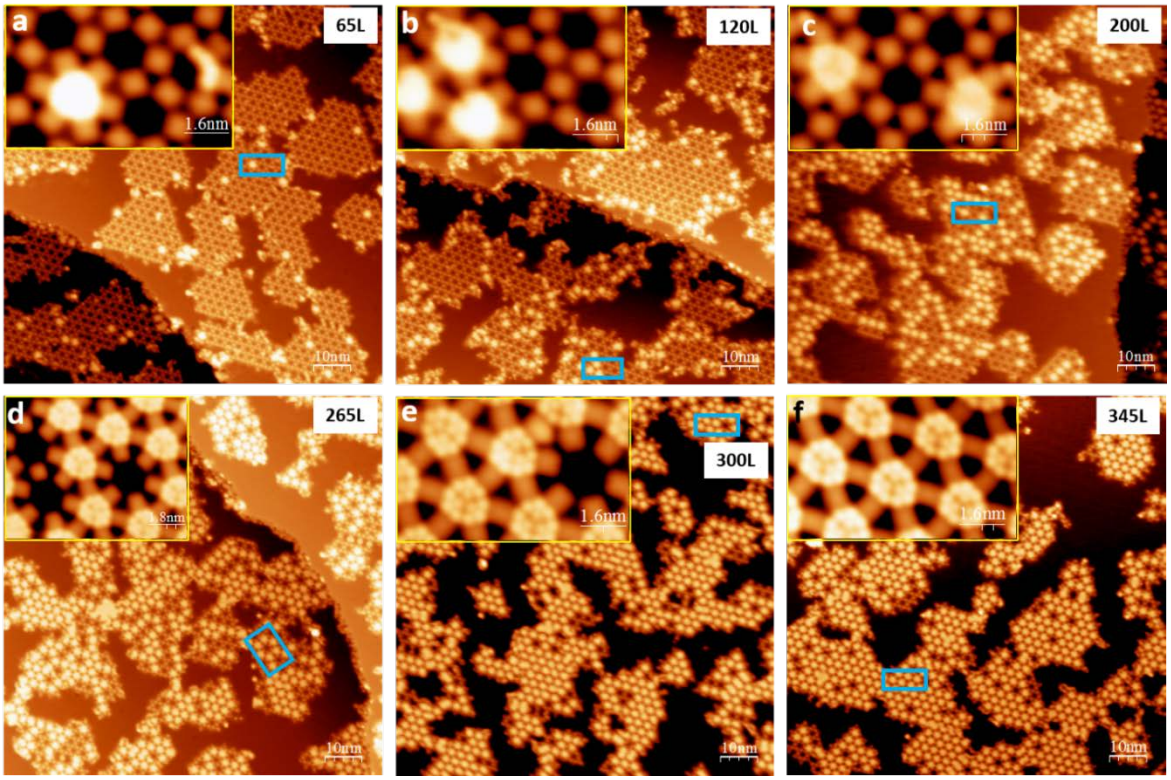


**SI-5. Coverage dependent diffusion studies in DPDI networks.** (a) with 65L exposure of Xe, some pores are fully saturated by Xe atoms and few with different occupancies while most of them are empty that is clearer in inset. (b) 120L exposure of Xe the ratio of fully filled pores is increased but still have with high ratio of partially filled pores indicated in inset. This trend of filling up pores to their maximum capacity gradually increase from 50%, 61%, 88% to 89% with increasing exposure with 200L (c), 265L (d), 300L (e) and 345L (f) respectively while this trend is also clear from the graph below the figure. All samples are exposed to Xe at 9K with follow up annealing to 40K for 30 minutes and scanned back at 4K. STM scanning parameters (V=1 V, I=10 pA, image size 100 nm X 100 nm, inset images 8nm x 5nm)

## 5. Graph, exposure dependent filling up pores

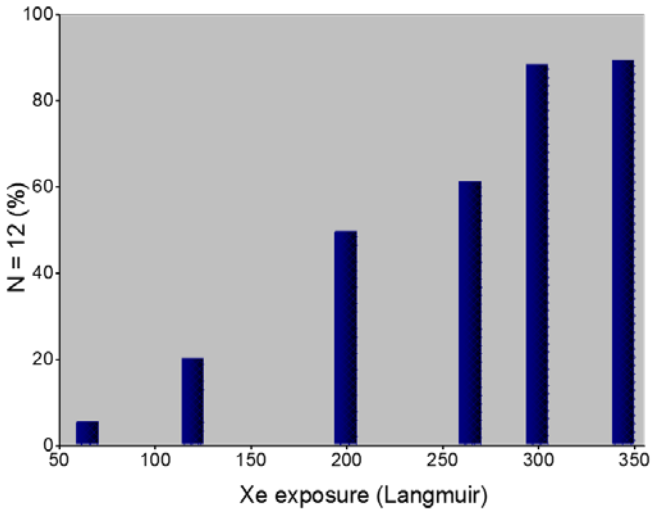


| a | 65L | 5% |
|---|---|---|
| b | 120L | 20% |
| c | 200L | 49% |
| d | 265L | 61.% |
| e | 300L | 88% |
| f | 345L | 89% |

**SI-Graph2. Exposure dependent filling up of pores with Xe atoms by diffusion in DPDI networks.** This trend of filling the pores based on diffusion/coarsening procedure shows from the graph, increases with increasing the exposure of Xe atoms over the sample. Letters a, b, c, d, e and f correspond to images a, b, c, d, e, f in figure S5.

# Chapter [[3]] and Supplementary Information

| | |
|---|---|
| [[3]] | **$Xe_3^+$ Trimers: Stabilisation of linear Xe trimer in the DPDI quantum confinements** |
| | Aisha Ahsan, S. Fatemeh Mousavi, T. Nijs, S.Nowakowska, Olha Popova, A. Wäckerlin, T. Nijs, J. Björk, L. H. Gade, T. A. Jung, *manuscript preparation*. |
| | Contribution of A. Ahsan: carried out experimental investigations (STM), analysed and interpreted the data, wrote the manuscript. |

# $Xe_3^+$ Trimers: Stabilization of a linear Xe trimer in the DPDI quantum confinements

Aisha Ahsan *et al.,*

**Literature:**

The charged linear $Xe_3^+$ and $Xe_4^+$ clusters form the core of larger clusters and photo absorption cross sections depends on these charged linear cores.[1] Xe cluster physics: Photoabsorption cross section for $Xe_3^+$ and $Xe_n^+$ shows that positive charge can localize on a trimer and tetramer ion core and only these cores of trimer and tetramer are surrounded by neutral atoms.[2] In situ behaviour of $^{129}Xe$ in the nanochannels of tris-cyclotriphosphazene (TPP) observed with NMR measurements that showed Xe-Xe internuclear average distance is 0.54 nm. Since pore diameter of TPP is almost same size of van der Waals diameter of xenon, thereby confined atoms cannot bypass each other in nanochannel.[3]

**Distance calculation:**

- Xe atoms distance in dimer and trimer inside pore is shorter than for Xe adsorbed on bare Cu(111) surface.
- Xe-trimer is stable and linear in quantum confinement.
- Could be no other reason than $Xe_3$ or $Xe_3^+$ in quantum confinement because of its stability and linearity otherwise it could be cluster or banana shape like other occupancies.[4–8]

Here in the STM image and table below, is measurement of distance between Xe atoms as linear dimer and trimer in DPDI pore.

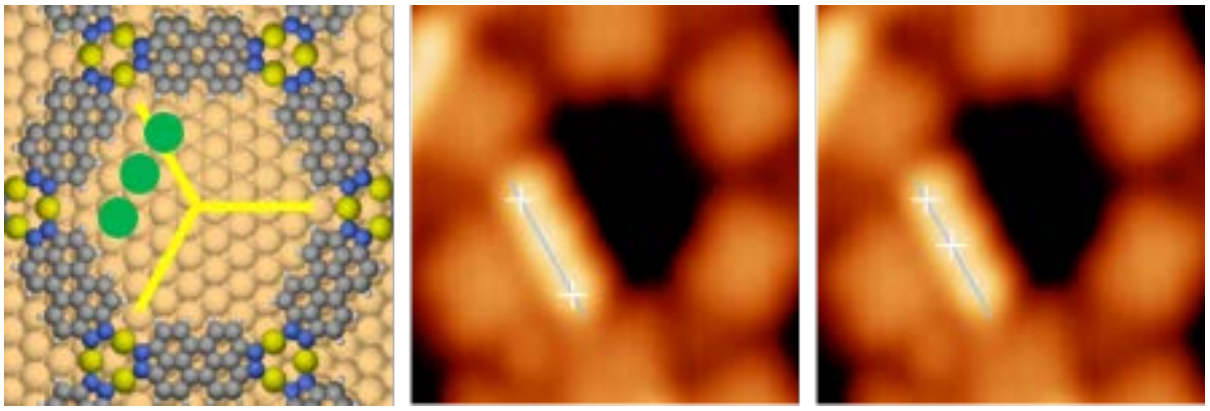

**Figure 1: Distance calculation between Xe trimer atoms in quantum confinement.**

| Xe-occupancy | Distance (STM) in pores | Distance calculated on bare surface | Distance (published) | Ionization Energy (vacuum) |
|---|---|---|---|---|
|  | 0.445 nm<br>4.45 ˚A | 0.475 nm<br>4.75 ˚A<br><br>*+6.7% bigger* | 0.4363 nm ($Xe_2$)<br>J. Chem. Phys. 138, 104313 (2013)<br>0.308 nm ($Xe_2^+$)<br>Drews / Seppelt Angew. Chemie Int. Ed. 1997, 36, 3 273 f<br>{$Xe_2^{+2}$ $Xe_2^o$}<br>Dimer is smaller in vacuum | 33.11 eV ($Xe_2^+$)<br>R. Dutil, P. Marmet, International Journal of Mass Spectrometry and Ion Physics 35, (1980) 371-379 |
|  <br>  | 0.38 ± 0.02 nm<br>3.8 ˚A<br><br>0.757 nm<br>7.57 ˚A | 0.415 nm<br>4.15 ˚A<br>*+9.2% bigger*<br><br>0.836 nm<br>8.36 ˚A<br>*10.4% bigger* | 0.327-0.368 nm<br>J. Chem. Phys. 131, 214302 2009<br><br>0.654-0.736 nm | 64.35 eV ($Xe_3^+$)<br>R. Dutil, P. Marmet, International Journal of Mass Spectrometry and Ion Physics 35, (1980) 371-379 |

**Table 1:** Distance calculation in dimer and trimer of Xe in pores of DPDI and also some comparison with literature**.**

Here we have some results from DFT calculations (peformed by Jonas Bjoerk, University of Linkoeping, Sweden), in the following, adsorption energy $E_{\text{ads}}$ is defined as

$$\mathbf{E_{ads} = E_{3Xe@Cu(111)} - E_{Cu(111)} - 3E_{Xe}}$$

where $E_{3\text{Xe@Cu(111)}}$ is the total energy of three Xe atoms on Cu(111), either on clean surface or in DPDI network on surface, $E_{\text{Cu(111))}}$ the total energy of the Cu(111) surface without Xe (with or without DPDI network) and $E_{\text{Xe}}$ the total energy a Xe atom in the vacuum. Thus, $E_{\text{ads}}$ gives the total adsorption energy of the three Xe atoms.

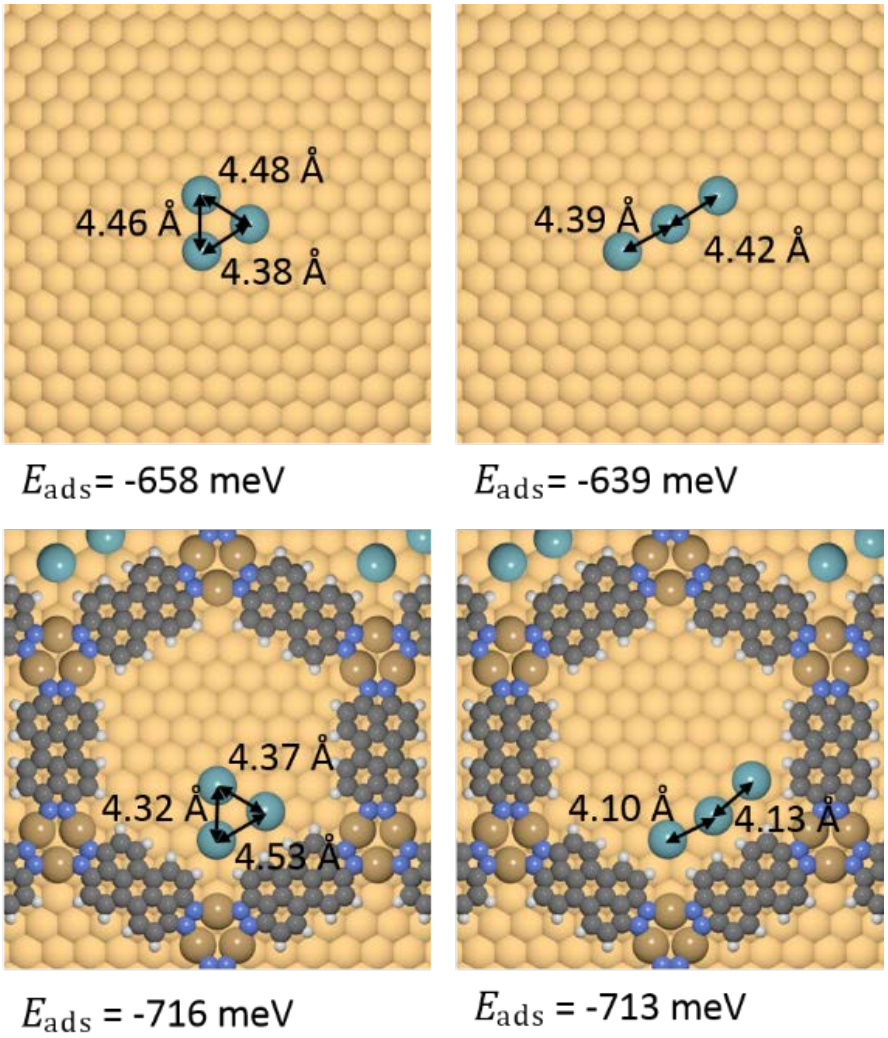


**Figure 2: DFT calculations of trimer xenon in DPDI pore.** The system is reported by the theoretician very difficult to calculate as it is very shallow in the energy landscape. The shortest trimer is also the most linear one, but in DFT the linearity is not as perfect as the experiment. The energy resolution at this DFT level is not sufficient to map energy minima at 5K – which is the experimental temperature.

**STM hopping calculation**:

Here in the Figure-3 below, STM Xe mobility traces have been measured for occ-3 of Xe atoms in the DPDI pore. This experiment is performed by using current verses time plots after halting the tip at a single point above the moving atoms inside the confinement. The monitoring started at 4K but there was no sign of hops until 7.5K. In the occ-3 pore at 8k the hopping starts in a way very different to other occupancies like occ-4—occ-6. There is also comparison to other occupancies, in Figure-4, started at 8k which is way different than the hopping at occ-3. This provides some evidence of occ-3 being present as a stable trimer $Xe_3$ or $Xe^{+}_3$ in the on-surface confinement. At higher temperatures i.e. ~>9.5K this trimer breaks up into single atoms as clear from independent hops with no broader width.

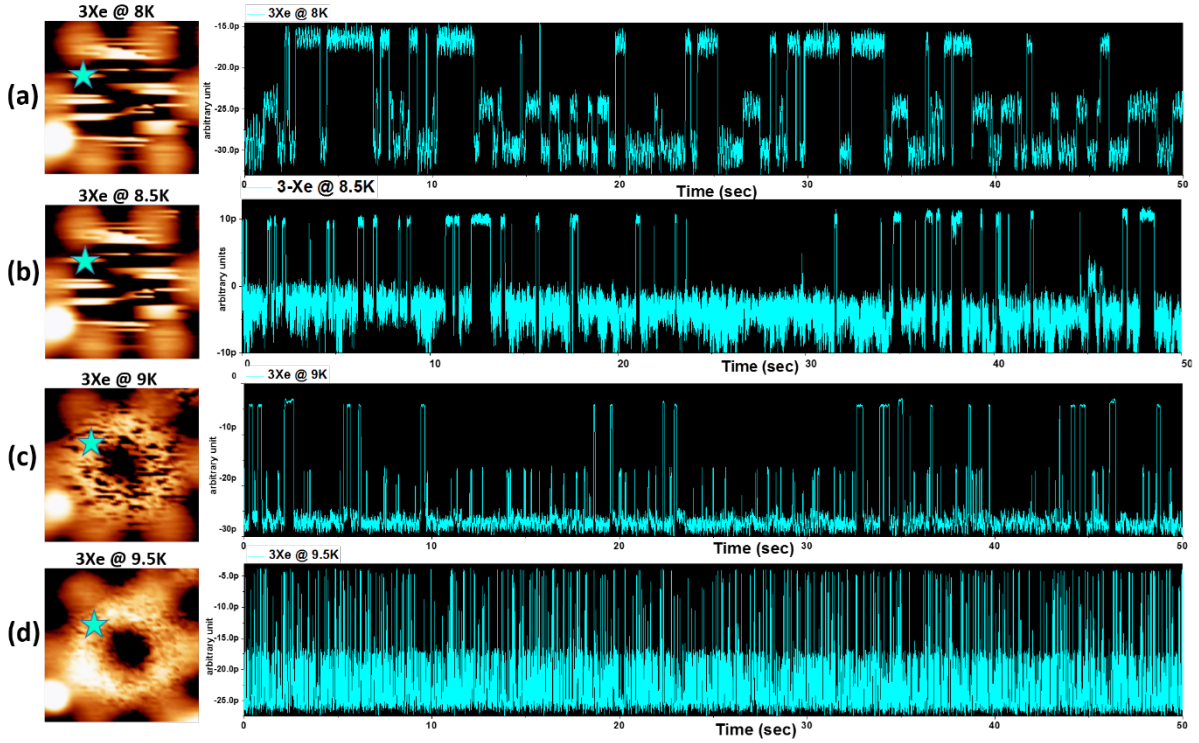


**Figure 3: Evidence of linear charged $Xe_3^+$ trimer footprints in DPDI pore.** a, b, c, d) Current versus time I(t) plot recorded at 8 K, 8.5K, 9K and 9.5 K in the pore containing linear Xe-trimer. The measurement has been performed at the tip position indicated by the blue star in the STM micrograph (inset). a) The broad width of the spikes in the tunnelling current imprints provide evidence for the presence of a larger entity, possibly the Xe3 trimer moving in the pore at 8 K, (b) the width of the spikes is reducing with increasing temperature to 8.5K, (c) the broadness in spikes almost vanishing at 9K, and (d) independent spikes deliver evidence for the breakup of trimer into individual Xe atoms below at higher temperature 9.5 K. Furthermore, the comparison with other occupancies see Figure-4.

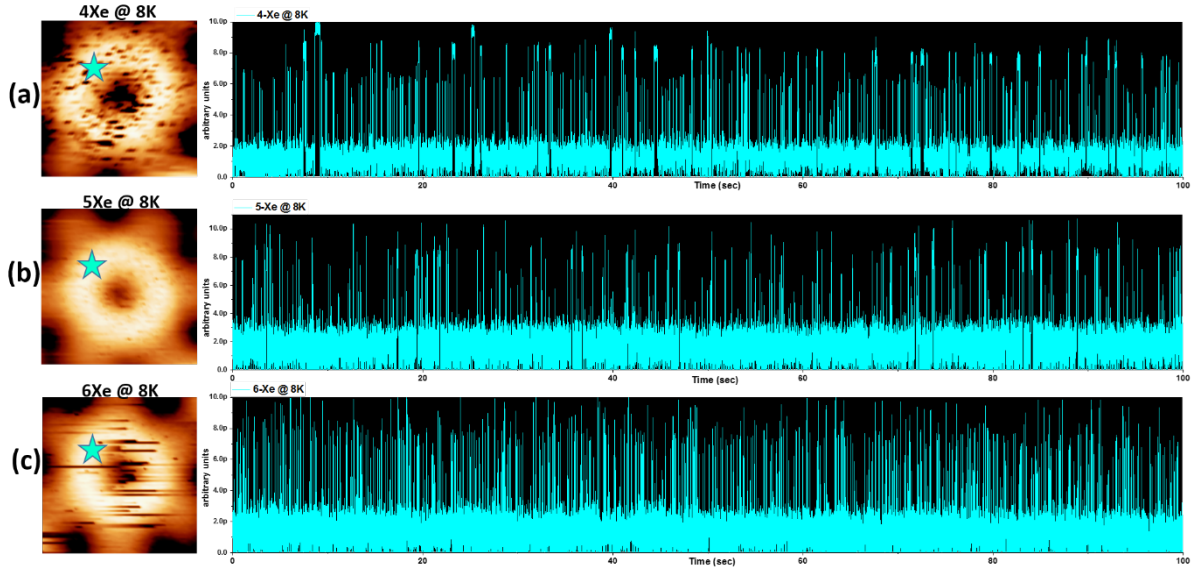


**Figure 4: Hopping of occ-4—occ-6 in pore.** a-c) Current versus time I(t) plot recorded at 8 K for occ—4-6 in the pore. The measurement has been performed at the tip position indicated by the blue star in the STM micrograph (inset). In all STM footprints the independent hops show the individual Xe atoms below. All these (occ-4, occ-5, occ-6) tip excursion trajectories taken at 8K look similar to occ-3 at 9.5K.

**STM Pulse induced excitation experiments**:

A local field has been applied by the STM tip held at a fixed position above a certain pore occupied with '**occ-n**'. These experiments are all performed at 4K for Xe **occ-1-6** in pores. In all cases voltage parameters have been found to induce excitations from the condensed state to the mobile state. In each occupancy case this slow 'pulsing' is performed in the centre of the pore. In a first series of investigations the holding time at elevated voltage was experimented with. For each occupancy case the voltage is such determined that the Xe excitation is observed with a considerable and optimized success rate (~ typically 65%) Sample-negative voltage pulsing at -5 V was observed to start rotation Fig 5(b,c) while sample-positive voltage pulsing at +5 V stopped 4-Xe rotating atoms inside the pore Fig 5(d,e). The dynamicity of the Xe atoms after their 'solid to fluid' transition was monitored in STM time-lapse imaging sequences following the initial excitation experiment. Very remarkably the excited mobility persisted for variable durations in the order of minutes which provides an unexpectedly slow relaxation of the Xe in its excited state at close to 4K. In all observed cases, however, the system relaxed to a state which was typically identified as containing many less atoms in the pore. The atoms leaving the box were at times identified to reposition to one or the other of the neighbouring node positions. We take this slow evolution of the excited state as evidence for the very limited interaction of the excited Xe with its surrounding pores. In the analysis of this behaviour, we assign a key role to the quantum well state present in the pore. This state, which has been observed to repulsively interact with Xe:[9] Xe can only be taken out, but not pushed in—at least for lower filling levels that weakens the Xe adsorption in the pore in comparison to Xe directly adsorbed on Cu(111) terraces. This interaction is reflected also in a modified quantum well state.[10] Thereby the system is characterized by Xe atoms with a reduced binding to the bottom substrate but surrounded by the metalorganic DPDI network which provide confining barriers for Xe atoms also in their excited states. To what effect the small size of the quantum box and the nature of the confinement are also destabilizing the Xe clusters compared to similar sized clusters on extended surfaces remains to be investigated e.g. by an in-depth theoretical analysis. This reliably (60%) induces condensation of the Xe inside the pore and there has been no evidence from our experiments that in this process Xe is prone to leave the sample. It is important to note that the excited mode induced by 'destabilizing' ramps and the thermally induced mobile mode are inequivalent as recognized by comparing Fig. 5c and 5d. This is not too surprising as a thermal excitation will be more uniformly inducing all available degrees of freedom of the Xe atoms while the tip bias will predominantly act in out of plane direction.

We assign the excitation / dexcitation of the Xe in the confinement to the polarity dependent stabilization or destabilization of the polarization of Xe in the surface dipolar field as depicted in Fig 5. Xe atoms are adsorbed with a considerable dipole moment pointing away from the Cu(111) surface, by its interaction with the surface. This polarization may be further strengthened due to the surface state present in the pore[11]. As also reported by, the adsorption strength of noble gases scales with the size of their polarizable electron shell. This indicates that a modified polarisation – here by an external applied field, leads to destabilization or stabilisation of the Xe in either the surface adsorbed state or in its excited mode above the surface.

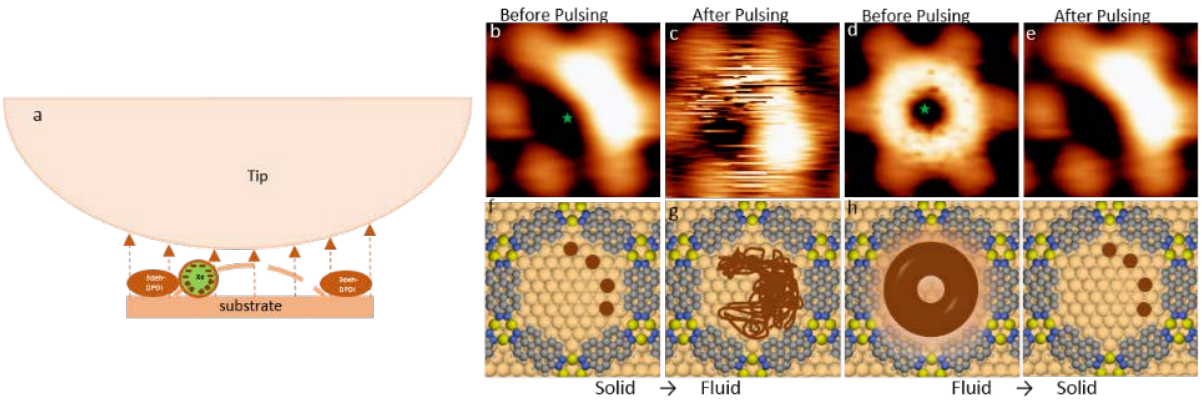


**Fig. 5 STM bias voltage induced phase transition in quantum confinements.** (a) Shows schematic sketch of an ideal tip asperity above one singly Xe occupied by quantum confinement. The central pore brown dashed line indicates the electron density of the confined state. Arrows indicate the electric field (estimated magnitude) which is applied to induce the phase transition in quantum confinement. Note that the tip radius has been taken from Field Ion Microscopy studies. STM micrographs of quantum confinements containing 4 Xe atoms measured in constant height mode (b, d) before and (c, e) after a voltage ramp has been provided with a holding time of 300 – 2000 msec. Applying a voltage ramp with +5 V sample bias in the center of the quantum box destabilizes the polarization dipole in the Xe and transforms adsorbates from (b) fixed adsorption to the (c) mobile mode. Reversely, upon applying a voltage ramp with a peak voltage of -5 V to the sample, the initially mobile **occ-4** (d) is forced to condense (e). The green asterisks indicate the position of STM tip upon applying the voltage ramps. In the second row, corresponding atomic models have been provided (f-i). (STM images size 3nm x 3nm, tunnelling parameters: I = 10pA, V = 1V; STM pulse parameters I = 10pA, V = 1V, Pulse Voltage (b) -5V and (d) +5 V).

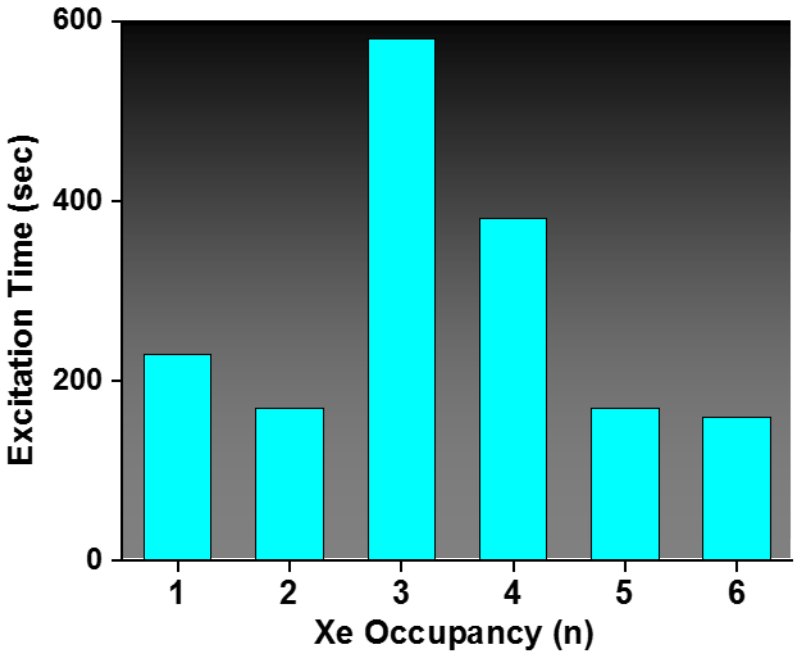


**Table 2: Histogram of STM pulsed excitation time of occ—1-6.** In this graph it is the pulsed excitation

time for occ-3 is higher than the other occupancies. Related time lapse images of occ—1-6 are in figure-3 below.

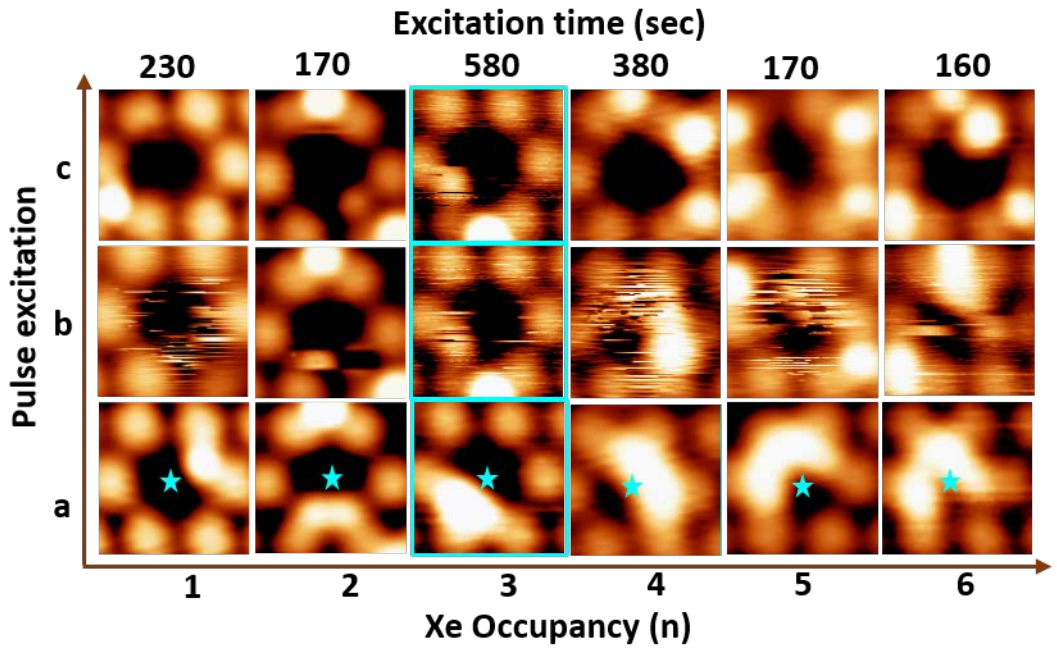


**Figure 6: STM Pulse induced excitation in confinements.** Horizontal axis shows Xe occupancy in bottom with corresponding duration of the excitation dynamic state inside pore on top, as observed in STM time-lapse imaging sequences. STM images measured at constant height before (a), after (b) the voltage pulse and (c) until adsorption on the nodes of pore. Blue asterisks indicate the position of STM tip upon pulsing. In all cases after the pulse Xe atoms are diffusing until their adsorption on the node of the network. The 580 sec excitation time for linear trimer is much higher than dimer and tetramer. (STM images size 3 nm x 3 nm, tunnelling parameters: I = 10pA, V = 1V, scan speed = 6 nm / sec, scan time = 2 min 8 sec; STM pulse parameters I = 10pA, V = 1V, Pulse Voltage -5V)

In conclusion, most remarkable property of the presented system is the exceptionally long relaxation times (~ min) of the Xe after excitation which is indicative of a very weak coupling of the atoms to their environment. Remarkably, the excited mobility persisted for variable durations in the order of minutes which provides an unexpectedly slow relaxation of the occ-3 Xe in its excited state, close to 4K. In all observed cases, however, the system relaxed to a state which was typically identified for containing much less atoms in the quantum box. We take this slow evolution of the excited state in case of occ-3 as evidence for the existence of trimer $Xe_3^+$ as compared to the relaxation time of other occupancies.

## References:


1. Oliveira, M. J. T., Nogueira, F., Marques, M. A. L. & Rubio, A. Photoabsorption spectra of small cationic xenon clusters from time-dependent density functional theory. *J. Chem. Phys.* **131,** 214302 (2009).
2. Haberland, H. *et al.* Electronic and geometric structure of Ar n + and Xe n + clusters: The solvation of rare-gas ions by their parent atoms. *Phys. Rev. Lett.* **67,** 3290–3293 (1991).
3. Kobayashi, H., Ueda, T., Miyakubo, K. & Eguchi, T. Intermolecular Interactions of Xe Atoms Confined in One-dimensional Nanochannels of Tris(o-phenylenedioxy)cyclotriphosphazene as Studied by High-pressure 129Xe NMR. *Z. Für Naturforschung A* **58,** (2003).
4. Nowakowska, S. *et al.* Interplay of weak interactions in the atom-by-atom condensation of xenon within quantum boxes. *Nat. Commun.* **6,** 6071 (2015).
5. Drews, T. & Seppelt, K. The Xe2+ Ion—Preparation and Structure. *Angew. Chem. Int. Ed. Engl.* **36,** 273–274 (1997).
6. Emmons, E. D. *et al.* Photoionization and electron-impact ionization of Xe 3 +. *Phys. Rev. A* **71,** (2005).
7. Formisano, F., Barocchi, F. & Magli, R. Long-range interactions in xenon. *Phys. Rev. E* **58,** 2648–2651 (1998).
8. Bressanini, D. & Morosi, G. What Is the Shape of the Helium Trimer? A Comparison with the Neon and Argon Trimers. *J. Phys. Chem. A* **115,** 10880–10887 (2011).
9. Nowakowska, S. *et al.* Interplay of weak interactions in the atom-by-atom condensation of xenon within quantum boxes. *Nat. Commun.* **6,** 6071 (2015).
10. Nowakowska, S. *et al.* Configuring Electronic States in an Atomically Precise Array of Quantum Boxes. *Small* (2016). doi:10.1002/smll.201600915
11. Lobo-Checa, J. *et al.* Band Formation from Coupled Quantum Dots Formed by a Nanoporous Network on a Copper Surface. *Science* **325,** 300–303 (2009).

# Supporting Information

# $Xe_3^+$ Trimers: Stabilization of a linear Xe trimer in the DPDI quantum confinements

**Contents**



## 1. Methods

### Sample preparation and STM measurement:

The samples are prepared and examined in an ultrahigh vacuum (UHV) system with a base pressure of 6 x $10^{-11}$ mbar. The Cu(111) crystal (MaTecK GmbH) is prepared by rounds of $Ar^+$ sputtering at E = 1 KeV performed at room temperature followed by annealing at 480 $^oC$. The DPDI molecules are deposited with the use of nine-cell commercial evaporator (Kentax, GmbH, Germany) on the Cu(111) by sublimation at ~240 $^oC$ and the rate is controlled before deposition by a quartz crystal microbalance. After deposition, the sample is annealed to 300 $^oC$ in order to convert DPDI into 3deh-DPDI, which crafts the Cu-coordinated network. Xe of purity 99.99% is dosed to the sample placed in the STM (Omicron Nanotechnology GmbH) functioned at 4.2 K, with the cryoshields open and the leak valve being in straight shot with the sample. STM data acquired after exposure of the Cu-coordinated 3deh-DPDI network to 120 L of Xe performed at a pressure equal to 1.3 x $10^{-7}$ mbar for 1,200 s causing the increase in the sample temperature to 9 K. Xe is found to be adsorbed in the pores as well as in the nodes of the network. Then with closed cryoshields, temperature is progressively raised up from the thermal equilibrium in the He cryostat (~4.2K) by resistive heating to a maximum temperature of 10K by using a temperature controller [LakeShore-331] at 0.2 K/min, experiments are performed at each required temperature by switching off the temperature ramping.

STM measurements are performed in the constant current mode with Pt–Ir tips (90% Pt, 10% Ir), prepared by mechanical cutting followed by sputtering and controlled indentation in the bare Cu(111). The STM images are acquired with such prepared metallic tip. To avoid modification of the condensates via interaction with the tip, the sample bias is selected 1V whereas the tunnelling current set 10 pA. To further assess the dynamics within the confinements, the STM tip is used as a fixed probe at certain positions (middle and periphery) of the pores to measure the tunnelling current fluctuations which are caused by the presence or absence of Xe, which is dependent on the diffusive motion of the Xe in the pore.

Points: 50,000-100,000, sample bias = 2 volts, set current = 60pA, sweep time = 102 s, initial setting time = 5 msec

**2. DFT calculations (text and images from Jonas Bjoerk).**

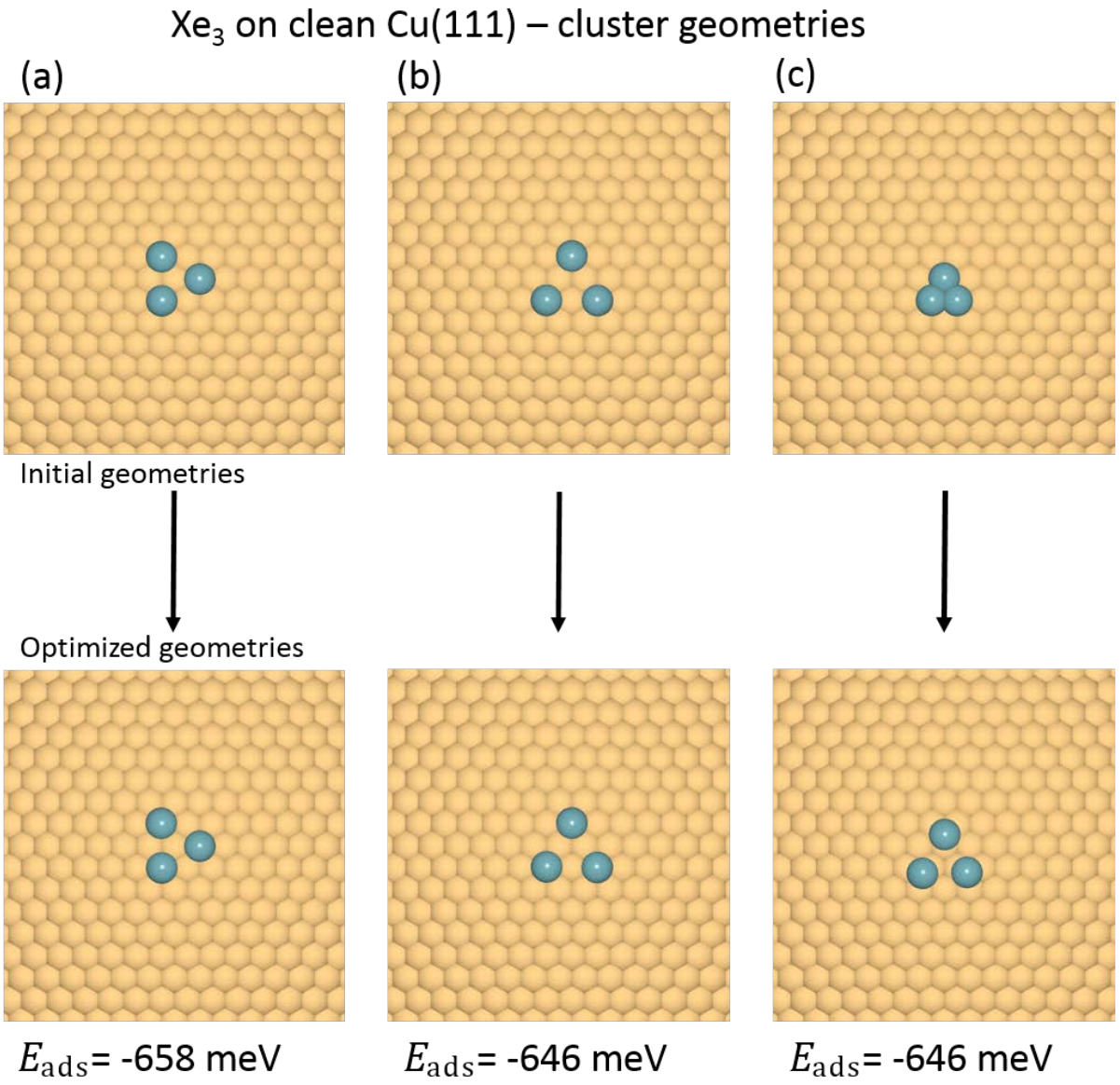

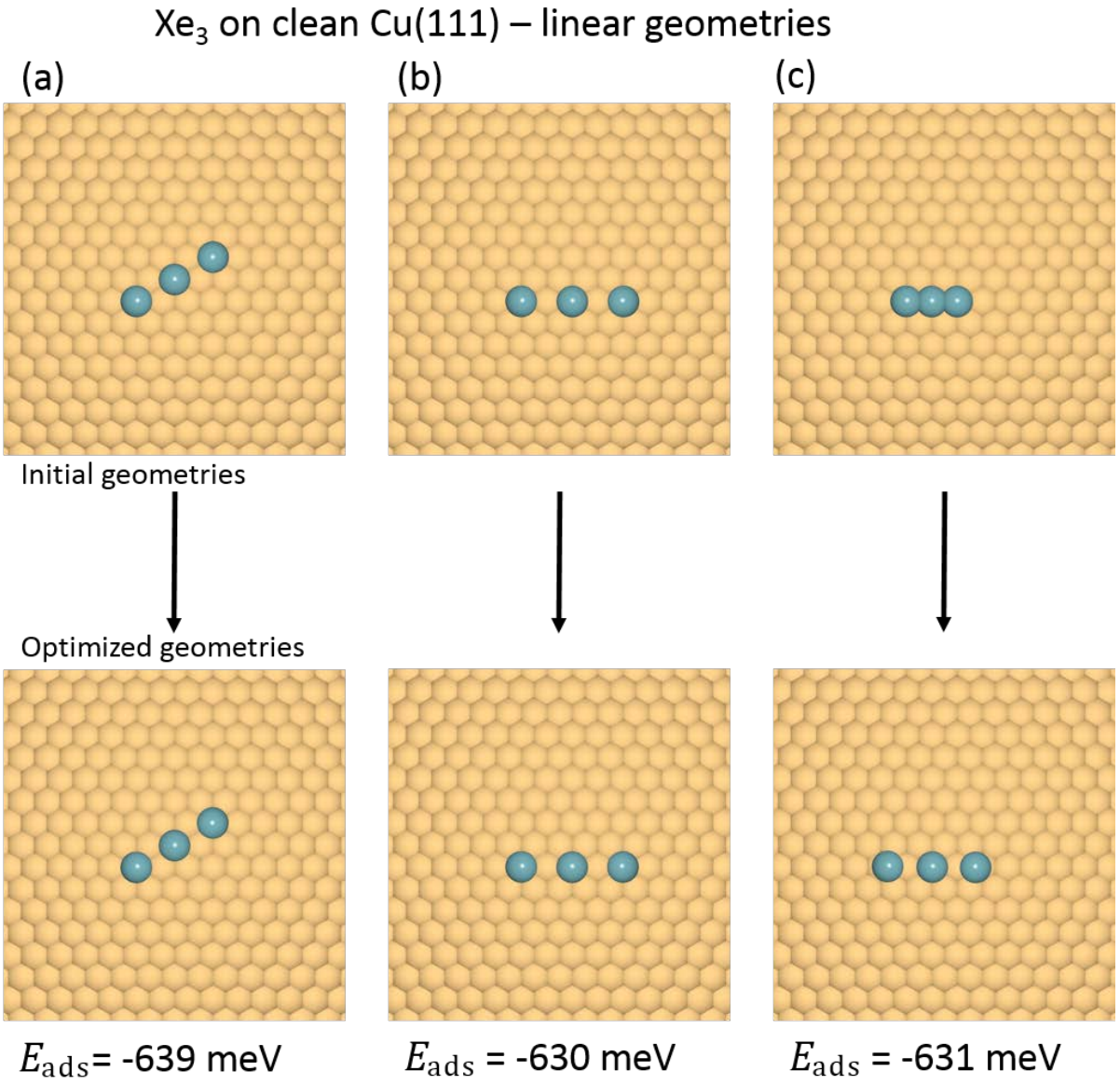
Xe3 on clean Cu(111) – linear geometries
(a)
(b)
(c)
Initial geometries
Optimized geometries
Eads= -639 meV
Eads = -630 meV
Eads = -631 meV

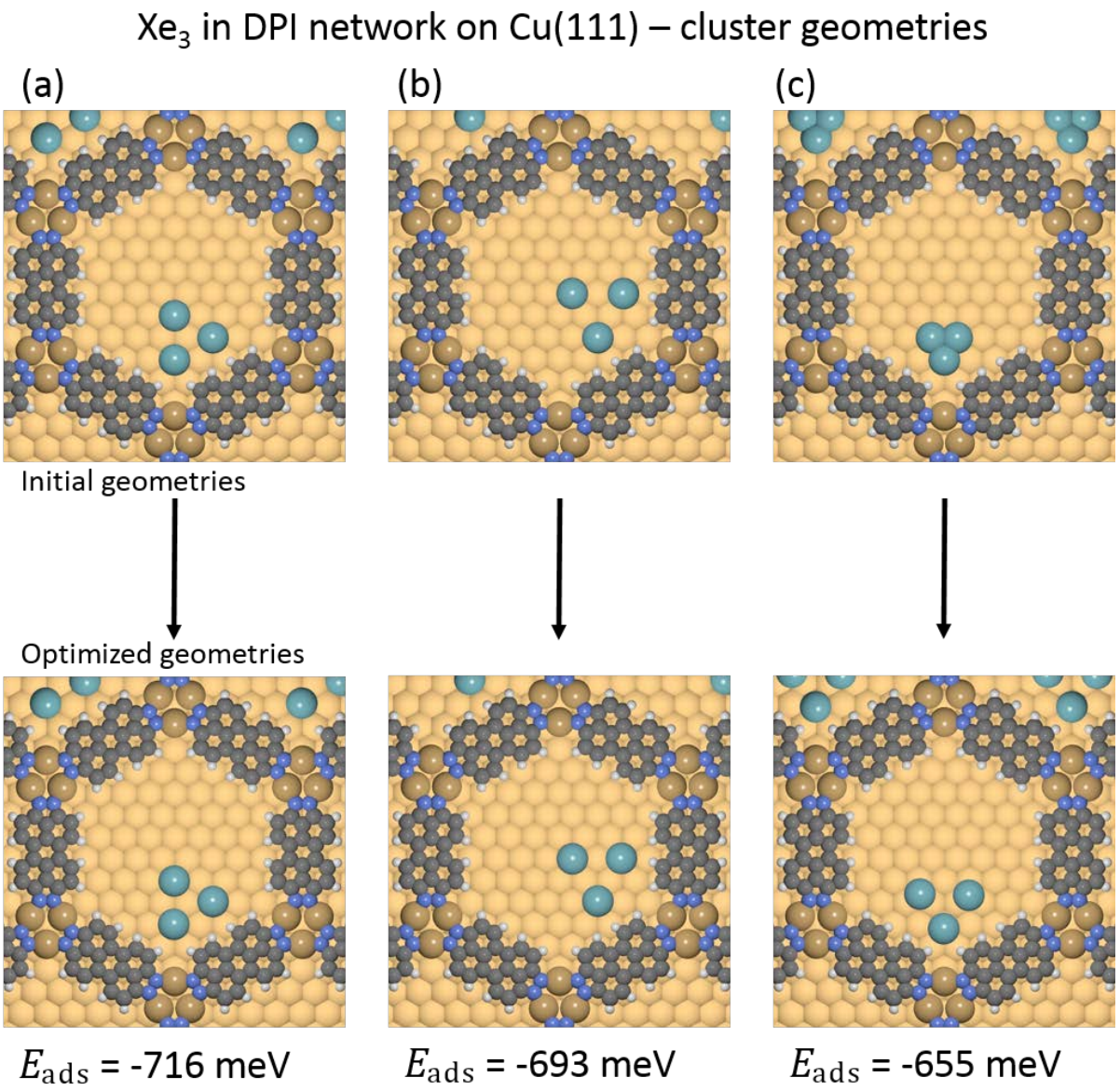
Xe3 in DPI network on Cu(111) – cluster geometries
(a)
(b)
(c)
Initial geometries
Optimized geometries
Eads = -716 meV
Eads = -693 meV
Eads = -655 meV

Xe$_3$ in DPDI network on Cu(111) – linear geometries 1

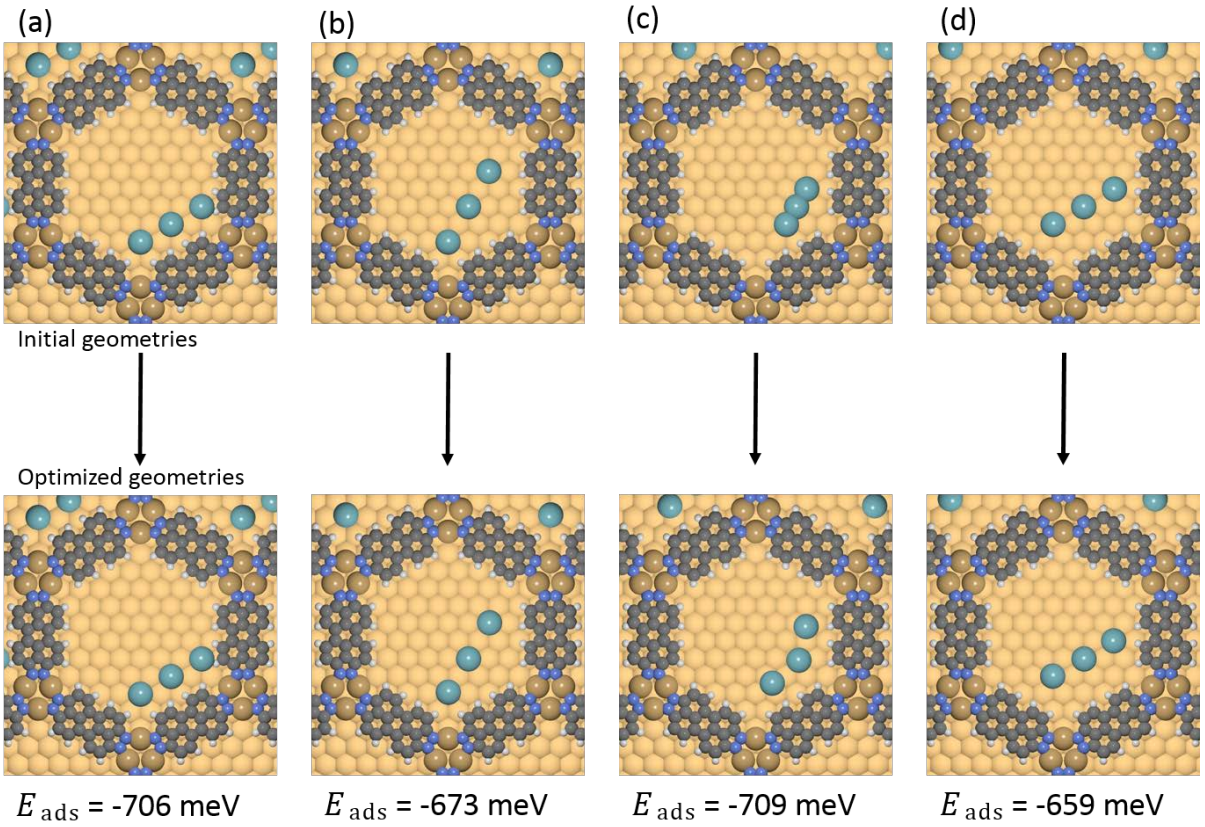


Xe$_3$ in DPDI network on Cu(111) – linear geometries 2

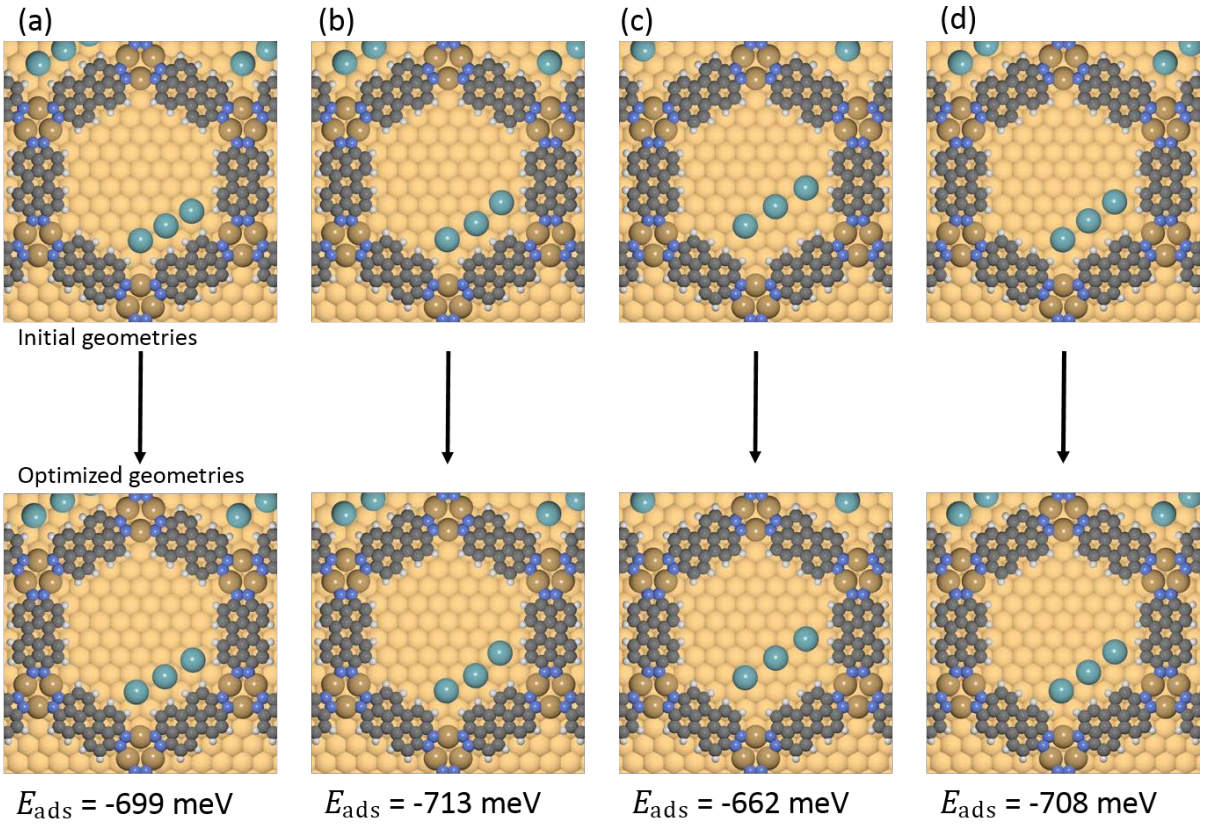

# Chapter [[4]] and Supplementary Information

| | |
|---|---|
| [[4]] | **Size dependent molecule by molecule condensation of cyclo-alkanes in on-surface nano-traps** |
| | Aisha Ahsan, S. Fatemeh Mousavi, T. Nijs, S.Nowakowska, Olha Popova, T. Nijs, J. Björk, L. H. Gade, T. A. Jung, *manuscript preparation.* |
| | Contribution of A. Ahsan: carried out experimental investigations (STM), analysed and interpreted the data, wrote the manuscript. |

# Size dependent molecule-by-molecule condensation of different cyclo-alkanes in confinements

Aisha Ahsan[a], S. Fatemeh Mousavi[a], Thomas Nijs[a], Sylwia Nowakowska[a], Olha Popova[a], Aneliia Wäckerlin[a,b], Jonas Björk[c], Lutz H. Gade[d], Thomas A. Jung[a,e]

[a]Department of Physics, University of Basel, 4056 Basel, Switzerland.
[b]Nanoscale Materials Science, Empa, Swiss Federal Laboratories for Materials Science and Technology, 8600 Dübendorf, Switzerland.
[c]Department of Physics, Chemistry and Biology, IFM, Linköping University, Linköping 581 83, Sweden.
[d]Anorganisch-Chemisches Institut, Universität Heidelberg, Im Neuenheimer Feld 270, 69120 Heidelberg, Germany.
[e]Laboratory for Micro- and Nanotechnology, Paul Scherrer Institut, 5232 Villigen PSI, Switzerland.

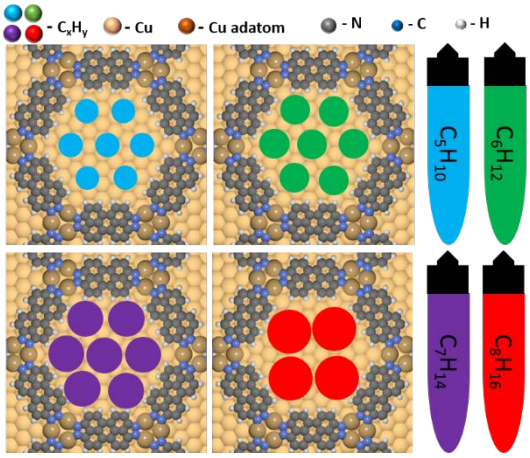


The condensation of cyclo-alkanes from cyclopentane to cyclooctane in the nanometer sized confinements of an on-surface metal organic coordination network is observed. It is conceptually interesting to probe condensation events in nanometer sized confinements for the investigation of inter-molecular and molecular-surface interaction forces in these cavities which are architecture with atomic precision. Molecule-by-molecule condensation is depicted by the Scanning Tunnelling Microscope, which provides direct real-space access to the aggregates and allows to monitor the structural evolution of the planar condensate from a single adsorbed molecule to the maximum size reachable in the pore. In such experiments the subtle interplay of different e.g. van der Waals, ionic forces as well as forces in e.g. electric fields and in the presence of specific electronic features of the pore can be investigated. Novel functional surfaces are expected as well as results to verify quantum chemical models.

## Results and Discussion

Understanding the adsorption and condensation of molecular species at solid surfaces provides one of the fundamental subjects during the evolution of surface science over the past half-century. In growth studies, the nucleation and adsorption of an ever-increasing number of molecules on crystallographic surfaces with steps and defect sites has been studied. Here, condensation is a fundamental process, and the interaction forces involved in the aggregation of atoms or molecules manage the structure of condensates.[1–3] Moreover at the nanoscale level, the properties of a condensate liable on its size, structure and bonding between the atoms or molecules. The condensation in a confinement usually proceeds under the competing influence of different forces, i.e. of the interacting walls and between the composing atoms or molecules.[4] The conformation of cycloalkanes is compromised by the tetrameric angle between the sp3 bonds linking to one C atom. This makes cycloalkenes particular interesting as depending on the number of carbon atoms in the ring different non-planar conformations occur which depending on the temperature exhibit different dynamics and affect the crystal packing, for example.[5–9]

We employ a highly ordered Cu-coordinated, triply dehydrogenated 4,9-diaminoperylene quinone-3,10-diimine (3deh-DPDI) porous network grown on Cu(111) as a template.[10] The electronic Shockley surface state of the underlying substrate is confined in the pores, resulting in a single quantum confinement state per pore.[11] Cyclo-alkanes mainly interact via van der Waals because of their closed shell architecture. Upon deposition of cyclo-alkanes onto the structured surface, the pores of the network were found to host a certain occupation distribution of cyclo-alkanes, as revealed in the scanning tunnelling microscopy (STM) overviews. The spontaneously occurring occupancies ranging from 0 to 7 molecules in case of $C_5H_{10}$-$C_6H_{12}$-$C_7H_{14}$ and 0 to 4 molecules with $C_8H_{16}$ cyclo-alkanes molecules are found across the pores as shown in Figure 1 (top) and the network areas shown in SI-1—SI4. Note that the occupancy of a pore is hereafter denoted as occ-0—occ-7. Figure 1 (bottom) presents the spatial arrangements of different cyclo-alkane molecules, with two different forms of aggregation being observed for occ-7 and occ-4.

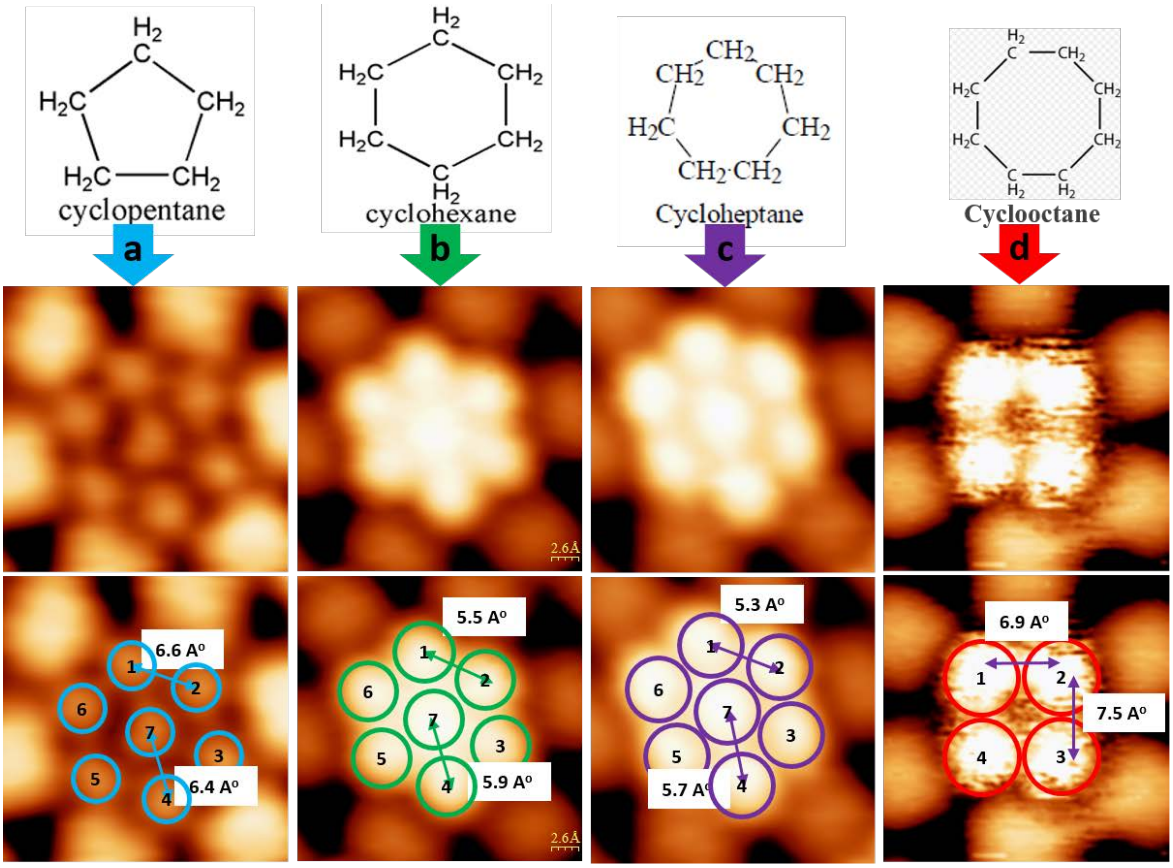


**Figure 1: Size dependent cyclo-alkanes condensation within quantum confinements influenced by van der waals forces.** *Top Row STM images*: Pores with different numbers of adsorbed cyclo-alkane molecules varying with their sizes from seven ($C_5H_{10}$, $C_6H_{12}$, $C_7H_{14}$) to four ($C_8H_{16}$) occupancy inside quantum confinement. *Bottom row STM images:* as a guide to the eye coloured circles (blue- $C_5H_{10}$, green- $C_6H_{12}$, indigo- $C_7H_{14}$, red- $C_8H_{16}$) have been added that define the adsorption position and the type of corresponding cycloalkanes in addition with the intermolecular distances (2.4 nm x 2.4 nm, 1V, 6pm).

For an analysis of the self-assembled patterns of cyclo-alkanes molecules within the pores, a closer inspection of the metal–organic surface structure is essential especially because of its

central quantum confinement state. Notably, no single cycloalkane molecule is observed to adsorb spontaneously in the centre of a pore. We attribute this behaviour to the repulsive interaction between centrally located quantum confinement state with the molecules. In contrast, the occupancy of CO molecules inside the pores of another on-surface network was found to preferentially adsorb in the centre of pores in the high electron density area.[12] In our case, the cycloalkanes prefer to adsorb around the outer rim of the confinement because of the centrally located quantum well state. Cyclohexane provides a special case in that it is mobile at single occupancy and in that it is not only observed at the outer rim. This indicates a reduced interaction of cyclohexane with the bottom substrate in the pore, which might possibly be attributed to the presence of the surface state and/or to the puckering.[13] Even in the case of single occupancy we identify unstable adsorption in the pore. This may be attributed to the puckering of the cycloalkenes and possibly assisted by the repulsivity of the confined state. Moreover, all observed condensates were found to be stable at full occupancy.

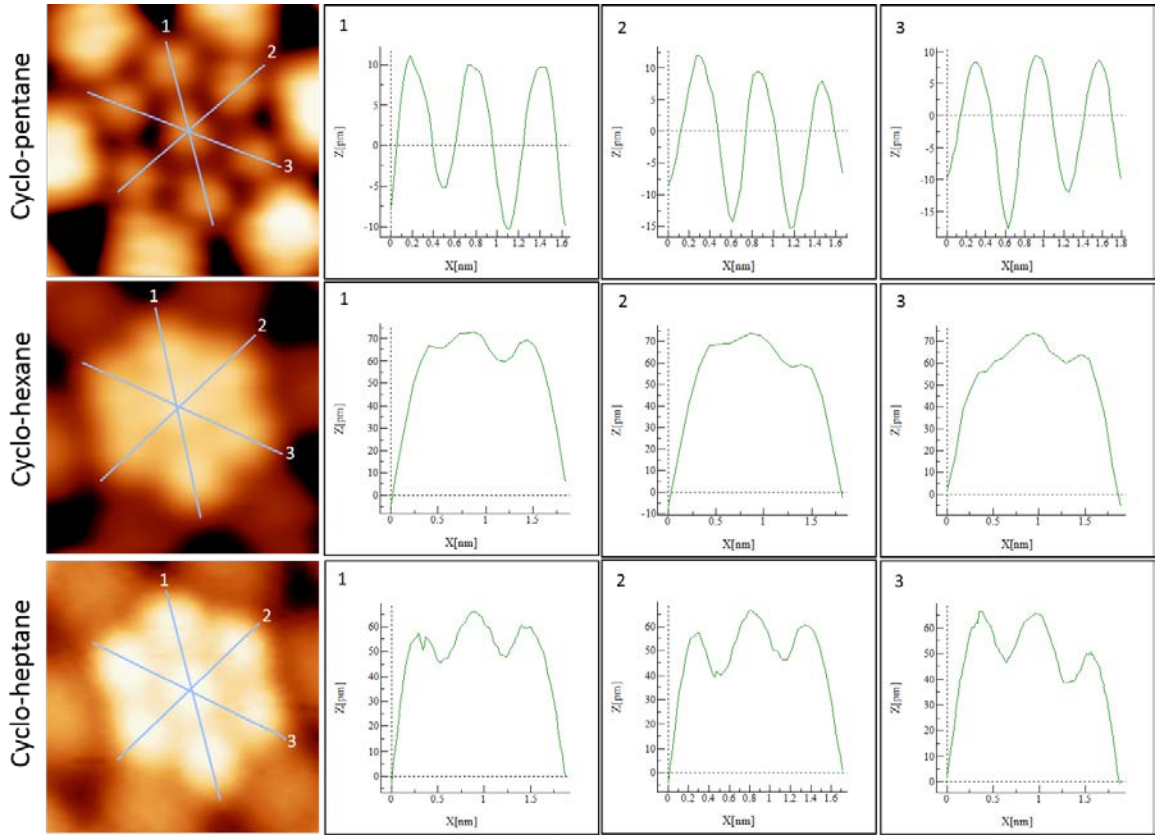


**Figure 2: Height profile analysis of cycloalkanes in the confinement of the DPDI pore.** *Top Row*: Pore with seven cyclopentane molecules found to be in planar configuration indicated by corresponding three line profiles with same height. *Middle row:* Pore with seven cyclohexane molecules found to be in different conformations indicated by corresponding three line profiles with varying height. *Bottom row:* Pore with seven cycloheptane molecules found to be in different conformation configuration indicated by corresponding three line profiles with varying height importantly with higher adsorbed position of central molecule. (2.4 nm x 2.4 nm, 1V, 6pm).

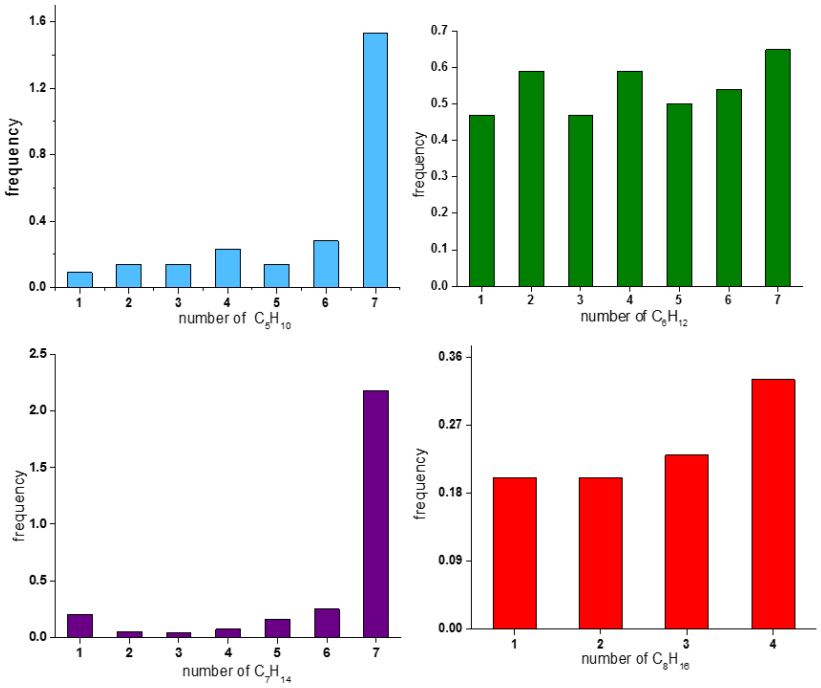


**Figure 3: Histogram of occupancy of pores**. The histogram of the occupancy of the pores obtained from one sample exposed to 120 L of cycloalkanes (separately-one by one) at 20K, resulting in the coverage Ø = 0.178 is displayed.

Figure 3 shows the histogram of pore occupancy (S1-1—SI-4) and reveals the presence of favoured occupancies, which may be related to particularly stable forms of condensates. The most favoured occupancies are occ-7 in case of especially cyclopentane and cycloheptane where condensates with greater occupancies (occ-0—occ-6) are significantly less frequently observed. Comparatively this sharp contrast is much less dominant in the cyclohexane case, where a slight preference for occ-7 is observed. The same trend of adsorption is observed in case of cyclo-octane with maximum occupancy 4 which occurs frequently. Notably there are differences between the different pores occupying the pores at the same occupancy. Some of the cases, in particular cyclohexane at single, chycloheptane at 1-3 fold occupancy and also cyclooctane at 4-fold occupancy exhibit some mobility. Also the STM apparent height of the different molecules is characteristically different, cyclopentane appears far lower than DPDI indicating a close contact with the metal surface, cyclohexane and cyclopentane both appear considerably higher than the DPDI and most interestingly, cyclooctane appears low in the case of occ-1 to occ-3, but high and dynamic in the case of occ-4. This may indicate that the cyclooctane does not fit any more in the pore, -- or not with a continuation of the trimeric structure of occ-3 – but rather is floating above the pore, possibly suspended by the confined quantum well state in conjunction with some conformational dynamics. Note that there are different conformations e.g. chair, boat and also there are ring flips possible while it is not exactly clear to what extent these can be activated at ~5K. The last interesting case is provided by cycloheptane which forms a ring structure unlike the compact structures of the other investigated alkanes. This ring strcture is then occupied between occ-5 and the maximum occ-7 in a nonstandard way in that first the center position is taken and then the last position at the border is occupied. The STM contrast of the center cycloheptane is different from the other molecules which indicates a different adsorption height.

Further research is needed to fully exploit the richness of this cycloalkane condensation and analyse the data with regard to the conformational flexibility.

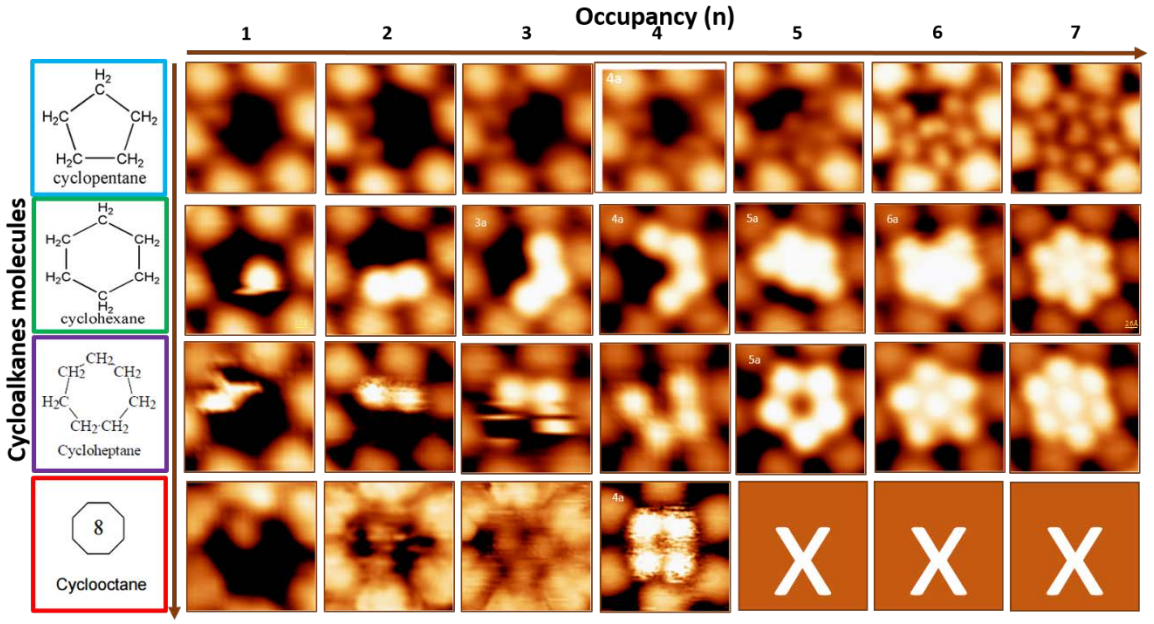


**Figure 4: Molecule by molecule self-assembly of cyclo-alkanes within quantum boxes.** STM images (2.4nm x 2.4nm) of pores with different numbers of cyclo-alkane molecules are indicated by the numbers placed along the horizontal axis at the top: time lapse images have been used to denominate condensates with the same number of cyclo-alkane molecules but in different arrangements. At the left side the vertical axis shows the choice of molecule from the cyclo-alkane series. STM parameters 1V, 6pA, image size 2.4 nm x 2.4 nm, pixels per frame: 256 px, scan speed 2nm/sec.

In summary, the molecule-by-molecule condensation of cyclo-alkanes in the pores of the Cu-coordinated 3deh-DPDI network results in a wide range of occupancies (occ-1—occ-7 & occ-1—occ-4) which do not follow a single set of 'hierarchic filling rules, but adapt their structures in the different regimes. This work demonstrates that the confinement of adsorbates in the pores of a metal–organic on-surface network provides the opportunity to study condensation under the influence of the subtle interplay of van der Waals forces with the effect of the different degree of puckering of the cycloalkanes and therefore their different stacking with single-molecule precision. The experimental resolution providing the real-space structure of molecular condensates adsorbed on an atomically defined patterned surface provides the unique opportunity to compare experimental data and theoretical models. We note that our approach can benefit from the comparison of the condensation behaviour in differently sized pores, as owing to that, the interference of weak interactions involved can be tuned, which is expected to be stronger/weaker with decreasing/increasing pore size.

## *References:*


1. *HANDBOOK OF NANOPHYSICS: clusters and fullerenes.* (CRC PRESS, 2017).
2. Lennard-Jones, J. E. On the Forces between Atoms and Ions. *Proc. R. Soc. Math. Phys. Eng. Sci.* 109, 584–597 (1925).
3. Jansen, J. & Dawson, L. M. On Intermolecular Forces and the Crystal Structures of the Rare Gases. *J. Chem. Phys.* 23, 482–486 (1955).
4. Nowakowska, S. *et al.* Interplay of weak interactions in the atom-by-atom condensation of xenon within quantum boxes. *Nat. Commun.* 6, 6071 (2015).
5. Bocian, D. F., Pickett, H. M., Rounds, T. C. & Strauss, H. L. Conformations of cycloheptane. *J. Am. Chem. Soc.* 97, 687–695 (1975).
6. Pakes, P. W., Rounds, T. C. & Strauss, H. L. Conformations of cyclooctane and some related oxocanes. *J. Phys. Chem.* 85, 2469–2475 (1981).
7. Hendrickson, J. B. Molecular geometry. V. Evaluation of functions and conformations of medium rings. *J. Am. Chem. Soc.* 89, 7036–7043 (1967).
8. Xiao, D. J., Oktawiec, J., Milner, P. J. & Long, J. R. Pore Environment Effects on Catalytic Cyclohexane Oxidation in Expanded Fe $_2$ (dobdc) Analogues. *J. Am. Chem. Soc.* 138, 14371–14379 (2016).
9. Kilpatrick, J. E., Pitzer, K. S. & Spitzer, R. The Thermodynamics and Molecular Structure of Cyclopentane [1]. *J. Am. Chem. Soc.* 69, 2483–2488 (1947).
10. Matena, M. *et al.* On-surface synthesis of a two-dimensional porous coordination network: Unraveling adsorbate interactions. *Phys. Rev. B* 90, (2014).
11. Lobo-Checa, J. *et al.* Band Formation from Coupled Quantum Dots Formed by a Nanoporous Network on a Copper Surface. *Science* 325, 300–303 (2009).
12. Cheng, Z. *et al.* Adsorbates in a Box: Titration of Substrate Electronic States. *Phys. Rev. Lett.* 105, (2010).
13. Nowakowska, S. *et al.* Configuring Electronic States in an Atomically Precise Array of Quantum Boxes. *Small* 12, 3757–3763 (2016).

# Supplementary Information

# Size dependent molecule-by-molecule condensation of cyclo-alkanes in confinements

**Contents**



## 1. Methods

**Sample preparation and STM measurement:**

The samples are prepared and examined in an ultrahigh vacuum (UHV) system with a base pressure of 6 x $10^{-11}$ mbar. The Cu(111) crystal (MaTecK GmbH) is prepared by rounds of $Ar^+$ sputtering at E = 1 KeV performed at room temperature followed by annealing at 480 $^oC$. The DPDI molecules are deposited with the use of nine-cell commercial evaporator (Kentax, GmbH, Germany) on the Cu(111) by sublimation at ~240 $^oC$ and the rate is controlled before deposition by a quartz crystal microbalance. After deposition, the sample is annealed to 300 $^oC$ in order to convert DPDI into 3deh-DPDI, which crafts the Cu-coordinated network. Cycloalkanes of purity 99% are frozen by liquid nitrogen and pumped well to and then separately dosed to the sample placed in the STM (Omicron Nanotechnology GmbH) functioned at 4.2 K, with the cryoshields open and the leak valve being in straight shot with the sample. SI-1 to SI-4 present STM data acquired after exposure of the Cu-coordinated 3deh-DPDI network to 120 L of each corresponding cycloalkanes performed at a pressure equal to 1.3 x $10^{-7}$ mbar for 1,200 s in the sample temperature to 20 K. all cycloalkanes are found to be adsorbed in the pores as well as around the network on bare surface. Then with closed cryoshields in the He cryostat (~4.2K) experiments are performed.

STM measurements are performed in the constant current mode with Pt–Ir tips (90% Pt, 10% Ir), prepared by mechanical cutting followed by sputtering and controlled indentation in the bare Cu(111). The STM images shown in Figure 1,4 and SI 1—4 are acquired with such prepared metallic tip. To avoid modification of the condensates via interaction with the tip, the sample bias is selected 1V whereas the tunnelling current set 6 pA.

## 2. $C_5H_{10}$---molecule by molecule condensation in Cu-coordinated DPDI pores

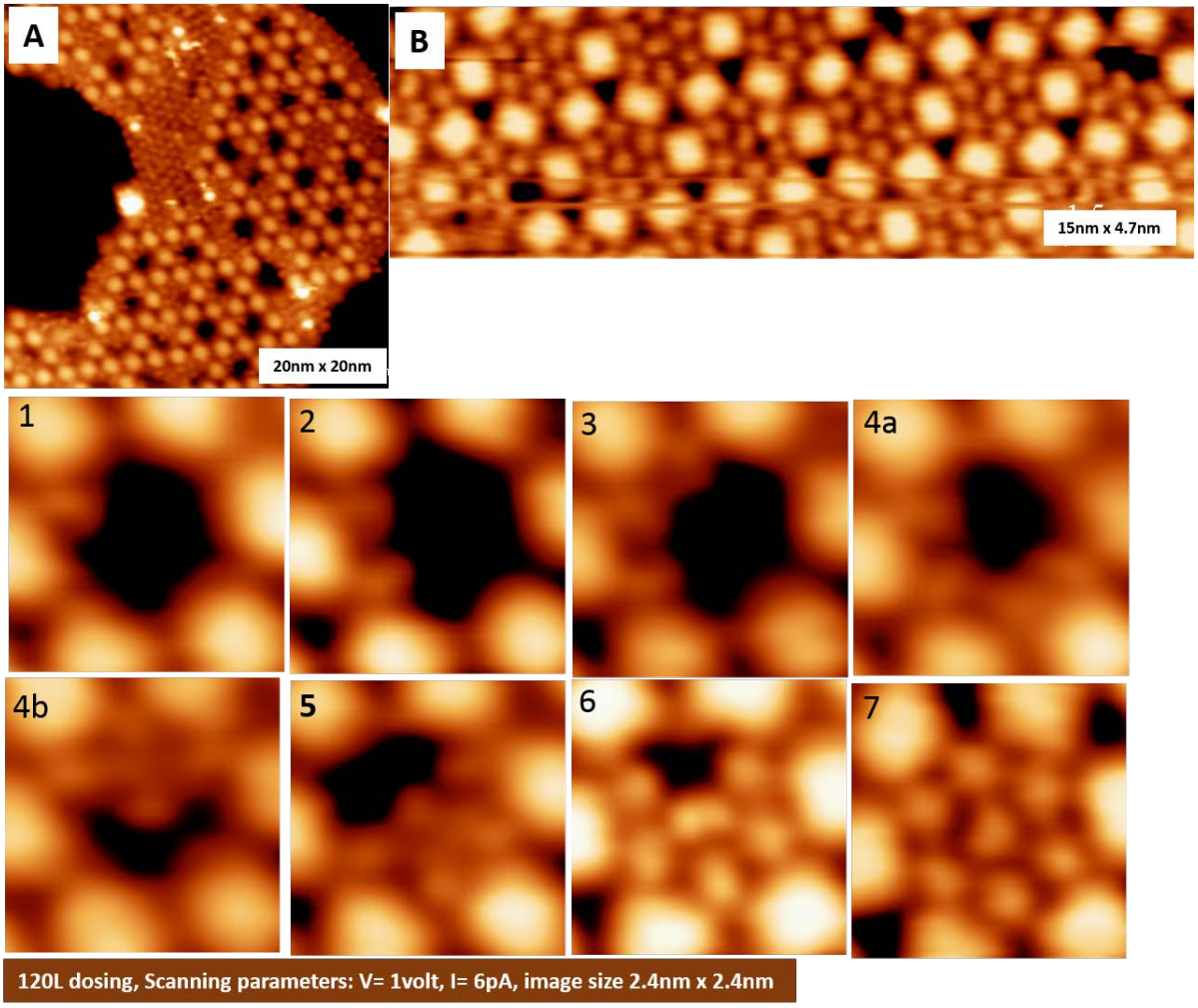


**Figure SI-1: Molecule by molecule self-assembly of cyclopentane within DPDI pores.** (A, B) Overview STM images with 120L dose of $C_5H_{10}$ exposed DPDI network sample at 20K resulting in pore condensation regimes with bare surface adsorption. At the bottom, STM images (2.4nm x 2.4nm) of pores with different numbers of cyclopentanes molecules are indicated by the numbers placed on top of horizontal axis with alphabetic letters denominate condensates with the same number of cyclopentanes molecules but having different arrangements. STM parameters 1V, 6pA, image size 2.4 nm x 2.4 nm, pixels per frame: 256 px, scan speed 2nm/sec.

### 3. $C_6H_{12}$ ---molecule by molecule condensation in Cu-coordinated DPDI pores:

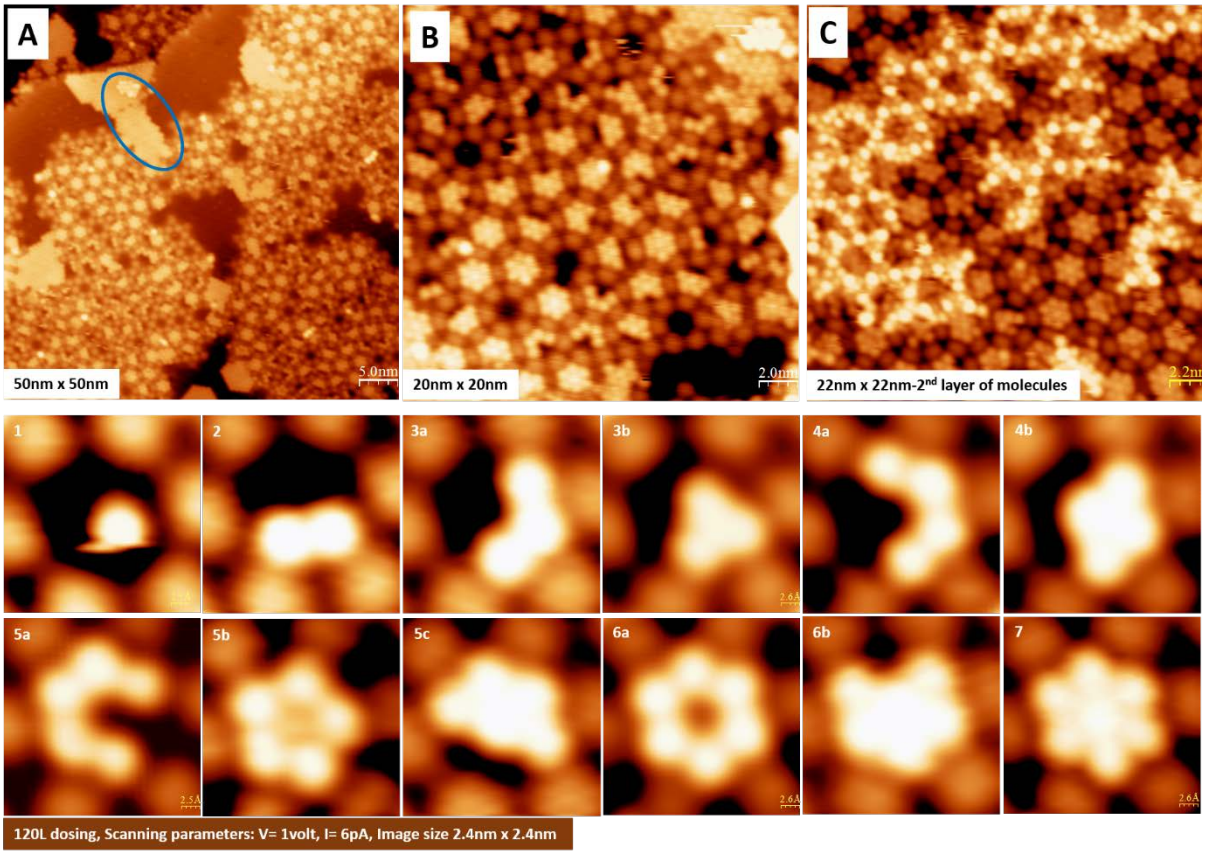


**Figure SI-2: Molecule by molecule self-assembly of cyclohexane within DPDI pores.** (A, B) Overview STM images with 120L dose of $C_6H_{12}$ exposed DPDI network sample at 20K resulting in pore condensation regimes with bare surface adsorption. (C) shows second layer absorption of molecules over the nodes of network with more 30L dosing at 20K over previously dosed sample. At the bottom, STM images (2.4nm x 2.4nm) of pores with different numbers of cyclohexane molecules are indicated by the numbers placed on top of horizontal axis with alphabetic letters denominate condensates with the same number of cyclohexane molecules but having different arrangements. STM parameters 1V, 6pA, image size 2.4 nm x 2.4 nm, pixels per frame: 256 px, scan speed 2nm/sec.

### 4. $C_7H_{14}$---molecule by molecule condensation in Cu-coordinated DPDI pores:

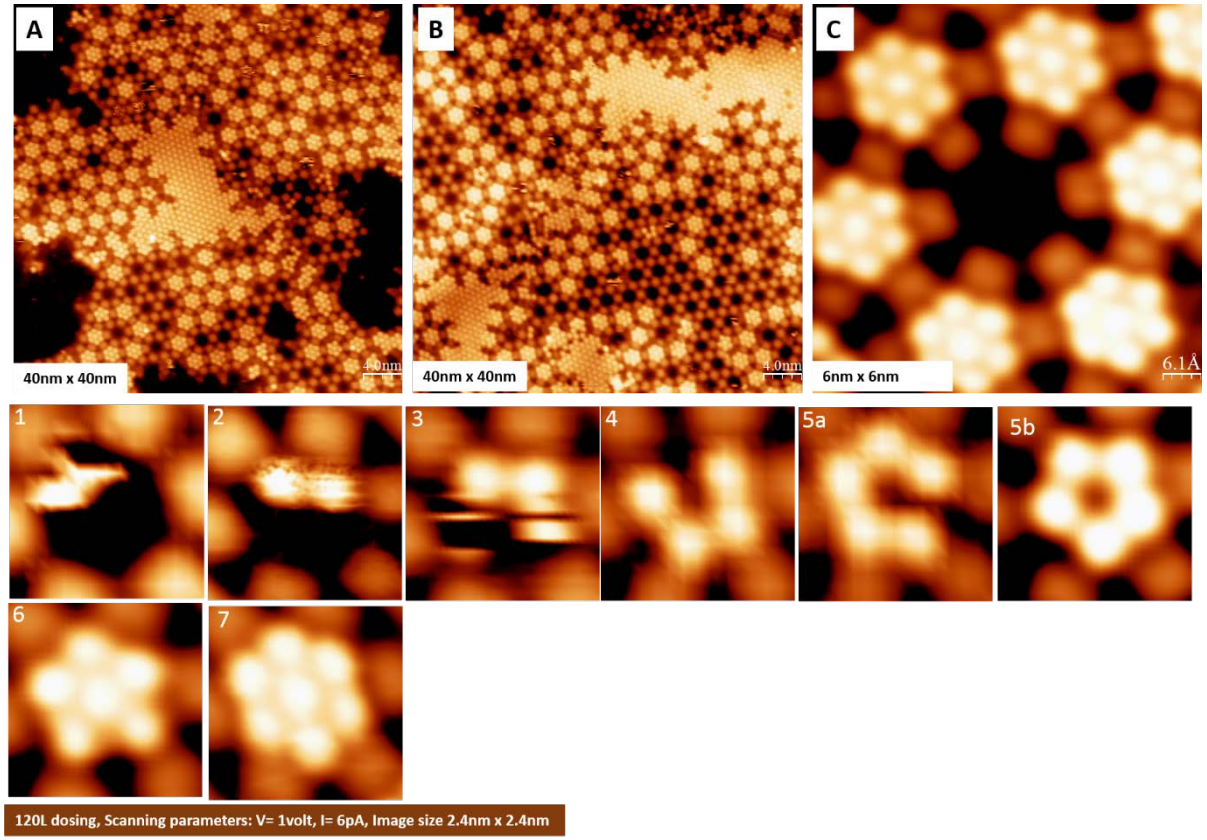


**Figure SI-3: Molecule by molecule self-assembly of cyclopheptane within DPDI pores.** (A, B) Overview STM images with 120L dose of $C_7H_{14}$ exposed DPDI network sample at 20K resulting in pore condensation regimes with bare surface adsorption. At the bottom, STM images (2.4nm x 2.4nm) of pores with different numbers of cycloheptanes molecules are indicated by the numbers placed on top of horizontal axis with alphabetic letters denominate condensates with the same number of cyclopheptanes molecules but having different arrangements. STM parameters 1V, 6pA, image size 2.4 nm x 2.4 nm, pixels per frame: 256 px, scan speed 2nm/sec.

## 5. $C_8H_{16}$---molecule by molecule condensation in pores.

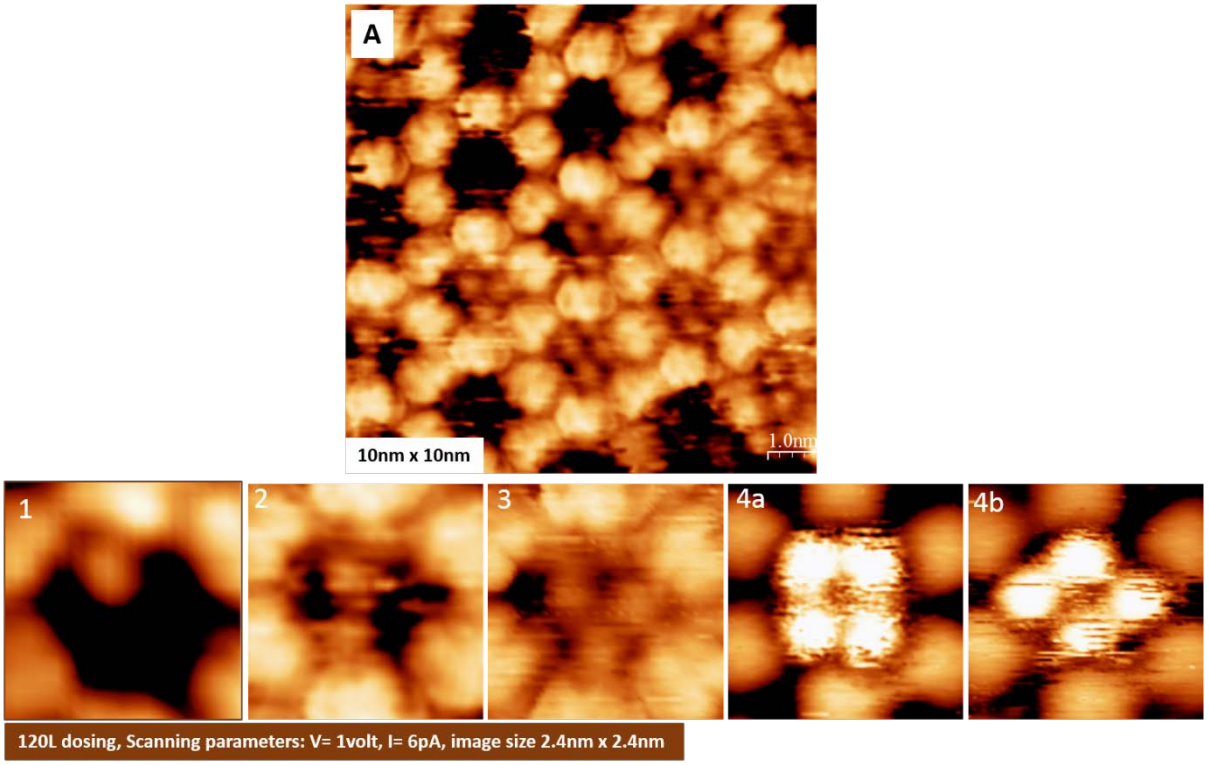


**Figure SI-4: Molecule by molecule self-assembly of cyclo-octane within DPDI pores.** (A) Overview STM images with 120L dose of $C_8H_{16}$ exposed DPDI network sample at 20K resulting in pore condensation regimes with bare surface adsorption. At the bottom, STM images (2.4nm x 2.4nm) of pores with different numbers of cyclo-octanes molecules are indicated by the numbers placed on top of horizontal axis with alphabetic letters denominate condensates with the same number of cyclo-octanes molecules but having different arrangements. STM parameters 1V, 6pA, image size 2.4 nm x 2.4 nm, pixels per frame: 256 px, scan speed 2nm/sec.

# Summary and outlook

In this thesis an innovative approach of a real space atomic level phase transitions investigation of the minimal number of condensates in confinements [[1]] as well as an achievement of fully atomically nucleated confinement arrays observed on a range of energy landscape [[2]], with a remarkable discovery of stable real space access to linear $Xe_3^+$ in on-surface confinement [[3]] and differently size dependent molecule-by-molecule condensation in confinements [[4]] are presented. The realization of these concepts utilized the capability of the scanning tunneling microscope (STM) tip to locally originate structural transformation in single adsorbates as well as the ability of self-assembled on-surface porous networks to trap different adsorbates (atoms & molecules) and to confine the surface state electrons. Therefore, each pore functions as a confinement (nano-trap) and a network can be viewed as a confinement array (nano-trap array). The first scheme comprised of xenon and a Cu-coordinated 3deh-DPDI network grown on Cu(111). Each pore of the network can host each number of xenon atoms ranging from 1 to 9. Our studies show that *globally* induced thermal activation of atomic level phase transition in condensates between their solid to fluid form is dependent on (i) the increasing temperature (ii) the number of confined atoms (iii) the registry of the underlying substrate (iv) the repulsive interaction between adsorbates and confinement state localized therein and (v) the attractive interaction between adsorbates and molecule. Moreover, STM fingerprint of the hopping signal analysed in the confinements at varying temperatures, allowing the determination of the Arrhenius activation energy for the site exchange. This system is also *locally* characterized by electric field excitation to assess active switching between mobile and static states of condensates [[1]]. This work is a fundamental achievement in that only very few (1-9) atoms change their phase behavior individually within a 2D confinement array. Also it is remarkable, that the patterning of such future 'patterned storage media' is provided by self-assembly and not by top-down nanostructuring. The latter provides a major hurdle for the implementation of patterned media technology in the market.

With the second presented approach of this system [[1]] is a demonstration of spatial distribution of Xe in its different modes of mobility with the time structure of the motion at increasing temperatures up to 40K within on-surafce nano-traps and after cooling down to 4K again. The system provides unprecedented insight in the diffusion of a van der Waals gas on a complex energy landscape defined by an on-surface sample architecture and its nucleation and coarsening / growth into 12-fold symmetry of larger condensates It is notable, that Xe can be captivated and re-distributed in an almost non-interacting state across different topologies defined by the architecture of an array [[2]]. In that way, we find new states of 'condensed matter' which may

provide alternatives trapping atoms or molecules at surface with unprecedented characteristics as modified by the surface and trapping potential.

The third project by using system [[1]] explores the stable linear charged $Xe_3^+$ trimer in on-surface confinement where experiments and theory give support each other for the existence of this remarkable new discovery. Distance calculation of trimer atoms inside confinements reveals smaller distance as compared to bare surface clustering. STM fingerprint of tip excursions indicate that in case of three xenon atoms in confinement, atoms diffuse in a more condensed way which is quite distinguishable from other condensates until 9 K. Furthermore, in local field excitation experiments: most notable property of the presented system is the exceptionally long relaxation times (~ min) of the Xe after excitation which is indicative of a very weak coupling of the atoms to their environment. Interestingly, the excited mobility persisted for variable durations in the order of minutes which provides an unexpectedly slow relaxation of the occ-3 Xe in its excited state, close to 4K. We take this slow evolution of the excited state in case of occ-3 as evidence for the existence of trimer $Xe_3^+$ as compared to the relaxation time of other occupancies time in case of trimer is much higher than other condensates [[3]].

The fourth system present an original approach allowing us to study condensation in a molecule-by-molecule way, which involves the size dependent adsorption of cyclo-alkanes molecules in the pores of a Cu-coordinated 3deh-DPDI network generated on the vacuum/solid interface. It is the imaging by scanning probe microscopy which enables us to gain real-space access to the condensates' architecture and our analysis of their structure formation provides much greater detail of the clustering process at an interface than hitherto available [[4]]. Condensation processes are of fundamental importance in chemistry and physics. As small condensates constitute the link between single atoms or molecules and the bulk state of condensed matter, the analysis of their size-dependent structure plays a crucial role in understanding the interatomic and intermolecular interactions involved.

On one hand the fascination with the present results is the unique achievement to observe textbook physics occuring in time lapse sequences under the microscope. On the other hand, the discrete number of components in the single digit range is impressive. Last but not least the complexity of the surface network architecture with the different adsorption sites and diffusion pathways activated at increasing temperature is another uniquely attractive characteristics of the here investigated system. The processes investigated involve (1) site specific condensation of different gases at different sites of a complex surface architecture, (2) phase transition like structural transitions, (3) diffusion pathways, (4) initial phases of reorganization / crystal structure formation with increasing number of atoms or molecules in a condensate. In this thesis

exclusively investigated noble gases and cycloalkanes in their condensation and temperature dependent phase evolution and diffusion in this particular network. The data and insight obtained so far triggers many new ideas to modify the surface architecture and/or the gas towards further insight and new conclusions. Some are briefly described in the following paragraph.

*Molecule-by-molecule* and *atom-by-atom* condensation studies can be performed for different adsorbates as well as in differently sized pores on different substrates. The former allows for change of the inter-atomic / intermolecular interactions: no experience with polar compounds has been gained yet and after that, also amphiphiles or even more complex molecules which are eligible for a combination of a subset of the following interactions H-bonding, pi-pi stacking and aliphatic chain aggregation and ionic bonding. While this requires larger pores, very interesting conclusions may arise about the hierarchy of interactions in competition of the energy minimal interaction and a rising temperatures which renders one or the other subunit mobile. Maybe even some insight can be gained on the dynamicity of substituents as they are occurring in biochemistry. In analogy to liquid crystals, a complex multi-stage phase evolution is expected for condensates from more complex molecular architectures. In the latter case, i.e. the modification of the pore size, the network backbones and the bottoms substrates the interplay of weak interactions can be probed as they govern the transition from a single layer condensate to a cluster which may exhibit a structure closer to the single crystal structure. Importantly also, local and non-local stimuli beyond temperature and the E-field in the STM junction should be exploited for inducing phase transitions. In ongoing work, it may also be interesting to look at desorption and chemical reaction processes as they initiate on condensates with different numbers of atoms/molecules. Last but not least, the topic of inter-pore coupling for differently sized condensates mediated via the substrate or via the elasticity of the network backbone provides another important parameter which is expected to increase the already high level of complexity of the observable phenomena. Even for the simpler systems, theoretical investigations are very useful to verify the numerical methods. In the case of the more complex systems such numerical calculations are essential to unravel and possibly also understand the detailed role of the different interatomic/intermolecular and/or the interaction with the confining walls of the network pore and the bottom substrate.

# Bibliography


1. Feynman, R. P. There's plenty of room at the bottom [data storage]. *J. Microelectromechanical Syst.* **1,** 60–66 (1992).

2. Maddox, M. W. & Gubbins, K. E. A molecular simulation study of freezing/melting phenomena for Lennard-Jones methane in cylindrical nanoscale pores. *J. Chem. Phys.* **107,** 9659–9667 (1997).

3. Zangi, R. & Mark, A. E. Bilayer ice and alternate liquid phases of confined water. *J. Chem. Phys.* **119,** 1694–1700 (2003).

4. Klein, J. & Kumacheva, E. Confinement-Induced Phase Transitions in Simple Liquids. *Science* **269,** 816–819 (1995).

5. Alba-Simionesco, C. *et al.* Effects of confinement on freezing and melting. *J. Phys. Condens. Matter* **18,** R15–R68 (2006).

6. Koga, K., Zeng, X. C. & Tanaka, H. Freezing of Confined Water: A Bilayer Ice Phase in Hydrophobic Nanopores. *Phys. Rev. Lett.* **79,** 5262–5265 (1997).

7. Coasne, B., Jain, S. K. & Gubbins, K. E. Freezing of Fluids Confined in a Disordered Nanoporous Structure. *Phys. Rev. Lett.* **97,** (2006).

8. Alabarse, F. G. *et al.* Freezing of Water Confined at the Nanoscale. *Phys. Rev. Lett.* **109,** (2012).

9. Sliwinska-Bartkowiak, M. *et al.* Melting/freezing behavior of a fluid confined in porous glasses and MCM-41: Dielectric spectroscopy and molecular simulation. *J. Chem. Phys.* **114,** 950 (2001).

10. Han, S., Choi, M. Y., Kumar, P. & Stanley, H. E. Phase transitions in confined water nanofilms. *Nat. Phys.* **6,** 685–689 (2010).

11. Sliwinska-Bartkowiak, M. *et al.* Phase Transitions in Pores: Experimental and Simulation Studies of Melting and Freezing †. *Langmuir* **15,** 6060–6069 (1999).

12. Javadian, S., Taghavi, F., Yari, F. & Hashemianzadeh, S. M. Phase transition study of confined water molecules inside carbon nanotubes: Hierarchical multiscale method from molecular dynamics simulation to ab initio calculation. *J. Mol. Graph. Model.* **38,** 40–49 (2012).

13. Valiullin, R. Diffusion in Nanoporous Host Systems. in *Annual Reports on NMR Spectroscopy* **79,** 23–72 (Elsevier, 2013).

14. Mitra, P. P., Sen, P. N., Schwartz, L. M. & Le Doussal, P. Diffusion propagator as a probe of the structure of porous media. *Phys. Rev. Lett.* **68,** 3555–3558 (1992).

15. Gelb, L. D., Gubbins, K. E., Radhakrishnan, R. & Sliwinska-Bartkowiak, M. Phase separation in confined systems. *Rep. Prog. Phys.* **62,** 1573–1659 (1999).

16. Knorr, K., Huber, P. & Wallacher, D. Thermodynamic and Structural Investigations of Condensates of Small Molecules in Mesopores. *Z. Für Phys. Chem.* **222,** 257–285 (2008).

17. Gubbins, K. E., Liu, Y.-C., Moore, J. D. & Palmer, J. C. The role of molecular modeling in confined systems: impact and prospects. *Phys Chem Chem Phys* **13,** 58–85 (2011).

18. Barth, J. V., Costantini, G. & Kern, K. Engineering atomic and molecular nanostructures at surfaces. *Nature* **437,** 671–679 (2005).

19. Müller, K., Enache, M. & Stöhr, M. Confinement properties of 2D porous molecular networks on metal surfaces. *J. Phys. Condens. Matter* **28,** 153003 (2016).

20. Nowakowska, S. *et al.* Configuring Electronic States in an Atomically Precise Array of Quantum Boxes. *Small* **12,** 3757–3763 (2016).

21. Nowakowska, S. *et al.* Interplay of weak interactions in the atom-by-atom condensation of xenon within quantum boxes. *Nat. Commun.* **6,** 6071 (2015).

22. Widmer, R., Passerone, D., Mattle, T., Sachdev, H. & Gröning, O. Probing the selectivity of a nanostructured surface by xenon adsorption. *Nanoscale* **2,** 502 (2010).

23. Dil, H. *et al.* Surface Trapping of Atoms and Molecules with Dipole Rings. *Science* **319,** 1824–1826 (2008).

24. Perry, J. J. *et al.* Noble Gas Adsorption in Metal–Organic Frameworks Containing Open Metal Sites. *J. Phys. Chem. C* **118,** 11685–11698 (2014).

25. Wahl, M., Stöhr, M., Spillmann, H., Jung, T. A. & Gade, L. H. Rotation–libration in a hierarchic supramolecular rotor–stator system: Arrhenius activation and retardation by local interaction. *Chem Commun* 1349–1351 (2007). doi:10.1039/B700909G

26. Lobo-Checa, J. *et al.* Band Formation from Coupled Quantum Dots Formed by a Nanoporous Network on a Copper Surface. *Science* **325,** 300–303 (2009).

# Acknowledgements

I am very happy that I received help and support in enormous amounts during my PhD studies.

Especially I owe my deepest gratitude to my PhD supervisor Thomas Jung for giving me room for creativity and personal growth, for openness and flexibility, for many scientific discussions and great help with writing of the manuscripts. Moreover, I acknowledge his effort to invite my little daughter Shanzay to Switzerland, and last but not least for organizing many great group events.

I would like to thank all my former and present colleagues Aneliia Wäckerlin, Sylwia Nowakowska, Marco Martina, Thomas Nijs, Seyedeh Fatemeh Mousavi and Olha Popova from the Nanolab, who made available their support in a number of ways. Especially I am thankful to Thomas Nijs, who introduced me to the UHV system, with whom I had great discussions and on whose help and creative approach for problem solving I could always count. Moreover, special thanks go to Seyedeh Fatemeh Mousavi for her priceless support during conference attendance in company of my daughter. I am thankful to all the technical support that has been provided by Marco Martina and Matthes Senn. I am also grateful to Shigiki Kawai, Robert Skonieczny and Mac Iwasaki for sharing their impressive scientific and technical knowledge.

I sincerely thank Lutz Gade from University of Heidelberg for providing the molecules used in this thesis, for sharing his remarkable knowledge and for his enthusiastic engagement in the projects. I am obliged to Jonas Björk for sharing his impressive knowledge during our scientific discussions.

Finally, I would like to thank the FCS grant for providing the funding which allowed me to undertake this research, and especially Mrs. Andrea Delpho of the University of Basel who was always present to solve any grant related problems.